Catalyzed Big Bang Nucleosynthesis and the Properties of Charged Relics in the Early Universe

by

Kristen Alanna Koopmans
B.Sc., McMaster University, 2005

A Thesis Submitted in Partial Fullfillment of the
Requirements for the Degree of

MASTER OF SCIENCE

in the Department of Physics and Astronomy

Catalyzed Big Bang Nucleosynthesis and the Properties of Charged Relics in the Early Universe

by

Kristen Alanna Koopmans
B.Sc., McMaster University, 2005

Supervisory Committee

Dr. Maxim Pospelov, Supervisor
University of Victoria Department of Physics and Astronomy
and Perimeter Institute for Theoretical Physics

Dr. Adam Ritz, Member
University of Victoria Department of Physics and Astronomy

Dr. Don A. Vandenberg, Member
University of Victoria Department of Physics and Astronomy

Dr. Richard H. Cyburt, External Member
National Superconducting Cyclotron Laboratory (NSCL) at Michigan State University
and The Joint Institute for Nuclear Astrophysics (JINA)

Supervisory Committee

Dr. Maxim Pospelov, Supervisor
University of Victoria Department of Physics and Astronomy
and Perimeter Institute for Theoretical Physics

Dr. Adam Ritz, Member
University of Victoria Department of Physics and Astronomy

Dr. Don A. Vandenberg, Member
University of Victoria Department of Physics and Astronomy

Dr. Richard H. Cyburt, External Member
National Superconducting Cyclotron Laboratory (NSCL) at Michigan State University
and The Joint Institute for Nuclear Astrophysics (JINA)

Abstract

The existence of charged electroweak-scale particles in the early universe can drastically affect the evolution of elemental abundances. Through the formation of Coulombic bound states with light nuclei, these exotic relic particles (hereafter referred to as X^-) act to catalyze nuclear reactions by reducing their threshold energies. This thesis examines the properties of the X^- bound states, and uses primordial element observations to constrain the abundance, lifetime, and mass of this exotic particle species. If the X^- is a Dirac Fermion, its abundance relative to baryons must be $Y_{X^-} \sim 0.01$, with a lifetime of $1500\,\mathrm{s} \lesssim \tau_{X^-} \lesssim 3000\,\mathrm{s}$, and a mass of $m_{X^-} \sim \mathcal{O}(100)\,\mathrm{GeV}$. Assuming that the X^- is a scalar particle that decays into gravitinos, then the resulting bounds are, $5 \times 10^{-4} \lesssim Y_{X^-} \lesssim 0.07$, $1600\,\mathrm{s} \lesssim \tau_{X^-} \lesssim 7000\,\mathrm{s}$, and $60\,\mathrm{GeV} \lesssim m_{X^-} \lesssim 1000\,\mathrm{GeV}$. These ranges are consistent with Dark Matter constraints.

Table of Contents

List of Tables

List of Figures

Acknowledgments

First and foremost, I would like to thank my professors and teachers, especially my supervisor, Dr. Pospelov, whose support and guidance has been greatly appreciated. I am also grateful for the excellent support staff in the Department of Physics, and the wonderful group of graduate students that I have become a part of. Special thanks go to my office mate who is always full of good advice, ranging from physics topics and LaTeX formatting, to suggestions that I go home and eat! You kept me sane! I am also lucky to have been blessed with a very supportive family, whose encouragement over the years has meant a lot to me. Thanks especially to my mother, who is never too busy for me, and who has become my good friend. Most of all, I would like to thank my Fighter Pilot out in the prairies, who has given me a wonderful goal to work towards, and is always able to remind me of the lighter side of life. I can't think of anyone I'd rather have on my team, and together I know that we will find our way Home. Final thanks go to my long-time friend the Laser Jock, who has always been there for me, and who pointed me towards this very fitting quotation,

> The general who wins a battle makes many calculations in his temple ere the battle is fought. The general who loses a battle makes but few calculations beforehand. Thus do many calculations lead to victory, and few calculations to defeat.
>
> ∼Sun Tsu, The Art of War, c.550 BC

Chapter 1

Introduction

Standard Big Bang Nucleosynthesis (BBN, or SBBN) is a remarkably successful framework which predicts the primordial abundances of the light elements using just one free parameter, the ratio of baryons to photons in the universe. Its predictions can be altered, however, by the presence of heavy metastable particles. In particular, if these relic particles are negatively charged, they can form electromagnetically bound states, allowing for catalyzed nuclear reactions. This novel mechanism allows particle physics to directly affect cosmological predictions. In this chapter, the motivation for including these heavy, charged relics in the theory will be discussed, both from a particle physics point of view, and from a cosmological standpoint. In the first section, an overview of the results and scope of this work will be presented, and the layout of this thesis will be explained.

1.1 Overview

The existence of metastable electroweak-scale particles is predicted by most Beyond-the-Standard-Model theories, but it wasn't until relatively recently that the interactions of these relic particles in the early universe were fully appreciated. Ref. [1] first proposed the mechanism of Catalyzed Big Bang Nucleosynthesis (CBBN), in which Coulomb bound states can form between the charged relic X^- and the light nuclei, N. These bound states can affect nuclear reaction rates, since the threshold energies for many interactions are reduced by the binding energy of the (NX^-) system. In addition, the Coulomb barrier for nuclear reactions is reduced by the presence of the bound states, as the nuclear charge is partially screened by the X^- particle. The catalysis of these nuclear reactions can affect the predictions of Nucleosynthesis. Observational bounds on primordial elemental abundances can therefore be used to constrain the properties of the X^- relic. The predictions are very model-independent and have broad applicability.

In this work, properties of the bound states (NX^-) will be established for several light nuclei, N, and constraints will be placed on the properties of the X^- particle.

Assuming that the X^- is a spin-1/2 Dirac Fermion, it will be shown that ^{6}Li constraints imply that the initial X^- abundance relative to baryons is $Y_{X^-} \sim 0.01$, while its lifetime is in the range $1500\,\mathrm{s} \lesssim \tau_{X^-} \lesssim 3000\,\mathrm{s}$. This indicates that the X^- mass should be about $m_{X^-} \sim \mathcal{O}(100)\,\mathrm{GeV}$.

In the case where the X^- takes the identity of a spin-0 Scalar particle, the X^- properties can be constrained much more definitely. A popular Supersymmetry (SUSY) scenario is one in which the spin-3/2 gravitino, $\tilde{g}_{3/2}$, is the Lightest Supersymmetric Particle (LSP), and the scalar stau, $\tilde{\tau}$, is the Next-to-Lightest Supersymmetric Particle (NLSP). If the X^- represents the $\tilde{\tau}$, then decays of the X^- into the gravitino also help to constrain its properties. Under these assumptions, it will be shown that the initial X^- abundance relative to baryons must be in the range $5 \times 10^{-4} \lesssim Y_{X^-} \lesssim 0.07$, while its lifetime is constrained to $1600\,\mathrm{s} \lesssim \tau_{X^-} \lesssim 7000\,\mathrm{s}$. The resulting bounds on the mass will be shown to be $60\,\mathrm{GeV} \lesssim m_{X^-} \lesssim 1000\,\mathrm{GeV}$.

These are very stringent constraints, and are based on the study of the CBBN implications of the ($^4\mathrm{HeX}^-$) system. The results are consistent with the best predictions coming from the CBBN study of the ($^7\mathrm{BeX}^-$) system [2], which uses ^{7}Li + ^{7}Be constraints to determine the properties of the X^-. The results of this work are also consistent with Dark Matter constraints, in the case where the X^- is the NLSP and decays into the LSP, presumed to be a Dark Matter candidate.

This thesis will be laid out as follows. In the Chapter 1, the theoretical and cosmological motivations for the work will be presented. The following two chapters will be devoted to a generic study of the properties of the system (NX^-), which represents the bound state between the X^- particle and a light nucleus N. Several isotopes of Hydrogen, Helium, Lithium, and Beryllium will be considered as the

nucleus in the bound state. The mechanisms for creating and destroying the bound state will also be discussed, and a temperature scale will be found at which the (NX^-) system can be expected to form.

In Chapter 4, the ($^7BeX^-$) system will be discussed in detail. In particular, the interesting possibility of the X^- decaying while within the bound state will be addressed. Ultimately, this scenario proves to have few consequences to standard Nucleosynthesis. On the other hand, the catalyzed nuclear reactions facilitated by the ($^7BeX^-$) system could lead to a possible solution to the Lithium Problem, which is a current discrepancy in cosmology that will be discussed in Section 1.3.

The main focus of this thesis is the study of the ($^4HeX^-$) system. In Chapter 5, the properties of the ($^4HeX^-$) system will be discussed, and the methodology for analysing the system will be established. In Chapter 6, cosmological ^6Li observations will be used to constrain the properties of the X^- through ($^4HeX^-$) considerations. Both the case where the X^- is a spin-1/2 particle, and the case where it is a spin-0 particle are considered. For the scalar particle, constraints on the decay of the X^- into a gravitino are also used to restrict the parameter space of allowed X^- properties.

Chapter 7 summarizes the results of this work, and shows that they are consistent with Dark Matter observations. Brief conclusions are given, and the importance of the continued study of the CBBN mechanism is emphasized.

A table of the abbreviations and symbols used in this text is provided in Appendix

A, and a list of the values of the physical constants relevant to this work is included in Appendix B. Units of $c = \hbar = k_B = 1$ are used throughout this text.

1.2 Theoretical Motivation

Although the Standard Model (SM) is a remarkably successful theory, it has many limitations, and there are several issues in physics that it does not address. For example, it cannot explain the small neutrino masses, or the smoothness of the universe (presumably due to an inflationary period in the early universe), or the matter-antimatter asymmetry that is observed. It also does not provide an explanation of the gravitational force. For these reasons, it is important to search for new physics beyond the Standard Model.

Heavy charged particles are predicted by many Beyond-the-Standard-Model theories, including Supersymmetry and Kaluza-Klein models. In particular, long-lived relics are found in the Constrained version of the Minimal R-parity conserving Supersymmetric Standard Model (CMSSM), and in Minimal Super Gravity (mSUGRA), which both predict gravitino Dark Matter, and often include a stau NLSP. There is compelling evidence that there must be some sort of new physics at the TeV-scale, and as such it is natural to expect a whole spectrum of new heavy particles, including the possibility of metastable charged particles such as those considered in the CBBN mechanism.

Supersymmetry and other Beyond-the-Standard-Model scenarios are motivated by three primary theoretical arguments [3]. First and foremost is to stabilize the Higgs mass, which otherwise gets radiative corrections from loop diagrams (involving mostly the top quark) that make the Higgs mass diverge quadratically. This is known as the weak scale Hierarchy problem, and Supersymmetry is able to offer a "natural" solution to this problem by the introduction of a symmetry between fermions and bosons. Secondly, SUSY provides a mechanism through which to unify the gauge couplings at high energy. The "Grand Unification" of the gauge couplings of the strong, weak, and electromagnetic forces is a strong theoretical motivation for looking for new physics at this scale. Supersymmetry also contains in its algebra the generator for space-time translations, which is a necessary component of quantum gravity. As such, Supersymmetry is required for String Theory, M-theory and other such Quantum Gravity models. The third important motivation for TeV-scale physics is to address the cosmological problem of Dark Matter. This particular issue will be discussed in more detail in Section 1.3.

Supersymmetry is a so-called "broken" symmetry. If it was a perfect symmetry, the masses of the sparticles (the SUSY partners to the SM particles) would be degenerate with the masses of their Standard Model partners, but it is known that no such particles exist below about 85 GeV [3]. The SUSY particles are expected to have masses around the TeV-scale, and searches at the Large Hadron Collider (LHC)

at CERN will commence in 2008 to attempt detection of these particles. Currently there is no experimental evidence for SUSY, and it is not known which form Supersymmetry will take if it is indeed a correct theory of nature. It is hoped that detector searches at the LHC will soon resolve this question.

1.3 Cosmological Motivation

One of the unsolved mysteries of physics today is to explain what the universe is made of. It is known that only about 24% of the energy density of the present universe comes from matter [4], and the rest is from an entity called Dark Energy, about which very little is known. Perhaps even more shocking, however, is the fact that all the stars and gas and matter that is observed in the universe can only make up about 4% of the energy density required for closure [4]. From the WMAP survey, it is now known that the universe is indeed flat, implying that most of this 24% matter is unaccounted for. As such, this unaccounted for matter it is generically known as Dark Matter.

Unlike for Dark Energy, there are possible solutions on the horizon for identifying the source of Dark Matter. It is generally agreed today that Dark Matter must be "cold," meaning that the particles that account for it must be non-relativistic and probably heavy. Dark Matter interacts only through the weak and gravitational forces, since any strong or electromagnetic interactions would have led to observation.

One of the attractive features of Supersymmetry is that it naturally supplies a Dark Matter candidate if R-parity is conserved. R-parity is a discrete symmetry that assigns R $= -1$ to all SUSY particles, and R $= +1$ to all Standard Model particles. It is a multiplicative quantum number, meaning that a SUSY particle must decay into an odd number of SUSY particles (plus some number of Standard Model particles). If R-parity holds, then that means that the lightest SUSY particle must be stable, since there is nothing it can decay into in an energy conserving process. This lightest SUSY particle (LSP) is therefore a Dark Matter candidate. The fact that Supersymmetry naturally provides a possible solution to the Dark Matter problem is an attractive feature of the theory, and one of its prime motivations.

The above theoretical and cosmological arguments have been motivations for some sort of TeV-scale physics beyond the Standard Model. Most of these theories include metastable charged relics such as the one presumed to be responsible for CBBN, but so far no real motivation for CBBN *itself* has been presented. Besides being a natural consequence of the presence of heavy metastable charged particles in the universe, the CBBN mechanism is itself an important addition to Big Bang Nucleosynthesis.

Big Bang Nucleosynthesis (BBN) predicts the primordial abundances of the light elements with just one free parameter, the ratio of baryons to photons in the universe. This parameter, η, has recently been well measured by the WMAP collabora-

tion through the study of the Cosmic Microwave Background anisotropies [4]. The combination of Nucleosynthesis and the dynamics of the universe itself (characterized by the Hubble Rate) are able to predict the evolution of the primordial abundances of the light elements in the universe. As such, the comparison of these Standard BBN (SBBN) predictions with observational data provides a good test of the combination of the Standard Model and General Relativity.

In order to make such comparisons, possible influences of non-standard cosmology and particle physics must be accounted for. Generic mechanisms that may affect the freezeout abundances of the elements include the following (see Ref. [2] and references therein). Models such as those predicting extra neutrino species can affect the timing of reactions, by altering the Hubble Rate, H(T). This in turn leads to a modification of the primordial elemental abundances. Unstable or annihilating heavy particles in the early universe can inject energy during or after BBN, thus adding a non-thermal component to nuclear reactions which can also have implications to the evolution of the light elements. Inhomogeneities in the universe during the BBN era and scenarios with time-dependent couplings can also have an impact. A new mechanism which has only recently been brought to the attention of the community is the possibility of thermally catalyzed reaction channels for nuclear reactions. This mechanism is the primary prediction of the Catalyzed BBN (CBBN) theory. If heavy charged particles form Coulomb bound states with the light nuclei, then many reactions can be

catalyzed, and the resulting implications to light element abundances can be severe [1].

Dispite the success of the SBBN, there is one outstanding issue in its ability to correctly predict elemental abundances. The amount of ^{7}Li predicted by the SBBN is about a factor of about 2-3 larger than the observational value found in the stellar atmospheres of low-metallicity halo stars. This is a statistically significant discrepancy that is known in cosmology as the Lithium Problem.

It is found that in very metal-poor Population-II stars, the ^{7}Li abundance becomes independent of metallicity. This is known as the "Spite Plateau," and is assumed to be indicative of the primordial ^{7}Li abundance [5]. Observations of metal-poor halo stars suggest a primordial abundance of ^{7}Li relative to hydrogen of $(1.23^{+0.68}_{-0.32}) \times 10^{-10}$ [6,7]. More recent observations of globular clusters using slightly different calibration factors to model stellar atmosphere found similar results, $(2.19^{+0.30}_{-0.26}) \times 10^{-10}$ [8] and $(2.34^{+0.35}_{-0.30}) \times 10^{-10}$ [9].

These observations are strikingly inconsistent with theoretical predictions based on the WMAP preferred value for η and Standard BBN [7,10]. Ref. [10] predicts that the primordial ^{7}Li abundance relative to hydrogen is $Y_{^7\mathrm{Li}} = (4.15^{+0.49}_{-0.45}) \times 10^{-10}$.

The discrepancy between prediction and observation is not easily attributed to trivial solutions, such as a discrepancy in nuclear rates or cross sections (see for example [10–12]). Recent understanding of diffusion in stars may help to alleviate some of the discrepancy, but cannot completely bridge the gap between experimental

findings and theoretical predictions [13]. In very old, metal-poor stars, diffusion has had time to allow heavier elements such as lithium to settle deep into the star. As lithium is fairly fragile, it is destroyed inside the star once it reaches layers with temperature greater than about 2.1×10^6 K [13]. This mechanism dilutes surface lithium, and may provide a partial explanation as to why less ^{7}Li is observed than Standard BBN predicts. It cannot, however, account for the whole difference that is observed, and just reduces the discrepancy from a factor of 2-3 to a factor of about 1.5-2.

Although the Lithium Problem may have its solution in an unaccounted for depletion mechanism for burning ^{7}Li inside stars, it is important to consider possible particle physics solutions as well. The CBBN predicts a ^{7}Li abundance lower than that predicted by the SBBN. By carefully choosing the values of the two important parameters in the model (namely, the abundance and the lifetime of the X^-), the CBBN predictions can be brought into agreement with the observational value, providing a possible solution to the Lithium Problem. For a full review of the Lithium Problem, the reader is referred to Refs. [13, 14], and references therein.

In addition to the well-established ^{7}Li problem, there is also an emerging ^{6}Li problem. The observed abundance of ^{6}Li is about a factor of 1000 larger than predictions from Standard BBN, and is thus attributed to cosmic sources. ^{6}Li can be produced by Galactic cosmic rays through α-α fusion and by proton and α spallation,

but observations find a relatively high ^{6}Li abundance even in very metal-poor systems, which cannot be explained by Standard BBN or Galactic cosmic rays. In addition, there appears to be an unexpected and unexplained ^{6}Li plateau region, where the abundance of ^{6}Li becomes independent of metallicity. There therefore appears to be an unsolved discrepancy with the ^{6}Li abundance. The ^{6}Li Problem is discussed in detail in Ref. [14]. A good review is also found in Ref. [15] and the references therein. Extra production of ^{6}Li in the BBN era of the early universe would help alleviate this problem. The CBBN mechanism may therefore also help to resolve this issue.

The CBBN mechanism is indeed an important addition to the understanding of the early universe, and it warrants further study. Many of the recent CBBN calculations in the literature are unreliable as they use inappropriate methods of analysis, relying on a Saha-type Equation to evaluate abundances rather than solving the full Boltzmann Equation. This thesis intends to improve upon these methods, and to provide constraints on the properties of the relic X^- particle species in various different scenarios.

Chapter 2

(NX^-) Bound State Properties

In this section, it will be demonstrated that if a metastable charged particle X^- with a lifetime $\tau_{X^-} \gtrsim 1000\,\mathrm{s}$ existed in the early universe, then it could have formed bound states with free nuclei in the early universe through Coulomb interactions. Since direct detector searches (for example at LEP 2) have excluded the possibility of exotic charged particles with $m \lesssim 85\,\mathrm{GeV}$ [3][1], then it is sufficient to consider just $m_{X^-} \sim \mathcal{O}(100)\,\mathrm{GeV}$ or more.

[1]The four experiments (ALEPH, DELPHI, L3, OPAL) at the Large Electron-Positron Collider (LEP) at CERN currently provide the best lower limits for the masses of exotic particles. Metastable scalar sleptons have been excluded for masses below 86 GeV, while spin-1/2 charginos must have masses greater than about 103 GeV in models with heavy sneutrinos. This limit may be slightly degraded for lighter sneutrinos. Assuming that the sneutrinos are heavier than the lightest chargino, then the lower limit on the chargino mass from LEP 2 reduces to 85 GeV. For even lighter sneutrino masses, there is no direct detector limit, but the Z width implies a lower limit of 45 GeV for the chargino mass. Light squarks with fractional charge have been excluded for masses below about 115 GeV by the Tevatron hadron collider experiments, although this limit may be less, depending on the model used. This information is summarized in Table 1 of Ref. [3].

2.1 Characteristic Energy and Distance Scales

At $t \simeq 1000\,\mathrm{s}$ after the Big Bang, the temperature of the universe was about $10^8\,\mathrm{K}$, or $40\,\mathrm{keV}$. At this time, the formation of most light nuclei had ended, and the elemental abundances were frozen out to their so-called 'primordial' values, after a period called Nucleosynthesis. The Nucleosynthesis era occurred during the first couple of minutes after the Big Bang, from about $t = 0.01\,\mathrm{s}$ to $t = 100\,\mathrm{s}$, corresponding to temperatures from $T = 10\,\mathrm{MeV}$ to just under $T = 100\,\mathrm{keV}$ (see, for example Ref. [16]). It was during this era that most of the creation of the light elements occured. By $t \simeq 1000\,\mathrm{s}$, the abundances of the light nuclei were all relatively constant with respect to each other. The universe was still much too hot for atoms to form, since typical atomic binding energies are on the order of $\frac{1}{2}Z^2\alpha^2 m_\mathrm{e} \sim \mathcal{O}(0.01\text{-}0.1)\,\mathrm{keV}$, so the universe consisted of a plasma of positively charged nuclei and negative electrons.

If free heavy X^- particles were also present in the early universe with $m_{\mathrm{X}^-} \gg m_\mathrm{N}$ for all the light nuclei, N, then there is the possibility that bound (NX^-) systems would have formed through Coulomb interactions [1]. These atom-like systems can be regarded as analogous to a hydrogen atom in which an electron is bound to the much heavier proton. In the case of the bound (NX^-) however, the X^- (at a mass of at least $100\,\mathrm{GeV}$) is much heavier than the positive nucleus, N. In the bound state (NX^-), the roll of the electron is therefore played by the nucleus, N, while the heavy X^- is the 'proton' of the system. Because $m_{\mathrm{X}^-} \gg m_\mathrm{N}$, the mass scales of the problem

will be entirely determined by the nuclear mass.

Naïvely, the binding energy of this (NX^-) system can be estimated by the Bohr-like Rydberg energy,

$$Ry = \frac{1}{2} Z^2 \alpha^2 m_{\mathrm{N}} \ \sim \ \mathcal{O}(100 - 1000)\,\mathrm{keV}. \tag{2.1}$$

Similarly, a 'Bohr' radius of the system can be defined as,

$$a_B = (Z\alpha m_{\mathrm{N}})^{-1} \ \sim \ (few)\,\mathrm{fm}. \tag{2.2}$$

These serve only to give an idea of the scales involved in the problem. Significant corrections to the binding energy will arise by considering another important difference between the (NX^-) bound state and a hydrogen atom. The nucleus N is not a point particle as is an electron, but rather, it has some finite size as well as a characteristic charge distribution. The binding energy can no longer be estimated by the simple point-particle Rydberg formula. This is especially evident when one considers the fact that the Bohr radius can often be well *within* the nuclear radius, which is also typically on the order of a few femtometers.

To determine the actual binding energy (or, equivalently, the ground state energy) of the (NX^-) system, the wave function must first be determined. In the following sections, two different methods are used to find the wave function. Firstly, a trial

wave function is employed, and a solution is found using the Variational Method of Quantum Mechanics. Secondly, a direct numeric solution is found to the Schrödinger Equation. It is confirmed that both methods yield the same results for the binding energy of the (NX^-) system. A table is presented in Section 2.2 comparing the Bohr radius, Rydberg energy, and the actual ground state energy of the light nuclei systems.

2.2 Binding Energy of (NX^-)

In this section, the Variational Method of Quantum Mechanics is used to determine the binding energy of (NX^-), taking into account the non point-like nature of the nucleus N. In order to study the effects of the finite charge radius of the nucleus, one must first model the charge distribution within the nucleus. A first-order approximation would be to assume a uniform spherical charge density, with a sharp drop-off to zero at the nuclear radius R_{N}. However, for light nuclei ($A \lesssim 40$), it has been found that the nuclear charge distribution is well characterized by a Gaussian distribution [17, 18],

$$\rho(r) = \rho_0 e^{-(r/r_0)^2}, \tag{2.3}$$

where $\rho_0 = \frac{Z\alpha}{(r_0\sqrt{\pi})^3}$. The parameter r_0 is chosen such that the root mean square (rms) value of the Gaussian radial distribution (2.3) is equal to the experimental rms charge

radius, R_N. As such, they are related by,

$$r_0 = \sqrt{\frac{2}{3}} R_N. \tag{2.4}$$

This charge distribution results in a potential between the X^- and a nucleus N with charge Z which is given by [18],

$$V(r) = -\frac{Z\alpha}{r} \operatorname{erf}(r/r_0). \tag{2.5}$$

With this potential in hand, it is now possible to use the Variational Method of Quantum Mechanics to find the binding energy and an optimized wave function for the (NX^-) system. It is assumed that the ground state of the system will be in an s-wave, and thus spherically symmetric. The angular wave function is therefore the trivial Y_0^0 spherical harmonic, $Y_0^0 = 1/\sqrt{4\pi}$. For the radial part of the wave function, a trial function is used which is inspired by the radial functions of the hydrogen atom. It comprises an exponential and a (third order) polynomial,

$$R(r) = N(1 + Br + Cr^2)e^{-Dr}, \tag{2.6}$$

where N is a normalization constant, and B, C and D are parameters. The Variational Principle (see for example Ref. [19, Chapter 7]) states that for *any* choice of ψ, the

following is true:

$$E_g \leq \langle\psi|H|\psi\rangle \equiv \langle H\rangle. \tag{2.7}$$

To find the correct ground state wave function, one therefore proceeds by minimizing the expectation value of the Hamiltonian, H, as a function of the parameters B, C and D. The Hamiltonian employed is the standard kinetic term plus the potential as given in Equation 2.5,

$$H = -\frac{1}{2m_N}\nabla^2 - \frac{Z\alpha}{r}\,\mathrm{erf}\left(\sqrt{\frac{3}{2}}\,\frac{r}{R_\mathrm{N}}\right), \tag{2.8}$$

where $\hbar = c = 1$.

Finding the values of B, C and D that minimize $\langle H\rangle$ gives the ground state wave function from Equation 2.6, and also the ground state energy of the (NX^-) system, since $E_g \approx \langle H\rangle_{min}$. For most of the nuclei considered, B and D are $\mathcal{O}(1)$ in some units (when r is measured in units of the Bohr radius a_B). For isotopes of Hydrogen, B is slightly less than unity, ranging from about 0.04 to 0.3 in these units. For ^{3}He and ^{4}He, $B \approx 0.7$. The parameter C is zero for all nuclei except for ^{7}Li (for which $C \approx 0.08$), and the two isotopes of Beryllium, ^{7}Be and ^{8}Be (for which $C \approx 0.2$).

The bound states of X^- with several light nuclei, N, were considered and the resulting properties are given in Table 2.1. It is interesting to note that ^{8}Be does not exist in nature, decaying immediately (in less than 0.1 fs [20, Appendix C]) to

two alpha particles. However, it *can* exist for finite time when bound with X^-. The Q-value for the decay $^8Be \rightarrow {}^4He + {}^4He$ is 91.84 keV [21–23], which is less than the binding energy of ($^8BeX^-$) as shown in Table 2.1.

Table 2.1: Properties of the bound state (NX^-) for several light nuclei N

Nucleus N	Z	Mass $(MeV)^2$	R_N $(fm)^3$	a_B (fm)	Ry (keV)	$\lvert E_g \rvert$ (keV)
^1H	1	938.280	0.862	28.82	25.0	25.0
^2H	1	1875.629	2.14	14.42	49.9	48.8
^3H	1	2808.945	1.68	9.63	74.8	72.5
^3He	2	2808.415	1.94	4.81	299	267
^4He	2	3727.411	1.72	3.63	397	346
^6Li	3	5601.566	2.54	1.61	1342	794
^7Li	3	6533.889	2.50	1.38	1566	870
^7Be	4	6534.240	2.48	1.03	2784	1336
^8Be	4	7454.914	2.44	0.91	3176	1427

It is clear from the table of results that it is indeed critical to consider the finite charge radius of the nucleus N, since the naïve Bohr orbit a_B is often well within the nuclear radius for the heavier nuclei, $a_B < R_N$. This indicates that the structure of the charge distribution is important to the determination of the properties of the bound state, and indeed quite a deviation is seen between the actual ground state energy and the Rydberg estimate.

[2]Atomic masses are given in Refs. [22, 23] for neutral atoms. The nuclear masses in Table 2.1 are obtained by subtracting $Z \cdot m_e$ from the atomic masses, to give the masses of the fully ionized nuclei (atomic binding energies are small enough to be neglected).

[3]The nuclear radii are from the experimental Gaussian rms charge densities given in Refs. [24–28] for all the nuclei except ^8Be. Since ^8Be is such an unstable nucleus, there is no experimental data on the nuclear radius, so the empirical formula $R_N = (1.22\,fm)\,x\,A^{1/3}$ [20] was employed, where A is the mass number.

2.3 (NX^-) Wave Functions

The second method of finding the ground state wave function and binding energy is to solve the Schrödinger Equation numerically. This method does not constrain the *form* of the wave function, as did the Variational Method through Equation 2.6, and so it will give a more accurate result. It is important to check the reliability of these numeric solutions, however, by ensuring that the binding energies they predict agree with those given by the Variational Method, which is also a valid method for finding the ground state energy.

The radial part of the wave function, $R = R(r)$ obeys the following equation,

$$\begin{aligned}
E\,\psi &= H\,\psi \\
E\,R &= -\frac{1}{2m_{\mathrm{N}}}\,\nabla^2 R \;-\; \frac{Z\alpha}{r}\,\mathrm{erf}\left(\sqrt{\frac{3}{2}}\,\frac{r}{R_{\mathrm{rms}}}\right) R \\
E\,R &= -\frac{1}{2m_{\mathrm{N}}}\,\frac{1}{r^2}\,\frac{\partial}{\partial r}\left(r^2\,\frac{\partial R}{\partial r}\right) \;-\; \frac{Z\alpha}{r}\,\mathrm{erf}\left(\sqrt{\frac{3}{2}}\,\frac{r}{R_{\mathrm{rms}}}\right) R \\
E\,\frac{\chi}{r} &= -\frac{1}{2m_{\mathrm{N}}}\,\frac{1}{r^2}\left(\frac{\partial^2\chi}{\partial r^2}\,r\right) \;-\; \frac{Z\alpha}{r}\,\mathrm{erf}\left(\sqrt{\frac{3}{2}}\,\frac{r}{R_{\mathrm{rms}}}\right)\frac{\chi}{r} \\
E\,\chi &= -\frac{1}{2m_{\mathrm{N}}}\,\frac{\partial^2\chi}{\partial r^2} \;-\; \frac{Z\alpha}{r}\,\mathrm{erf}\left(\sqrt{\frac{3}{2}}\,\frac{r}{R_{\mathrm{rms}}}\right)\chi. \qquad (2.9)
\end{aligned}$$

The Schrödinger Equation (2.9) is a second order ordinary differential equation for χ, where $\chi(r) = rR(r)$. From this definition of χ, it is clear that the boundary condition at $r = 0$ is $\chi(0) = 0$. Since Equation 2.9 is a *second* order differential equation, it

is also necessary to specify the slope at $r = 0$. This can be arbitrarily chosen (for example $\frac{\partial \chi}{\partial r}|_{r=0} = 1$), since normalizing the wave function later will fix this to the proper value. The only input needed to solve Equation 2.9 is the mass of the nucleus m_{N}, the charge Z, the rms nuclear radius R_{N}, and the energy E of the state. The first three parameters are taken from experimental nuclear data, and are listed in Table 2.1. For a first estimate, the ground state energy E_g can be approximated by the Rydberg energy, as defined in Equation 2.1.

Using the mathematical analysis package `Maple 9.5`, a numeric solution is found for the wave function. Of course, since the energy that was inserted was not the correct binding energy, the wave function will not properly reflect the ground state. Plotting the resulting solution will result in a function that looks qualitatively correct at small r, but that diverges to $\pm\infty$ at larger r. Depending on whether this large-r tail tends towards $+\infty$ or $-\infty$, one can adjust the input energy either downwards or upwards, respectively. A more accurate energy input will cause the divergence to happen at larger r. Iterating in this manner, one can push these divergences in the wave function out to arbitrarily large r (on the order of $50a_B$ or more) and get a binding energy precise to more than 10 digits. In the case of ^{7}Be, the amplitude of the radial wave function after $15a_B$ is less than 0.3% of the peak value, and the amplitude remains negligibly small well past $50\mathrm{a}_B$. Similar results are found for the other nuclei.

Therefore, from the numeric solution to the Schrödinger Equation, a very precise ground state energy is found which agrees with the energy found through the Variational Method, and is consistent with the values in Table 2.1. The resulting numeric wave function can also be used to calculate expectation values for certain quantities of interest.[4] As this numeric solution is less constrained than is the wave function found through the Variational Method, it is used for all further calculations and analysis.

As an example, the wave function found above can be used to calculate the expectation value of r, the average distance between the center of the nucleus and the X^- particle. In the case of the hydrogen atom, this quantity is exactly $\langle r \rangle = 1.5a_B$. Due to the finite size of the nuclei in the (NX^-) systems, it should be expected that $\langle r \rangle > 1.5a_B$, especially in the case of the heavier nuclei. Referring to the results in Table 2.2, it is clear that this is the case. For the bound states of X^- with hydrogen, $\langle r \rangle \approx 1.5a_B$, but for isotopes of beryllium, the average distance from the center of the nucleus to the X^- particle is about $3a_B$. In all cases, $\langle r \rangle$ is larger than the nuclear radius, R_N.

The fact that the nuclear radius is often larger than the naïve Bohr radius has a significant impact to the catalysis of nuclear reactions facilitated by the (NX^-) system. The Coulomb barrier of the nucleus N is partially screened by the presence

[4]Clearly, when finding an expectation value with these wave functions, one does not integrate up to infinity, but rather to some cut-off scale where the wave function $\chi(r)$ has gone to zero, but well before the scale at which the unphysical divergence mentioned above is encountered. In the case of ^{7}Be, this cut-off was set to $30a_B$.

Table 2.2: Distance scales involved in the (NX^-) systems

Nucleus N	R_N (fm)	a_B (fm)	$\langle r \rangle$
^{1}H	0.862	28.82	1.50 a_B
^{2}H	2.14	14.42	1.53 a_B
^{3}H	1.68	9.63	1.54 a_B
^{3}He	1.94	4.81	1.66 a_B
^{4}He	1.72	3.63	1.70 a_B
^{6}Li	2.54	1.61	2.47 a_B
^{7}Li	2.50	1.38	2.63 a_B
^{7}Be	2.48	1.03	3.00 a_B
^{8}Be	2.44	0.91	3.18 a_B

of the X^-, thereby reducing the nuclear reaction threshold.

As a demonstration of the impact of the finite size of the radius, the radial wave functions of two systems, (^{4}HeX^-) and (^{7}BeX^-), were plotted as a function of distance in units of the Bohr radius, a_B, in Figures 2.1 and 2.2. The hydrogen-like profile which assumes the nucleus is a point particle is compared to the more realistic profile in which the nucleus is given a Gaussian charge distribution characterized by the rms radius R_N from Table 2.1. Both the $R(r)$ and the $\chi(r) = rR(r)$ forms of the wave functions are shown. In the case of (^{4}HeX^-), $R_N = 1.72\,\text{fm}$, and $a_B = 3.63\,\text{fm}$. Since $R_N < a_B$, the realistic (^{4}HeX^-) profile does not differ much from the hydrogen-like case. With (^{7}BeX^-), on the other hand, $R_N = 2.48\,\text{fm}$ while $a_B = 1.03\,\text{fm}$, and the naïve Bohr orbit is *within* the nuclear radius since $R_N > a_B$. In this case, the two profiles are seen to differ significantly, and it becomes essential to include the finite radius effects.

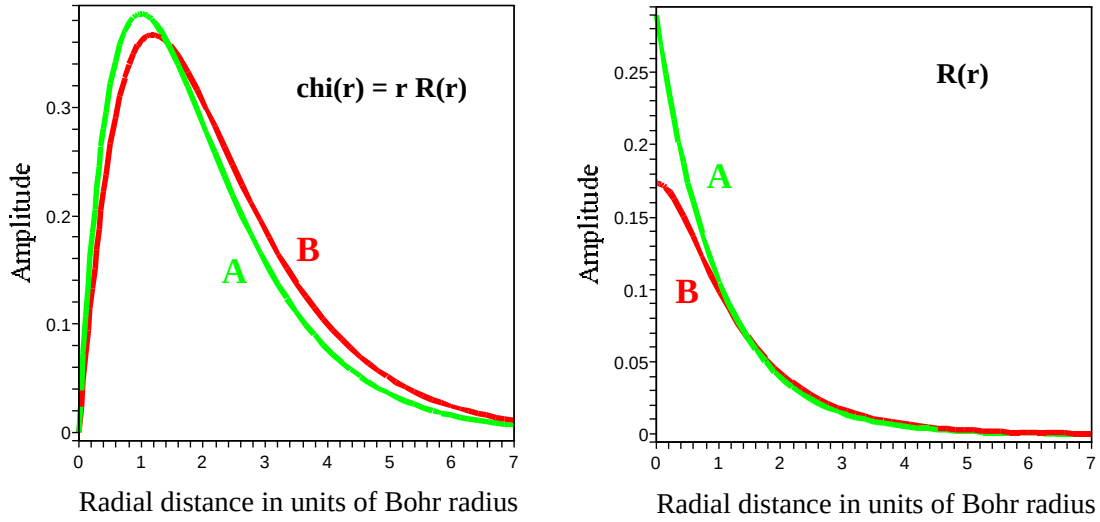

Figure 2.1: Normalized radial wave functions for the (^{4}HeX$^-$) system as a function of distance in units of $a_B = 3.63\,\text{fm}$. The green curves, A, are for the naïve point-like ^{4}He, while the red curves, B, represent a more realistic Gaussian charge distribution inside ^{4}He with an rms charge radius of $R_\text{N} = 1.72\,\text{fm}$

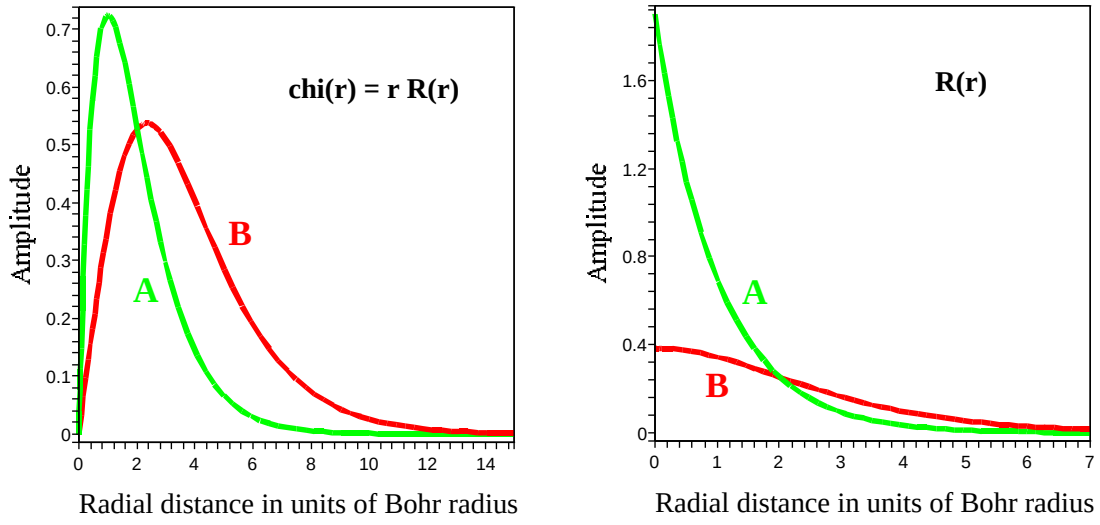

Figure 2.2: Normalized radial wave functions for the (^{7}BeX$^-$) system as a function of distance in units of $a_B = 1.03\,\text{fm}$. The green curves, A, are for the naïve point-like ^{7}Be, while the red curves, B, represent a more realistic Gaussian charge distribution inside ^{7}Be with an rms charge radius of $R_\text{N} = 2.48\,\text{fm}$

Chapter 3

Formation of (NX^-)

In this chapter, several important processes are examined in order to develop an understanding of the time-evolution of the abundance of the bound state (NX^-) in the universe. The mutual attraction between the nucleus N and the particle X^-, as well as the lower potential of the bound state with respect to the free particles, causes the formation of (NX^-) through the process of recombination. When the temperature of the universe is hotter than (or on par with) the binding energy of (NX^-), then the bound state will be destroyed by background photons through photodisintegration. In a non-static universe, the expansion rate of the universe must also be considered. The universe cools as it expands, and particles fall out of equilibrium with the photons as their interaction rates fall below the Hubble Rate [16]. These processes are examined in this chapter to quantify the abundance of (NX^-) as a function of time.

3.1 The Saha and Boltzmann Equations

The rate of change of the abundance Y_i of the species i can be understood simply as the difference of the rates of creation minus the rates of destruction, multiplied by the individual likelihoods of these processes. Schematically, this is represented as,

$$\frac{dY_i}{dt} = \sum \left(\Gamma_{ij} Y_j + \Gamma_{ikl} Y_k Y_l + \ldots\right), \tag{3.1}$$

where Y_i are the abundances of the particles i, and $\Gamma_{ij\ldots}$ are the generalized (positive or negative) rates for creation or destruction of the species i, involving interactions with the particles j, k, etc [2].

In cosmology and astrophysics, it is rarely useful to give rates or abundances in terms of their time dependence, but rather, it is usually their *temperature* dependence which is important. This is because nuclear and electromagnetic interactions fundamentally depend on energies, and not on time. The way in which time and temperature are related is given by the Friedmann Equation [16],

$$H^2 = \left(\frac{\dot{a}}{a}\right)^2 = \frac{8\pi G_N}{3}\,\rho - \frac{k}{a^2}, \tag{3.2}$$

where H is the Hubble rate, a is the scale factor, G_N is Newton's Constant, and ρ is the energy density of the universe (composed of matter, radiation, and Dark Energy).

In a flat universe, $k = 0$. Using the equation of state $p = w\rho$ to relate the pressure p of a fluid to its energy density ρ, it can be shown (see for example Ref. [16]) that the energy density evolves as $\rho \propto a^{-3(1+w)}$. The equation of state for radiation is $p = \frac{1}{3}\rho$, while for a pressure-less matter dust, it is $p = 0$. Dark Energy is thought to have negative pressure, $p = -\rho$. These lead to the following scalings of density with the scale factor:

$$\begin{aligned} \textit{Radiation} \quad & \rho_\gamma \propto a^{-4} \\ \textit{Matter} \quad & \rho_m \propto a^{-3} \\ \textit{Dark Energy} \quad & \rho_\Lambda = \textit{constant}. \end{aligned} \tag{3.3}$$

For a closed universe ($k = 0$), the scale factor a increases with time [16]. Since Nucleosynthesis occurred very early in the history of the universe (see discussion in Section 2.1), the scale factor was very small and the dominant component to the energy density of the universe was radiation. The radiation-dominated epoch of the universe lasted until $t \approx 10^6$ years [29] at which time matter became dominant. Dark Energy has only become important relatively recently as a becomes larger.

Solving the Friedmann Equation 3.2 in a flat radiation-dominated universe gives,

$$H(t) = \frac{1}{2t}. \tag{3.4}$$

The Hubble rate can also be expressed as a function of temperature [30],

$$\begin{aligned} H(T) &= \left(\frac{8\pi G_N \rho}{3}\right)^{1/2} \\ H(T) &= \left(\frac{8\pi\rho}{3}\right)^{1/2} M_{\rm Pl}^{-1}, \end{aligned} \tag{3.5}$$

where $M_{\rm Pl}$ is the Planck Mass, $M_{\rm Pl} = 1.22 \times 10^{19}\,{\rm GeV}$. At high temperatures, the energy density ρ can be expressed in terms of just the particles with mass $m \ll T$ [30],

$$\begin{aligned} \rho &= \frac{\pi^2}{30} g_* T^4 \\ \rho &= \frac{\pi^2}{30}\left(\sum_B g_B \left(\frac{T_B}{T}\right)^4 + \frac{7}{8}\sum_F g_F \left(\frac{T_F}{T}\right)^4\right) T^4, \end{aligned} \tag{3.6}$$

where the sums run over all bosons, B, and fermions, F, with masses much less than the temperature. Equation 3.6 defines g_*, where g_B and g_F are the number of degrees of freedom of the boson or fermion respectively, and the factor of 7/8 arises from the difference between Fermi-Dirac and Bose-Einstein statistics. The different particle species may no longer be in thermal equilibrium with the rest of the universe, and are characterized by temperature-like parameters T_i which may in general be different from the temperature T of photons.

During Nucleosynthesis, the temperature of the universe is less than about 100 keV (see discussion in Section 2.1), so the only particles to be included in the sums in Equa-

tion 3.6 are photons (with $g = 2$) and the three flavours of Standard Model neutrinos (each with $g = 2$). A well-known result (see for example Refs. [16, 30]) that arises due to the fact that neutrinos fall out of equilibrium with the thermal photon bath before $e^{\pm}$ pairs begin to annihilate, is that the photons are heated up with respect to the neutrinos, since they can absorb the energy from the $e^{\pm}$ annihilation. After $e^{\pm}$ annihilation (at temperatures less than about the mass of an electron, $T \lesssim 511\,\mathrm{keV}$), the ratio between the photon temperature, T_γ, and the neutrino temperature, T_ν, is

$$\frac{T_\nu}{T_\gamma} = \left(\frac{4}{11}\right)^{1/3}. \tag{3.7}$$

Using Equations 3.5 and 3.6, the Hubble Rate can be written as a function of the photon temperature, denoted by T hereafter.

$$\begin{aligned} H(T) &= \left(\frac{8\pi^3}{90}\right)^{1/2} \left(2 + \frac{7}{8}\,(3 \cdot 2) \left(\frac{4}{11}\right)^{4/3}\right) \frac{T^2}{M_{\mathrm{Pl}}} \\ H(T) &\approx 0.3798 \left(\frac{T}{\mathrm{MeV}}\right)^2 \mathrm{s}^{-1}. \end{aligned} \tag{3.8}$$

Equating Equations 3.4 and 3.8 finally gives a relation between temperature and time, $t \approx 1.316 T^{-2}$, with t in seconds and T in MeV. Using the relation $t = \frac{1}{2H(T)}$ and the

fact that $H(T)$ scales as T^2, then,

$$\begin{aligned} dt &= -\frac{1}{2}\, H^{-2}(T)\, \frac{dH}{dT}\, dT \\ dt &= -H^{-1}(T)\, T^{-1}\, dT. \end{aligned} \tag{3.9}$$

Now Equation 3.1 can be reformulated in terms of temperature:

$$\frac{dY_i}{dt} = -H(T)\, T\, \frac{dY_i}{dT} = \sum \left(\Gamma_{ij} Y_j + \Gamma_{ikl} Y_k Y_l + \ldots\right). \tag{3.10}$$

This is a generalized form of the Boltzmann Equation for the evolution of the abundance of the particle species i.

If recombination and photodisintegration are the dominant production and destruction mechanisms respectively, then the Boltzmann Equation becomes,

$$-H\, T\, \frac{dY_{(\mathrm{NX}^-)}}{dT} = \langle \sigma_{\mathrm{rec}} v \rangle n_{\mathrm{N}} Y_{\mathrm{X}^-} - \langle \sigma_{\mathrm{ph}} \rangle n_\gamma Y_{(\mathrm{NX}^-)}, \tag{3.11}$$

where n_i are the densities of the species i, Y_i are their abundances (relative to some common standard, such as the total baryon density, n_{B}) and all quantities are implicitly functions of temperature.

The Saha Equation (see for example Ref. [16]) relates the abundance of free particles and those bound in atoms. It can be applied to this example, but should be

taken as an approximation to the Boltzmann Equation. The Saha Equation assumes that the process $\mathrm{N} + \mathrm{X}^- \leftrightarrow (\mathrm{NX}^-) + \gamma$ is in chemical equilibrium, and that no other processes are involved. It predicts a rapid switch from a fully ionized state to a state where all of the N or X^- (whichever is less abundant) are bound into (NX^-). The modified Saha Equation for the (NX^-) system is,

$$\left(\frac{m_{\mathrm{N}} m_{\mathrm{X}^-}}{m_{(\mathrm{NX}^-)}}\right)^{3/2} \left(\frac{T}{2\pi}\right)^{3/2} = \frac{n_{\mathrm{N}} n_{\mathrm{X}^-}}{n_{(\mathrm{NX}^-)}} e^{I/T}, \tag{3.12}$$

where $I = E_B$ is the (positive) ionization energy of (NX^-). This equation can be rearranged to give the fraction of X^- particles locked into the bound state (NX^-), $F_{\mathrm{X}^-} = n_{(\mathrm{NX}^-)} / \, n_{\mathrm{X}^-}$. It is assumed below that $m_{\mathrm{X}^-} \approx m_{(\mathrm{NX}^-)}$.

$$\begin{aligned} F_{\mathrm{X}^-}^{(Saha)} &= \left(\frac{m_{\mathrm{N}} T}{2\pi}\right)^{-3/2} e^{I/T} \, n_{\mathrm{N}} \, (1 - F_{\mathrm{X}^-}) \\ &= \left(1 + \left(\frac{m_{\mathrm{N}} T}{2\pi}\right)^{3/2} e^{-I/T} \, n_{\mathrm{N}}^{-1}\right)^{-1}. \end{aligned} \tag{3.13}$$

The Boltzmann Equation can also be arranged to give a differential equation for F_{X^-},

$$-H\,T \, \frac{dF_{\mathrm{X}^-}^{(Boltz.)}}{dT} = \langle \sigma_{\mathrm{rec}} v \rangle n_{\mathrm{N}} (1 - F_{\mathrm{X}^-}^{(Boltz.)}) - \langle \sigma_{\mathrm{ph}} \rangle n_\gamma F_{\mathrm{X}^-}^{(Boltz.)} \tag{3.14}$$

Both of these expressions can be modified for a unstable X^- by including a factor of $n_{\mathrm{X}^-}^{initial} e^{-t/\tau_{\mathrm{X}^-}}$, where $n_{\mathrm{X}^-}^{initial}$ is the initial X^- abundance, and τ_{X^-} is the lifetime of

the X^-. Both τ_{X^-} and t can be converted from units of time to units of temperature using Equations 3.4 and 3.8.

The difference between the output of the Boltzmann and Saha Equations will be examined for the ($^4HeX^-$) system in Chapter 5. Although several recent publications [31–33] have used the Saha Equation for analysing the ($^4HeX^-$) system, this work finds that there are significant modifications to the final results when using the full Boltzmann Equation.

3.2 Photodisintegration

Photodisintegration is the primary mechanism for destroying (NX^-) bound states in a hot universe, and is initiated by an interaction with a thermal photon whose energy is at least equal to the ionization energy of the bound state,

$$(NX^-) + \gamma \rightarrow N + X^- , \ E_\gamma \geq I. \tag{3.15}$$

Because the energies of the photons in a thermal bath are distributed according to the Planck Distribution which has a large high-energy tail, there will be photons with sufficient energy to ionize the (NX^-) bound state even at temperatures much less than the ionization energy of the system. As will be shown, the rate of photodisintegration is Boltzmann-suppressed by a factor of $e^{-I/T}$, where I is the ionization energy of the

(NX^-) bound state. At temperatures $T \gtrsim I$, the rate becomes large, as there are many photons in the thermal distribution which can initiate the photoelectric effect. At these temperatures, the destruction rate of the bound state is expected to be so high that (NX^-) does not get a chance to form.

The following discussion is therefore restricted to temperatures much less that the ionization energy of the bound state. At such temperatures, the energy of the initiating photon, ω, is expected to be approximately equal to the ionization energy. As a rough estimate, the ionization energy should be of a similar magnitude as the Rydberg energy (Equation 2.1), which gives the naïve estimate of the binding energy for a point-particle system. From this, it is concluded that $\omega - \mathrm{I} \ll \mathrm{I}$, where $\mathrm{I} \sim Ry = \frac{1}{2}\mathrm{Z}^2\alpha^2 m_\mathrm{N}$. The photoelectric cross section in this limit is given in Ref. [34] as,

$$d\sigma_{\mathrm{p}h} = Z^2\alpha\frac{m_\mathrm{N}|\mathbf{p}|}{2\pi\omega}|\mathbf{e}\cdot\mathbf{v}_{fi}|^2 d\Omega, \tag{3.16}$$

where $\mathbf{p}$ is the momentum of the nucleus N, $\mathbf{e}$ is the photon polarization, and,

$$\mathbf{v}_{fi} = -\frac{i}{m_\mathrm{N}}\int \psi'^{*}\nabla\psi d^3\mathbf{r}\,. \tag{3.17}$$

The initial bound-state wave function is taken as the n=1 ground state, $\psi = \frac{1}{\sqrt{4\pi}}R(r)$, where $R(r)$ is the normalized radial wave function. In the final state, ψ' is the wave function of the free nucleus N. The asymptotic form of ψ' must comprise a plane

wave, $e^{i\mathbf{p}\cdot\mathbf{r}}$, together with an ingoing spherical wave, and must be in a p-wave ($l = 1$) to account for selection rules for transitions from the $l = 0$ ground state. Neglecting unimportant phase factors, the wave function ψ', as given in Ref. [34] is,

$$\psi' = \frac{3}{\mathrm{p}}\sqrt{\frac{\pi}{2}}(\hat{\mathbf{p}}\cdot\hat{\mathbf{r}})R_{p1}(r), \tag{3.18}$$

where R_{p1} is the radial function for $l = 1$. In the zero-energy limit[1], this becomes the Bessel Function [35],

$$R_{p1}(r) \to \sqrt{\frac{2\mathrm{p}}{r}}J_3\left(\sqrt{8r/a_B}\right). \tag{3.19}$$

Here a_B represents the Bohr radius of the (NX^-) system, $a_B = \frac{1}{Z\alpha m_{\mathrm{N}}}$. The Bessel Function $J_3(x)$ is a pure Coulomb function for the free wave function, and does not necessarily apply to the case of a system involving a nucleus of finite size. As such, it is an approximation to the true case. It will be shown later that this approximation causes the photodisintegration rate to be about 30% low for the ($^7\mathrm{BeX}^-$) system. For the ($^4\mathrm{HeX}^-$) system, the approximation is fair. Even in the bound state, the ($^4\mathrm{HeX}^-$) wave function is not significantly different than the purely Hydrogen-like profile, as can be seen in Figure 2.1 .

With Equations 3.18 and 3.19 to define ψ', and using $\psi = \frac{1}{\sqrt{4\pi}}R(r)$, the quantity

[1]The N momentum is small, $\mathrm{p} \to 0$, in the limit that the temperature of the universe is $T \ll I$. This is because $\omega \to I$ in this limit, and the photon barely has enough energy to ionize the system. It therefore does not have enough energy to give the recoiling nucleus much momentum.

$\mathbf{e}\cdot\mathbf{v}_{fi}$ is calculated as follows,

$$\begin{aligned}
\mathbf{v}_{fi} &= -\frac{i}{m_{\mathrm{N}}}\int \frac{3}{\mathrm{p}}\sqrt{\frac{\pi}{2}}(\hat{\mathbf{p}}\cdot\hat{\mathbf{r}})R_{p1}(r)\frac{1}{\sqrt{4\pi}}\left(\frac{\partial}{\partial r}R(r)\hat{\mathbf{r}}\right)d^3\mathbf{r} \\
|\mathbf{e}\cdot\mathbf{v}_{fi}| &= \frac{3}{2^{3/2}m_{\mathrm{N}}\mathrm{p}}\int(\hat{\mathbf{p}}\cdot\hat{\mathbf{r}})(\hat{\mathbf{r}}\cdot\mathbf{e})R_{p1}(r)\left(\frac{\partial}{\partial r}R(r)\right)d^3\mathbf{r} \\
&= \frac{3}{2^{3/2}m_{\mathrm{N}}\mathrm{p}}\int(\hat{\mathbf{p}}\cdot\hat{\mathbf{r}})(\hat{\mathbf{r}}\cdot\mathbf{e})d\Omega\int R_{p1}(r)\left(\frac{\partial}{\partial r}R(r)\right)r^2dr \\
&= \frac{3}{2^{3/2}m_{\mathrm{N}}\mathrm{p}}\cdot\frac{4\pi}{3}(\hat{\mathbf{p}}\cdot\hat{\mathbf{e}})\int R_{p1}(r)\left(\frac{\partial}{\partial r}R(r)\right)r^2dr \\
&= \frac{\sqrt{2}\pi}{m_{\mathrm{N}}\mathrm{p}}(\hat{\mathbf{p}}\cdot\hat{\mathbf{e}})\int\sqrt{\frac{2\mathrm{p}}{r}}J_3\left(\sqrt{8r/a_B}\right)\left(\frac{\partial}{\partial r}R(r)\right)r^2dr \\
&= \frac{2\pi}{m_{\mathrm{N}}\sqrt{\mathrm{p}}}(\hat{\mathbf{p}}\cdot\hat{\mathbf{e}})\int J_3\left(\sqrt{8r/a_B}\right)\left(\frac{\partial}{\partial r}R(r)\right)r^{3/2}dr.
\end{aligned}$$

This result can now substituted into Equation 3.16. Integrating over the solid angle to go from $d\langle\sigma_{\mathrm{ph}}\rangle$ to $\langle\sigma_{\mathrm{ph}}\rangle$ only affects the dot product between the incoming momentum and the photon polarization, $\int(\hat{\mathbf{p}}\cdot\hat{\mathbf{e}})^2d\Omega=\frac{4\pi}{3}$.

$$\begin{aligned}
\sigma_{\mathrm{p}h} &= Z^2\alpha\frac{m_{\mathrm{N}}|\mathbf{p}|}{2\pi\omega}\left(\frac{2\pi}{m_{\mathrm{N}}\sqrt{\mathrm{p}}}\right)^2\frac{4\pi}{3}\left(\int J_3\left(\sqrt{8r/a_B}\right)\left(\frac{\partial}{\partial r}R(r)\right)r^{3/2}dr\right)^2 \\
&= \frac{8\pi^2Z^2\alpha}{3m_{\mathrm{N}}\omega}\left(\int J_3\left(\sqrt{8r/a_B}\right)\left(\frac{\partial}{\partial r}R(r)\right)r^{3/2}dr\right)^2 \\
&= \frac{8\pi^2Z^2\alpha}{3m_{\mathrm{N}}Ry}\frac{Ry}{\omega}\left(\int J_3\left(\sqrt{8r/a_B}\right)\left(\frac{\partial}{\partial r}R(r)\right)r^{3/2}dr\right)^2. \qquad (3.20)
\end{aligned}$$

In Equation 3.20, Ry is the Rydberg energy of the system, which is the naïve estimate of the ionization energy, $Ry=\frac{1}{2}Z^2\alpha^2m_{\mathrm{N}}=\frac{1}{2a_B^2m_{\mathrm{N}}}$. The important limit is when $\omega\to I$, where I is the real ionization energy. Table 2.1 compares the real

ionization energies ($I = |E_g|$) of various (NX^-) systems with the naïve Rydberg energies. For example, the ratio I_{true}/Ry is approximately 0.9 for ($^4HeX^-$), or about 0.5 for ($^7BeX^-$). In the limit $\omega \to I_{true}$, the cross section from Equation 3.21 becomes,

$$\sigma_{\mathrm{p}h} = \frac{16Z^2\pi^2\alpha a_B^2}{3}\frac{Ry}{I_{true}}\left(\int J_3\left(\sqrt{8r/a_B}\right)\left(\frac{\partial}{\partial r}R(r)\right)r^{3/2}dr\right)^2. \tag{3.21}$$

An analytic solution can be found only for simple systems. Such an example is atomic Hydrogen, for which the ground-state radial wave function is $R(r) = 2a_B^{3/2}e^{-r/a_B}$, and Z=1. Plugging this into the above equation gives,

$$\begin{aligned}
\sigma_{\mathrm{p}h}(hydrogen) &= \frac{16\pi^2\alpha a_B^2}{3}\left(\int J_3\left(\sqrt{8r/a_B}\right)2a_B^{-5/2}e^{-r/a_B}r^{3/2}dr\right)^2 \\
&= \frac{16\pi^2\alpha a_B^2}{3}\left(\int J_3\left(\sqrt{8r/a_B}\right)2a_B^{-5/2}e^{-r/a_B}r^{3/2}dr\right)^2 \\
&= \frac{2^6\pi^2\alpha a_B^2}{3}\left(\int J_3\left(\sqrt{8x}\right)e^{-x}x^{3/2}dx\right)^2 \\
&= \frac{2^6\pi^2\alpha a_B^2}{3}\left(\sqrt{8}e^{-2}\right)^2 \\
&= \frac{2^9\pi^2\alpha a_B^2}{3e^4},
\end{aligned} \tag{3.22}$$

where e is the base of the natural logarithm, and x was defined as r/a_B. Using the Hydrogen Bohr Radius of 5.29×10^4 fm, this gives,

$$\sigma_{\mathrm{p}h}^{(hydrogen)} = 6.3 \times 10^6 \,\mathrm{barn}\,. \tag{3.23}$$

More interesting systems can also be analysed. For example, with the numerical ground state wave function for (^{7}BeX$^-$) from Section 2.3, and with Z=4, $I_{true}/Ry \approx 0.4799$, and $a_B \approx 1.03\,\mathrm{fm}$, Equation 3.21 gives,

$$\sigma_{ph}^{(^7\mathrm{BeX}^-)} \approx 8.67 \times 10^{-3}\,\mathrm{barn}\,. \tag{3.24}$$

For (^{4}HeX$^-$) with Z=2, $I_{true}/Ry \approx 0.8715$, and $a_B \approx 3.63\,\mathrm{fm}$, one finds,

$$\sigma_{ph}^{(^4\mathrm{HeX}^-)} \approx 0.118\,\mathrm{barn}\,. \tag{3.25}$$

To turn these cross sections into rates of photodisintegration, they must be averaged over the thermal distribution of photons and multiplied by the number density of photons, $\Gamma_{\mathrm{ph}} = \langle \sigma_{\mathrm{ph}} v \rangle n_\gamma$, where $v = c = 1$ in these units. In the limit where the cross sections are essentially independent of the photon energy, averaging the cross section over the thermal distribution of photons amounts to simply multiplying σ_{ph} by the number density of photons with enough energy to ionize (NX$^-$). This number density is a function of temperature and is obtained by integrating the Planck distribution (also often called the Bose-Einstein distribution) from the threshold energy to infinity. The Planck distribution (see for example Refs. [36,37]) for the number of photons per

unit volume at temperature T with energies between E_γ and $E_\gamma + dE_\gamma$ is,

$$dn_\gamma(T) = \left(\frac{1}{\pi}\right)^2 \frac{E_\gamma^2 \, dE_\gamma}{\exp\left(E_\gamma/T\right) - 1}. \tag{3.26}$$

The number of photons n_γ^{ionize} at a given temperature T with enough energy to ionize the system (NX^-) is obtained by integrating the above distribution from $E_\gamma = I$, to $E_\gamma = \infty$,

$$n_\gamma^{ionize}(T) = \int_I^\infty \left(\frac{1}{\pi}\right)^2 \frac{E_\gamma^2 \, dE_\gamma}{\exp\left(E_\gamma/T\right) - 1}. \tag{3.27}$$

Since the photodisintegration cross section is a scalar quantity, $\langle\sigma_{\rm ph}\rangle n_\gamma$ is equivalent to $\sigma_{\rm ph} n_\gamma^{ionize}$, and the photodisintegration rate is,

$$\Gamma_{\rm ph} = \langle\sigma_{\rm ph}\rangle n_\gamma = \sigma_{\rm ph} n_\gamma^{ionize}, \tag{3.28}$$

where $\sigma_{\rm ph}$ is from Equation 3.21, n_γ^{ionize} is from Equation 3.27, and n_γ is the *total* number density of photons at temperature T, obtained by integrating Equation 3.26 from zero to infinity.

3.3 Recombination

Recombination is the process through which N and X^- form an electromagnetically bound state (NX^-). The recombination process $N + X^- \rightarrow (NX^-) + \gamma$ is the inverse

of the photodisintegration process, and as such it is natural to expect that the cross sections are related. The Principle of Detailed Balance states [34] that the recombination cross section can be obtained from the photodisintegration cross section through the following equation,

$$\sigma_{\text{rec}} = \sigma_{\text{ph}} \cdot \frac{2k^2}{\text{p}^2}, \tag{3.29}$$

where $k = \omega$ is the momentum of the emitted photon, and p is the relative momentum of the incoming nucleus N and the X^- particle. In practice, the X^- can be considered to be at rest, since its mass is assumed to be much larger than that of the N, so p can be assumed to be just the momentum of the thermal nucleus.

Since the temperature of the universe is much less than the ionization energy of (NX^-) at the time of its formation,[2] then the N and X^- do not have much thermal energy when they interact. The energy available to the recoiling (NX^-) and the photon after recombination is therefore not significantly more than the binding energy that is released when the bound state (NX^-) forms. Assuming that the recoil energy of the heavy (NX^-) is negligible, then the photon energy is $\omega \approx I$.

Table 2.1 shows that the masses of the light nuclei are all around several GeV, while the ionization energies are on the order of hundreds of keV. Since the temperature of the universe (and therefore the kinetic energies of the N and X^-) is less

[2]This must be the case, otherwise the bound state would be completely destroyed by ionizing background photons.

than the ionization energy, it is appropriate to assume that the nuclei (and the X^- particles) are non-relativistic. In this limit, $p = m_N v$, and the expression for σ_{rec} can be written as,

$$\sigma_{rec} = \sigma_{ph} \frac{2I^2}{(m_N v)^2}. \tag{3.30}$$

In order to get the recombination rate, this cross section must be averaged over the thermal distribution of the nuclei. Note that technically, p is not the momentum of N, but rather the *relative* momentum of N and X^-, in which case $p = m_{red} v$, where $m_{red} = m_{X^-} m_N/(m_{X^-} + m_N)$. Since $m_N \ll m_{X^-}$, this reduces to $m_{red} \approx m_N$, and the relative momentum is approximately equal to $m_N v$. Similarly, σ_{rec} should be averaged over the *relative* speed, v_{rel}, not just the N speed. The 2-body Maxwell-Boltzmann velocity distribution is identical to that for a single particle [38] with the exception that the reduced mass must be used in place of the single particle mass. Again, since $m_{red} \approx m_N$, then one may just consider the N speed distribution. This is given by the Maxwell-Boltzmann distribution of the speed of a particle in the non-relativistic limit (see for example Ref. [39]),

$$f(v)dv = 4\pi \left(\frac{m}{2\pi k_B T}\right)^{3/2} v^2 e^{\frac{-mv^2}{2k_B T}} dv, \tag{3.31}$$

where $f(v)dv$ is the probability that the particle is at a speed between v and $v + dv$. The Boltzmann constant k_B is shown above for clarity, but is set back to k_B=1 for

the remainder of the discussion.

The thermally averaged cross section $\langle \sigma_{\rm rec} v \rangle$ is,

$$\begin{aligned}
\langle \sigma_{\rm rec} v \rangle &= \int \sigma_{\rm rec} v f(v) dv \\
&= \int \sigma_{\rm ph} \frac{2I^2}{(m_{\rm N} v)^2} v f(v) dv \\
&= 8\pi \frac{I^2}{m_{\rm N}^2} \sigma_{\rm ph} \left(\frac{m_{\rm N}}{2\pi T} \right)^{3/2} \int_0^1 v e^{-m_{\rm N} v^2/2T} dv \\
&= \frac{4\, I^2\, \sigma_{\rm ph}}{\sqrt{2\pi T}\; m_{\rm N}^{3/2}} \left(1 - e^{-m_{\rm N}/2T} \right) \\
&\approx \frac{4\, I^2\, \sigma_{\rm ph}}{\sqrt{2\pi}\; m_{\rm N}^{3/2}}\; T^{-1/2}. \qquad (3.32)
\end{aligned}$$

The exponential was set to zero in the last line since $m_{\rm N} \gg T$, and the units in the above expression are such that c=1.

To get the rate of recombination, one must multiply $\langle \sigma_{\rm rec} v \rangle$ by the number density of either N or X^-, and the abundance of the other. Clearly, this choice is arbitrary, since the abundance of a species i (measured relative to some constant, such as the total baryon density $n_{\rm B}$) is $Y_i = \frac{n_i}{n_{\rm B}}$. So, $Y_{\rm N} n_{\rm X^-} = n_{\rm N} Y_{\rm X^-} = Y_{\rm N} Y_{\rm X^-} n_{\rm B}$, and any of these combinations are equivalent, and moreover each also gives the correct units for the rate $\Gamma_{\rm rec}$. The rate is in units of inverse time, which matches with $\langle \sigma_{\rm rec} v \rangle Y_{\rm N} Y_{\rm X^-} n_{\rm B}$, since $\langle \sigma_{\rm rec} v \rangle$ has units of area times (distance/time), $Y_{\rm N}$ and $Y_{\rm X^-}$ are dimensionless,

and $n_{\rm B}$ has units of inverse volume. The recombination rate is thus,

$$\Gamma_{\rm rec} = \frac{4\, I^2\, \sigma_{\rm ph}}{\sqrt{2\pi}\; m_{\rm N}^{3/2}}\; T^{-1/2}\; n_{\rm B}\, Y_{\rm N}\, Y_{\rm X^-}\,. \tag{3.33}$$

3.4 Temperature of Formation

In the previous sections, there were several claims made as to the temperature of the universe at the time of the formation of (NX^-). Although an exact temperature of formation would be difficult to define (the processes occur over a range of temperatures), it is possible to quantify a rough scale at which the (NX^-) forms.

The photodisintegration decoupling temperature, T_f, is an estimate of the temperature scale at which the (NX^-) system is no longer ionized. This temperature is defined to be the temperature at which the photodisintegration rate becomes smaller than the Hubble Rate, $\Gamma_{\rm ph}(T_f) = H(T_F)$. Using the Hubble and photodisintegration rates from Equations 3.8 and 3.28 (with the optimized wave functions from Section 2.3), the temperature scale T_f of the formation of the bound state (NX^-) is found. The results are presented in Table 3.1, along with the binding energy from Section 2.2.

From Table 3.1, it is clear that T_f is typically about 2.5% of the ionization energy of the system. The claims earlier in this chapter that the bound state (NX^-) does

Table 3.1: Temperature of Formation of (NX^-)

Bound State	$I = \|E_g\|$ (keV)	T_f (keV)
^{1}H X^-	25.0	0.6
^{2}H X^-	48.8	1.2
^{3}H X^-	72.5	1.8
^{3}He X^-	267	6.3
^{4}He X^-	346	8.2
^{6}Li X^-	794	19
^{7}Li X^-	870	21
^{7}Be X^-	1336	33
^{8}Be X^-	1427	36

not form until the universe cools to a temperature well under its ionization energy are therefore justified.

Now that some general properties of the X^- bound states have been set, the following chapters are devoted to studying two specific systems in more detail. The (^{7}BeX^-) system will be studied first. This system is of interest to cosmology, as the catalysis effects that it causes could potentially provide a solution to the Lithium Problem [2]. The second system that is studied is that of (^{4}HeX^-). Because of fairly stringent limits on the ^{6}Li abundance in the universe, this system can be used to constrain the properties of the X^-.

Chapter 4

The (^{7}BeX$^-$) System

Study of the (^{7}BeX$^-$) system is of great importance to cosmology, and there has been considerable interest in it since the CBBN model was first proposed by Ref. [1] early in 2006. The catalyzed nuclear reactions facilitated by (^{7}BeX$^-$) offer a possible solution to the Lithium Problem,[1] in which standard BBN predicts twice the primordial ^{7}Li that is observed. ^{7}Li is produced primarily through neutron spallation on beryllium, $^7\mathrm{Be} + n \rightarrow {}^7\mathrm{Li} + p$, and much later through ^{7}Be electron capture decay. As such, any process that depletes ^{7}Be will also reduce the primordial abundance of ^{7}Li. This chapter reviews recent work on the topic of the (^{7}BeX$^-$) system, showing that with appropriate abundance and lifetime parameters for X$^-$, the CBBN ^{7}Li predictions can be brought into agreement with observation.

[1] See full discussion in Section 1.3.

4.1 The Abundance of (^{7}BeX$^-$)

As an illustrative example, the abundance of the (^{7}BeX$^-$) system can be studied through the use of the Boltzmann Equation.[2] Considering just photodisintegration and recombination, the Boltzmann Equation 3.11 is,

$$-H\,T\,\frac{dY_{(^7\mathrm{BeX}^-)}}{dT} = \langle\sigma_{\mathrm{rec}}v\rangle Y_{^7\mathrm{Be}} Y_{\mathrm{X}^-} n_{\mathrm{B}} - \langle\sigma_{\mathrm{ph}}\rangle n_\gamma Y_{(^7\mathrm{BeX}^-)}, \tag{4.1}$$

or, in terms of the total number N_i of species i,

$$-H\,T\,\frac{dN_{(^7\mathrm{BeX}^-)}}{dT} = \langle\sigma_{\mathrm{rec}}v\rangle n_{\mathrm{B}} Y_{\mathrm{X}^-} N_{^7\mathrm{Be}} - \langle\sigma_{\mathrm{ph}}\rangle n_\gamma N_{(^7\mathrm{BeX}^-)}. \tag{4.2}$$

Note that $N_{^7\mathrm{Be}}$ is the number of *free* ^{7}Be nuclei, and Y_{X^-} is the abundance (relative to baryons) of free X$^-$ particles.

^{7}Be freezes out of Standard BBN at a temperature of about 40 keV (see for example Ref. [16]). By the time the universe cools enough to start forming (^{7}BeX$^-$) (about 33 keV according to Table 3.1), the number of ^{7}Be from SBBN is relatively constant on the time scales important to this problem. The abundance of ^{7}Be relative to Hydrogen at that time was small, only about 10^{-11} [16]. On much longer

[2]The relative merits of the Boltzmann Equation over the Saha Equation for the study of the evolution of the abundance of a bound state (NX$^-$) will be discussed in detail in the following chapter, through the examination of the (^{4}HeX$^-$) system.

time scales, once the universe has cooled enough so that atomic ^{7}Be can recombine with electrons, ^{7}Be decays through electron capture to ^{7}Li with a half-life of about 53 days [22]. None survives to the present day. Since the ^{7}Be abundance is so small during the BBN era, it is useful to re-write the Boltzmann Equation in terms of the fraction, $F_{\rm BS}$, of ^{7}Be locked into a bound state with X$^-$, $F_{\rm BS} \equiv N_{(^7{\rm BeX}^-)}/\ (N_{(^7{\rm BeX}^-)} + N_{^7{\rm Be}})$. Dividing Equation 4.2 by the total number of free and bound ^{7}Be gives,

$$-H\,T\,\frac{dF_{\rm BS}}{dT} = \langle\sigma_{\rm rec}v\rangle n_{\rm B} Y_{\rm X^-}(1-F_{\rm BS}) - \langle\sigma_{\rm ph}\rangle n_\gamma F_{\rm BS}, \tag{4.3}$$

It is clear from this equation that $F_{\rm BS}$ depends on the abundance $Y_{\rm X^-}$ of the X$^-$ particle in the universe.

Using the formulae developed in Sections 3.2 and 3.3, the photodisintegration and recombination cross sections are,

$$\langle\sigma_{\rm ph}\rangle n_\gamma = \left(6.87\times10^{15}T^3 + 9.18\times10^{15}T^2 + 6.13\times10^{15}T\right) e^{-1.336/T}\,{\rm s}^{-1} \tag{4.4}$$

$$\langle\sigma_{\rm rec}v\rangle n_{\rm B} = 22.65T^{5/2}\,{\rm s}^{-1} \tag{4.5}$$

where temperature T is measured in MeV.

Incidentally, there are several important factors not taken into account in Equations 4.4 and 4.5. In the derivation of the photoelectric cross section (on which the recombination cross section also depends), the final state wave function of the free

^{7}Be and X$^-$ was taken to be the Bessel function given in Equation 3.19. This is an approximation to the true case, however, as it assumes a point-particle behaviour of ^{7}Be. As demonstrated in Section 2.3, the (^{7}BeX$^-$) wave function in the bound state deviates significantly from one which assumes point-particle behaviour, so it is reasonable to expect a similar effect in the free wave function. Including finite radius effects increases the photodisintegration cross section (and thus also the recombination cross section) by about 30% [2]. The recombination rate gets additionally enhanced due to resonant states in ^{7}Be that facilitate the creation of (^{7}BeX$^-$) states as described by Ref. [2]. The photodisintegration and recombination cross sections including all these effects are given in [2], and in the units used here, they are,

$$\langle\sigma_{\rm ph}\rangle n_\gamma = \left(8.76\times10^{15}T^3 + 1.13\times10^{16}T^2 + 7.48\times10^{15}T\right) e^{-1.329/T}\ {\rm s}^{-1} \qquad (4.6)$$

$$\langle\sigma_{\rm rec}v\rangle n_{\rm B} = \left(47.18T^{5/2} + 12.87T^{3/2}e^{-0.121/T} + 10.16T^{3/2}e^{-0.140/T}\right)\ {\rm s}^{-1}, \qquad (4.7)$$

where T is again in MeV.

Using these rates in the Boltzmann Equation 4.3, The fraction of ^{7}Be locked into (^{7}BeX$^-$) is calculated as a function of temperature, denoted by $F_{\rm BS}(T)$. In the limit of long X$^-$ lifetime, this only depends on the one parameter, $Y_{\rm X^-}$.[3] A plot of $F_{\rm BS}$ as a function of temperature is presented in Figure 4.1 for several values of $Y_{\rm X^-}$ =

[3]For finite lifetime, a decaying exponential is added to the X$^-$ abundance, $Y_{\rm X^-} \rightarrow Y_{\rm X^-}\ e^{-t/\tau_{\rm X^-}}$ $= Y_{\rm X^-}\ e^{-1.32/T^2\tau_{\rm X^-}}$, where $\tau_{\rm X^-}$ is the X$^-$ lifetime in seconds, and T is the temperature in MeV.

$n_{\mathrm{X}^-}/n_{\mathrm{B}}$, in the limit of long X^- lifetime. The functions were calculated numerically using the `Maple 9.5` software package.

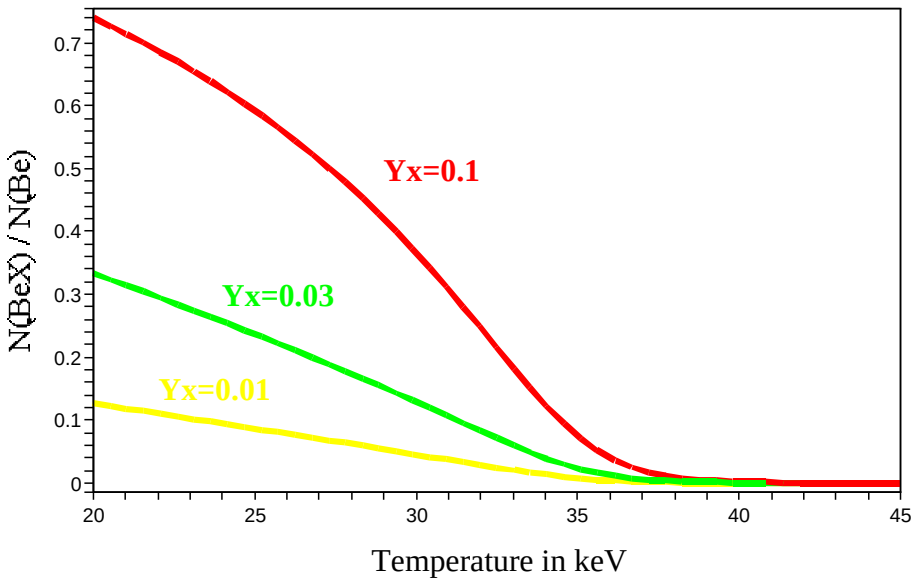

Figure 4.1: The fraction, F_{BS}, of ^{7}Be locked into the bound state (^{7}BeX$^-$) as a function of temperature, in the limit of long X^- lifetime. In this limit, $F_{\mathrm{BS}}(T)$ depends only on one parameter, the abundance Y_{X^-} of X^- relative to baryons. The solution is plotted for three different values of Y_{X^-} for illustrative purposes.

Figure 4.1 gives a qualitative depiction of the evolution of the abundance of the bound state (^{7}BeX$^-$), but still does not represent a complete treatment of the (^{7}BeX$^-$) system. The only creation and destruction mechanisms that were inserted into the Boltzmann Equation were recombination and photodisintegration. Other important nuclear processes exist that destroy (^{7}BeX$^-$), as discussed in Ref. [2]. The simplified picture represented by Figure 4.1 is still useful in giving a scale to the problem, as it shows that for $Y_{\mathrm{X}^-} < 0.01$, less than 15% of ^{7}Be nuclei enter the bound state (^{7}BeX$^-$)

at temperatures greater than 20 keV. There is little point considering temperatures significantly lower than this scale. If it is assumed that the X^- has a lifetime on the order of 1000 s, then by the time the universe is 1000 s old (cooled to a temperature of about 40 keV), the X^- population has significantly decayed, and the fraction $F_{\rm BS}$ will drop significantly. Figure 4.1 implies that $Y_{X^-} > 0.01$ if there are to be observable effects on cosmology. With Y_{X^-} less than 0.01, only 15% or fewer ^{7}Be are in the state (^{7}BeX$^-$), and one would not expect drastic consequences to BBN due to X^- catalyzed depletion of ^{7}Be.

There are many subtleties in the (^{7}BeX$^-$) system, including nuclear processes such as the catalysis of proton- and neutron-destruction, that affect the evolution of (^{7}BeX$^-$). In addition, catalyzed internal conversion, (^{7}BeX$^-$) $\rightarrow$ ^{7}Li + X^0, can cause the early creation of ^{7}Li. Since ^{7}Li is much more fragile than ^{7}Be, this leads to an overall depletion of the predicted ^{7}Li abundance. These mechanisms go beyond the scope of this current work, and a full treatment of the (^{7}BeX$^-$) system will not be considered here, as it is not the main focus of this thesis. This author did, however, contribute to the work in Ref. [2] through a calculation of the consequences that would follow if the X^- decayed while *inside* the bound state (^{7}BeX$^-$). These calculations are presented in Section 4.2. For a detailed analysis of the complete (^{7}BeX$^-$) system, the reader is referred to Ref. [2]. The main conclusions of this study are summarized in Section 4.3, and in Section 6.4.

4.2 Break-up of ^{7}Be in the Decay of X^-

When examining how the bound states (NX^-) affect cosmology, the primary considerations are catalyzed nuclear reactions. The threshold energies for processes involving the bound nucleus N are reduced by the binding energy of (NX^-), and the Coulomb barrier is partially screened. These processes are thus altered for a cosmology with a heavy metastable X^-. These nuclear reactions are said to be "catalyzed" by the presence of the X^-. Another consideration is the possibility that the unstable X^- may decay while inside the bound (NX^-) system, dissociating the bound state before nuclear processes can proceed with the bound N.

For the ($^7BeX^-$) system, nuclear processes are studied in detail in Ref. [2], and will not be repeated here. The possibility of X^- decay inside the ($^7BeX^-$) system is an interesting possibility to discuss, however, and the three main mechanisms for ^{7}Be break-up in X^- decay will be presented below.

1. ($^7BeX^-$) $\rightarrow$ ^{7}Be + products of X^- decay + hard $\gamma \rightarrow$ ^{3}He + ^{4}He + $\cdots$

   If the decay of X^- produces a "hard" photon (with energy greater than the photodestruction threshold of ^{7}Be, $E_{th} = 1.59\,\mathrm{MeV}$ [40]), this photon could be absorbed by the ^{7}Be to induce a photodestruction, $^7\mathrm{Be} \rightarrow {}^3\mathrm{He} + {}^4\mathrm{He}$. This hard photon may be a virtual particle radiated off by the X^- or the charged decay products that it creates.

2. $(^7\mathrm{BeX}^-) \rightarrow {}^7\mathrm{Be}\ (E \gg T)$ + background particles + $\cdots \rightarrow {}^3\mathrm{He} + {}^4\mathrm{He} + \cdots$

   If the decay of the X^- occurs "instantaneously," then the free ^{7}Be after the decay has the same momentum distribution that it had while in the bound state. This momentum distribution is given by the Fourier Transform of the wave function from Section 2.3. Typical momenta of the free ^{7}Be would be on the order of the binding energy of the $(^7\mathrm{BeX}^-)$ system, about 1.3 MeV from Table 3.1, while the temperature of the universe is cooler than about 30 keV. In this case, the decay of X^- therefore causes ^{7}Be to be injected non-thermally into the universe. Other thermal particles and photons in the universe will consequently appear blue-shifted to the ^{7}Be, and reaction thresholds will be effectively lowered, increasing the possibility of break-up of the recoiling ^{7}Be.

3. $(^7\mathrm{Be}^*\mathrm{X}^-) \rightarrow {}^3\mathrm{He} + {}^4\mathrm{He} + \cdots$

   In this mechanism, one considers the fact that the electromagnetic field created by the X^- particle could polarize the ^{7}Be such that the ^{7}Be bound into $(^7\mathrm{BeX}^-)$ is actually an admixture of the ground state of ^{7}Be as well as all the excited states, including those belonging to the continuum. When the X^- decays, these continuum states are released as ^{3}He + ^{4}He.

The first two mechanisms will be discussed in detail below. The third mechanism proves ineffectual for CBBN, as the admixture of excited states is only about 1% [2].

4.2.1 ^{7}Be Break-up through Hard Photons

In this mechanism, the break-up of ^{7}Be is induced when the nucleus is struck by an energetic photon. In order to produce these energetic photons, the X^- must release significant energy in its decay. As a model of this interaction, one can consider the generic possibility of the X^- decaying into a charged Standard Model particle, with or without some non-Standard Model relics accompanying it [2],

$$X^- \rightarrow SM^- [+ X^0], \quad \Delta E \sim m_{X^-}. \tag{4.8}$$

Assuming large energy release (which may not be the case in certain models where there is small mass splitting between relic particles), the charged decay product can be relativistic, causing a perturbation in the electromagnetic field around the ^{7}Be as it passes by. As the charged particle passes by the ^{7}Be nucleus, it emits hard photons which can cause the break-up of the nucleus. This process can be studied through the Weizsäcker-Williams Method of Equivalent Photons [34]. It is represented by the Feynman Diagram in Figure 4.2 for the case where the X^- is given the identity of the stau, $\tilde{\tau}$, in the model where $\tilde{\tau} \rightarrow \tau + \tilde{g}_{3/2}$, with a relic non-Standard Model gravitino, $\tilde{g}_{3/2}$.

The relativistic energy of the charged decay product, γm, and the maximum photon energy, E_{max}, can both be safely assumed to be on the order of the mass of

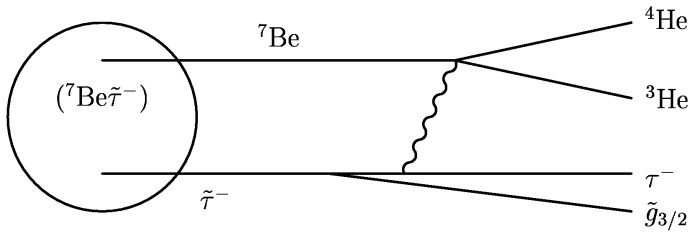

Figure 4.2: Feynman diagram for the "Equivalent Photon" mechanism of inducing the break-up of ^{7}Be in the decay of X^-. In this case, X^- has been given the identity $\tilde{\tau}$, and in this diagram, a model has been chosen where $\tilde{\tau} \to \tau + \tilde{g}_{3/2}$.

the X^-: $\gamma m \sim E_{max} \sim \mathcal{O}(100)\,\text{GeV}$. Under these assumptions, the cross section for the radiative break-up of ^{7}Be due to the electromagnetic perturbation caused by the charged decay products of the X^- is [34],

$$\sigma = \int_{E_{thr}}^{E_{max}} \frac{2Z\alpha}{\pi} \ln\left(\frac{E_{thr}}{\omega}\right) \sigma_{rad}(\omega)\, \frac{d\omega}{\omega}, \tag{4.9}$$

where Z is the charge of the X^- decay product, here assumed to be 1, ω is the virtual photon energy, and $\sigma_{rad}(\omega)$ is the cross section for the regular radiative break-up of ^{7}Be due to interaction with a photon of energy ω. To turn this cross section into a branching ratio or probability of break-up, one must multiply it by a "flux" of virtual photons through the ^{7}Be nucleus. This is where the wave function dependence enters, as the flux is given by the expectation value of $1/4\pi r^2$, the inverse of the surface area of a sphere (centred on the X^-) that is occupied by the ^{7}Be nucleus.

Combining these elements, the branching ratio for induced radiative break-up of

the ^{7}Be nucleus in the decay of X^- is,

$$P_{rad\ br} = \frac{1}{4\pi} \int_0^\infty |R(r)|^2 dr \int_{E_{thr}}^{E_{max}} \frac{2\alpha}{\pi} \ln\left(\frac{E_{thr}}{\omega}\right) \sigma_{rad}(\omega) \frac{d\omega}{\omega}, \tag{4.10}$$

where $R(r)$ is the radial wave function from Section 2.3. The maximum photon energy, E_{max}, is taken to be on the order of the X^- mass, $E_{max} \sim 100\,\mathrm{GeV}$, however the upper limit of the integral is rather inconsequential, as the integrand goes to zero for large ω. The only other dependence on E_{max} is logarithmic, so precision is not crucial.

The threshold energy and radiative break-up cross section are taken from Ref. [40]. For ^{7}Be break-up into ^{3}He + ^{4}He,

$$\begin{aligned} \sigma_{rad}^{helium} &= 0.504\,\mathrm{mb}\left(\frac{2371\,\mathrm{MeV}^2}{\omega^2}\right)\exp\left(\frac{-5.1909}{\sqrt{\mathrm{E_{cm}}}}\right)\times \\ &\quad \exp\left(-0.548E_{cm}\right)\left(1 - 0.428E_{cm}^2 + 0.534E_{cm}^3 - 0.115E_{cm}^4\right), \end{aligned} \tag{4.11}$$

with $E_{thr} = 1.586627\,\mathrm{MeV}$, and $E_{cm} \equiv \omega - E_{thr}$. ^{7}Be can also radiatively break up into p + ^{6}Li. From Ref. [40],

$$\sigma_{rad}^{lithium} = 32.6\,\mathrm{mb}\,\frac{\mathrm{E_{thr}^{10.0}\,E_{cm}^{2.0}}}{\omega^{12.0}} + 2.27\times10^6\,\mathrm{mb}\,\frac{\mathrm{E_{thr}^{8.8335}\,E_{cm}^{13.0}}}{\omega^{21.8335}}, \tag{4.12}$$

with $E_{thr} = 5.605794\,\mathrm{MeV}$, and again the definition $E_{cm} \equiv \omega - E_{thr}$ is used.

The radiative break-up cross sections were calculated by Ref. [40] from reverse reaction data, and are not necessarily good analytic forms for the cross sections at all photon energies. In particular, the $^7\mathrm{Be} \rightarrow {}^3\mathrm{He} + {}^4\mathrm{He}$ cross section goes negative at $\omega \approx 5.4\,\mathrm{MeV}$. For this analysis, the cross section was set to zero after this energy, so that the integral only goes up to the point where the cross section becomes negative. With these input data, and using the ^{7}Be wave function from Section 2.3, the probabilities of ^{7}Be break-up into ^{3}He + ^{4}He or p + ^{6}Li are,

$$P_{rad\ br}^{helium} = 1.0 \times 10^{-4}$$
$$P_{rad\ br}^{lithium} = 1.3 \times 10^{-4}. \tag{4.13}$$

Clearly, these results show that the radiative break-up of the recoiling ^{7}Be is rather inefficient. Since break-up occurs for fewer than 0.1% of the cases of X^- decay, it is concluded that the catalysis effects in this case are not important to cosmology.

4.2.2 ^{7}Be Break-up from Non-Thermal Ejection

If the X^- decays while within the bound state ($^7\mathrm{BeX}^-$), then the ^{7}Be nucleus can be suddenly ejected into the universe as a free particle. It gets a "kick" of kinetic energy from the decay, acquiring an energy on the order of the binding energy of the ($^7\mathrm{BeX}^-$) system. Since this energy ($\sim 1.3\,\mathrm{MeV}$) is greater than the temperature of the universe

($\sim 30\,\mathrm{keV}$), then the ^{7}Be enters the universe out of equilibrium. The photons and other particles in thermal equilibrium with the universe appear blue-shifted to the ^{7}Be. As such, it is important to re-evaluate nuclear and photon-induced processes that destroy ^{7}Be.[4] These processes were important to the evolution of the ^{7}Be abundance when the universe was much hotter (during Nucleosynthesis), but froze out long before ($^7BeX^-$) started to form. By giving a kick of kinetic energy to ^{7}Be, the X^- decay may be able to recreate the conditions for these reactions, because the universe will appear hotter to the ^{7}Be.

In analysing this mechanism, there are two effects playing off one another. The non-thermal ^{7}Be may interact either elastically or inelastically with the photons and other particles in the universe. Elastic collisions will cause the ^{7}Be to slow down and thermalize, while inelastic collisions will result in the break-up of ^{7}Be. If the ^{7}Be thermalizes before it has a chance to undergo inelastic collisions, then the decay of the X^- will have freed the ^{7}Be from the bound state, but it will not have changed ^{7}Be abundances relative to Standard BBN results.

It will be useful to first study the elastic processes in order to determine a time scale in which the ^{7}Be nucleus would be expected to thermalize, if it was ejected into the universe with energy on the order of an MeV.

[4]These are especially important if one wants to address the ^{7}Li problem, since any depletion of ^{7}Be will reduce the primordial ^{7}Li abundance as well. All the primordial ^{7}Be eventually ends up as ^{7}Li, so when one speaks of the primordial lithium abundance, the observable is actually $^7Li + {}^7Be$.

The primary thermalization modes to consider in the early universe are inverse Compton scattering with photons, hard-sphere scattering from protons, and Coulomb scattering off of electrons and positrons in the universe. According to the analysis of Ref. [41] (and verified by this author's own calculations), the thermalization is dominated by the Coulomb interactions with electrons and positrons. The cross section for the interaction of a particle of mass m with electrons is in general factor of $(m/T)^2$ larger than the cross section of the same particle with photons. As long as electrons and positrons are sufficiently abundant in the universe (which is the case until about $T < 0.05 m_{\rm e}$), then the Coulomb cross section will dominate the thermalization rate. In the case of the thermalization of ^{7}Be (at a mass of about 7 GeV) this suppression of the photon cross sections is significant when the universe at a temperature of about 30 keV.

Following the detailed analysis in the "Thermalization" Appendix of Ref. [41],[5] one finds that the ^{7}Be energy decays roughly exponentially in time, with dE/dt on the order of $10^6\,{\rm s}^{-1}$ at 30 keV. With this rate of thermalization, it takes an MeV-scale ^{7}Be nucleus less than 10^{-6} s to slow down to thermal temperatures. The thermalization is even faster if the X^- decays when the universe is hotter than 30 keV. Even at 25 keV,

[5]The electron number density, needed as input for the thermalization rate of Ref. [41], is not just the ambient number of electrons needed for charge neutrality of the universe, as pointed out by Ref. [42]. Rather, it is the combination of this number plus the number of e^+e^- pairs created out of the vacuum as a function of temperature. From Equation D4 in Appendix D of Ref. [42], one finds that the e^+e^- pairs are about 5 orders of magnitude more abundant than ambient electrons at the temperatures relevant for the (^{7}BeX^-) problem.

when the universe is more than 2100 s old, the ^{7}Be thermalizes in about 10^{-5} s.

It is clear that the time-scale of thermalization is very small. It takes only about 10^{-6} s for an MeV-energy ^{7}Be to come into equilibrium with the universe, at which time all processes will continue as per the usual Standard BBN evolution. Unless the enhanced inelastic destruction rates are very high, the CBBN effect of X^- decay inside the bound state (^{7}BeX^-) will not be substantial.

The two main inelastic processes that will cause ^{7}Be to break up are non-thermal photodisintegration, $^7\mathrm{Be} + \gamma \rightarrow {}^3\mathrm{He} + {}^4\mathrm{He}$, and proton-destruction, $^7\mathrm{Be} + \mathrm{p} \rightarrow {}^9\mathrm{B} + \gamma$. The photodisintegration cross section for ^{7}Be is taken from Ref. [40], and was given earlier as a function of photon energy ω in Equation 4.11. In order to convert the cross section into a rate of reaction, one must integrate the cross section over the thermal distribution of photons, given by the Planck distribution. The Planck distribution (see for example Refs. [36,37]) for the number of photons per unit volume at temperature T with energies between E_γ and $E_\gamma + dE_\gamma$ is,

$$dn_\gamma(T) = \left(\frac{1}{\pi}\right)^2 \frac{E_\gamma^2 \, dE_\gamma}{\exp\left(E_\gamma/T\right) - 1}. \tag{4.14}$$

Integrating the photodisintegration cross section over the Planck distribution of photons from the threshold energy to infinity gives the thermal photodisintegration rate

of ^{7}Be,

$$\Gamma_\gamma^{thermal} = \left(\frac{1}{\pi}\right)^2 \int_{E_{thr}}^{\infty} \frac{E_\gamma^2}{\exp\left(E_\gamma/T\right) - 1}\, \sigma_{rad}^{helium}(E_\gamma)\, dE_\gamma. \tag{4.15}$$

To account for the fact that the ^{7}Be is injected non-thermally into the universe, one can apply the Doppler formula to shift the effective energy of the photons. The cross section σ_{rad}^{helium} will become a function of the effective energy, while the thermal distribution remains the same. The lower limit of the integral will be reduced to the lowest energy of a thermal photon that can be Doppler shifted up to the threshold energy. The Doppler shift in photon energy for an "observer" traveling at a non-relativistic speed v is,

$$\omega_{eff} = \sqrt{\frac{1+v}{1-v}}\, \omega \;\equiv\; F_D\, \omega, \tag{4.16}$$

where F_D has been defined as the "Doppler Factor." Using this formula, the non-thermal photodisintegration rate for ^{7}Be injected into the universe at a non-relativistic speed v is,

$$\Gamma_\gamma^{non-thermal} = \left(\frac{1}{\pi}\right)^2 \int_{E_{thr}/F_D}^{\infty} \frac{E_\gamma^2}{\exp\left(E_\gamma/T\right) - 1}\, \sigma_{rad}^{helium}(F_D \cdot E_\gamma)\, dE_\gamma. \tag{4.17}$$

Using the cross section σ_{rad}^{helium} from Equation 4.11, one can evaluate the above integrals to find the thermal and non-thermal photodisintegration rates of ^{7}Be. An injection energy of 1.336 MeV was chosen, corresponding to a speed of $v/c \approx 0.02$.

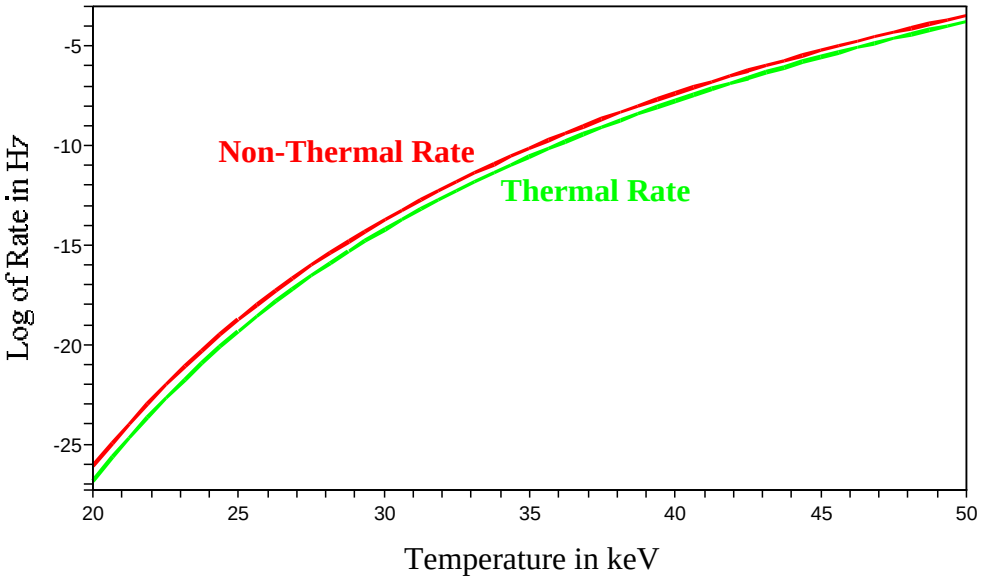

Figure 4.3: Thermal and non-thermal photodisintegration rates of ^{7}Be as a function of temperature in the universe. The thermal rate is the standard BBN rate, while the non-thermal rate arises due to the possibility of ^{7}Be being ejected at high energy after the decay of X^- inside the (^{7}BeX^-) system.

As shown in Figure 4.3, the enhanced non-thermal rate is indeed larger than the thermal rate. The enhancement is about a factor of 2 at 50 keV, increasing to a factor of about 5 at 20 keV. Although the energetic injection of ^{7}Be does indeed induce an enhancement of the photodisintegration rate over the thermal rate, it is not significant over the small time-scale of thermalization, 10^{-6} s. Even at 35 keV, the probability of break-up (given approximately by the rate of photodisintegration times the time for ^{7}Be to thermalize) is only about 10^{-16}, and above that temperature, the universe is still too hot to form (^{7}BeX^-) in the first place, as discussed in Section 3.4. Thus it is evident that this mechanism is inefficient at destroying ^{7}Be.

The other inelastic process to consider is proton-induced break-up, $^7\mathrm{Be} + \mathrm{p} \rightarrow {}^9\mathrm{B}$

$+ \gamma$. The cross section for this process as a function of centre-of-mass energy is taken from the NACRE collaboration database, Ref. [21]. It is more useful, however, to have the cross section as a function of the proton speed, $v_{\rm p}$, with the ^{7}Be injection energy as an additional input. As such, the cross section can be averaged over the thermal distribution of protons, and multiplied by the proton number density to give the rate. In order to make this conversion, first note that in the centre-of-mass system,

$$\begin{aligned} m_{\rm p}\, v'_{\rm p} &= m_{^7{\rm Be}}\, v'_{\rm Be} \\ v'_{\rm p} &= \frac{m_{^7{\rm Be}}}{m_{\rm p}}\, v'_{\rm Be}, \end{aligned} \tag{4.18}$$

and the centre-of-mass energy for non-relativistic protons and ^{7}Be is,

$$\begin{aligned} E_{COM} &= \frac{1}{2}\, m_{\rm p}\, {v'_{\rm p}}^2 + \frac{1}{2}\, m_{^7{\rm Be}}\, {v'_{\rm Be}}^2 \\ &= \frac{1}{2}\, \frac{m_{^7{\rm Be}}^2}{m_{\rm p}}\, {v'_{\rm Be}}^2 + \frac{1}{2}\, m_{^7{\rm Be}}\, {v'_{\rm Be}}^2 \\ &= \frac{1}{2}\, m_{^7{\rm Be}}\, {v'_{\rm Be}}^2 \left(1 + \frac{m_{^7{\rm Be}}}{m_{\rm p}}\right). \end{aligned} \tag{4.19}$$

The relative speed between the two particles approaching one another is $v_{\rm rel} = v'_{\rm Be} + v'_{\rm p}$ in the centre-of-mass system, and $v_{\rm rel} = v_{\rm Be} + v_{\rm p}$ in the thermal "universe frame." Setting these two equal, and noting that in the "universe frame," the speed of the ^{7}Be nucleus is $v_{\rm Be} = \sqrt{\frac{2I}{m_{^7{\rm Be}}}}$ when the ^{7}Be is injected into the universe with an energy

equal to the ionization energy, I, of the (^{7}BeX^-) system, then the thermal proton speed can be found.

$$\begin{aligned}
v_{\mathrm{Be}} + v_{\mathrm{p}} &= v'_{\mathrm{Be}} + v'_{\mathrm{p}} \\
\sqrt{\frac{2I}{m_{^7\mathrm{Be}}}} + v_{\mathrm{p}} &= v'_{\mathrm{Be}} + \frac{m_{^7\mathrm{Be}}}{m_{\mathrm{p}}}\, v'_{\mathrm{Be}} \\
v_{\mathrm{p}} &= v'_{\mathrm{Be}} \left(1 + \frac{m_{^7\mathrm{Be}}}{m_{\mathrm{p}}}\right) - \sqrt{\frac{2I}{m_{^7\mathrm{Be}}}} \\
v_{\mathrm{p}} &= \sqrt{\frac{2E_{COM}}{m_{^7\mathrm{Be}}}} \left(1 + \frac{m_{^7\mathrm{Be}}}{m_{\mathrm{p}}}\right)^{-1/2} \left(1 + \frac{m_{^7\mathrm{Be}}}{m_{\mathrm{p}}}\right) - \sqrt{\frac{2I}{m_{^7\mathrm{Be}}}} \\
v_{\mathrm{p}} &= \sqrt{\frac{2E_{COM}}{m_{^7\mathrm{Be}}}} \left(1 + \frac{m_{^7\mathrm{Be}}}{m_{\mathrm{p}}}\right)^{1/2} - \sqrt{\frac{2I}{m_{^7\mathrm{Be}}}}. \qquad (4.20)
\end{aligned}$$

With this relation, the cross section data from Ref. [21] is converted into a function of proton speed, rather than of centre-of-mass energy. Averaging this cross section over the Maxwell-Boltzmann Equation 3.31 for proton thermal speeds, and multiplying by the proton number density gives the rate of the proton-destruction. A numeric evaluation of the integrals gives a rate of about $1.4 \times 10^{-5}\,\mathrm{s}^{-1}$ at 30 keV, decreasing with decreasing temperatures to about $2.6 \times 10^{-6}\,\mathrm{s}^{-1}$ at 20 keV. So again, this rate is ineffective at destroying ^{7}Be on the timescale of thermalization.

The combined analysis of Section 4.2 shows that all mechanisms for the break-up of ^{7}Be following an X^- decay within the bound state (^{7}BeX^-) are ineffective. The decay of X^- therefore does *not* significantly deplete the ^{7}Be abundance, and as such

does not on its own alter the conclusions of BBN.

4.3 Impact of (^{7}BeX$^-$) in CBBN

Though the (^{7}BeX$^-$) system will not be considered further here, it remains important, as it may offer a solution to the Lithium Problem. In the preceding section, it was shown that the unstable nature of the X$^-$ inside the (^{7}BeX$^-$) system did not have noticeable effects on cosmology. The primary impact of the (^{7}BeX$^-$) system is therefore through catalyzed nuclear reactions with ^{7}Be, in which the reaction thresholds are reduced by the binding energy of the (^{7}BeX$^-$) system, as examined in detail in Ref. [2]. The main conclusions of this paper will be briefly summarized here.

In Ref. [2], it was found that both proton-destruction, $^7\mathrm{Be} + \mathrm{p} \rightarrow \gamma + {}^8\mathrm{B}$, and neutron-destruction, $^7\mathrm{Be} + \mathrm{n} \rightarrow {}^7\mathrm{Li} + \mathrm{p}$, of beryllium are enhanced due to catalysis effects of the (^{7}BeX$^-$) system. The proton-destruction reduces the abundance of ^{7}Be, and consequently also the primordial ^{7}Li abundance. Despite the fact that the neutron-destruction of ^{7}Be produces ^{7}Li, this reaction also acts to decrease the overall primordial abundance of ^{7}Li. This is because of the fact that ^{7}Li is significantly more fragile than ^{7}Be, so if ^{7}Be is converted into ^{7}Li too early (due to the catalysis effects), then it is quickly destroyed in the hot early universe. In a model with a neutral relic X^0 close in mass to the X$^-$, Ref. [2] also finds that the internal conversion process $^7\mathrm{Be} + \mathrm{X}^- \rightarrow {}^7\mathrm{Li} + \mathrm{X}^0$ is catalyzed. Similar to the neutron-destruction process, this

acts to reduce the overall predicted ^{7}Li primordial abundance. As the Standard BBN scenario predicts a ^{7}Li abundance that is a factor of about 2-3 times larger than the observed amount [6–10], these catalysis effects may help solve the discrepancy.

The rates of ^{7}Be destruction through catalyzed nuclear reactions depend on only two parameters in a simple model. In Ref. [2], these two parameters were chosen to be the initial abundance of X$^-$ and its lifetime, τ_{X^-}. It was found that with $Y_{\mathrm{X}^-} \gtrsim 0.02$ relative to baryons, and with the lifetime of X$^-$ in the range $1000\,\mathrm{s} \lesssim \tau_{\mathrm{X}^-} \leq 2000\,\mathrm{s}$, the Lithium Problem was solved, and the CBBN predictions were brought into agreement with experimental observations.[6]

Although the conclusions of Ref. [2] are extremely model-independent, two possible scenarios are suggested that could explain the existence of a heavy particle that is nonetheless long-lived. Either the couplings between the X$^-$ and its decay product are small, or the X$^-$ and its daughter may be nearly degenerate in mass. Either case would result in a long X$^-$ lifetime. The first scenario corresponds to the case of gravitino Dark Matter, where the X$^-$ is the NLSP (usually assumed to be the stau in these models) which decays into a gravitino LSP. In the second scenario, the small mass splitting between the X$^-$ and its daughter implies nearly degenerate LSP and NLSP. In this case, the LSP Dark Matter candidate would presumably be a neutralino.

The (^{7}BeX$^-$) system continues to be studied, and is of considerable interest to

[6]It will be shown in the following chapters that this is consistent with restrictions on the X$^-$ properties based on the catalyzed production of ^{6}Li through (^{4}HeX$^-$).

both particle physics and cosmology, because of the tantalizing possible solution that it offers to the Lithium Problem, and because of the fairly model-independent predictions that it can make of the properties of the relic X^-.

Chapter 5

The (^{4}HeX$^-$) System

The production of ^{6}Li through the interaction ^{2}H + ^{4}He $\rightarrow$ ^{6}Li + γ, is catalyzed by the (^{4}HeX$^-$) system. Since an upper limit on the primordial ^{6}Li abundance is fairly well established (observational limits vary within a factor of a few [40, 43]), this can be used as a limit on the catalyzed reaction, and therefore also on the properties of the X$^-$ particle. The (^{4}HeX$^-$) system is highly constrained by the ^{6}Li abundance, and as such, it a suitable system to study in order to deduce limits on the properties of the X$^-$. This has important implications to particle physics beyond the Standard Model, as the X$^-$ could represent one of the light SUSY particles. Since most of the analysis in this work is fairly model-independent (the primary assumptions being just the existence of a heavy, metastable charged particle), then the conclusions will hold for many different Beyond-the-Standard-Model scenarios.

5.1 The Abundance of (^{4}HeX$^-$)

In Section 3.1, the Boltzmann and Saha Equations were developed to give the abundance of a particle species in the early universe as a function of temperature. In Section 4.1, the Boltzmann Equation was used to study the (^{7}BeX$^-$) system, without a full demonstration of the differences between the Boltzmann Equation and the Saha Equation. The Saha Equation should be taken as an approximation to the Boltzmann Equation, as it assumes a rapid switch-on from fully ionized to fully bound states, whereas the Boltzmann Equation is a differential equation which takes into account the dynamic evolution of the states. The differences between the output of these two equations will be examined here for the (^{4}HeX$^-$) system.

The (^{4}HeX$^-$) system is somewhat easier to study than the (^{7}BeX$^-$) system, as it does not have many of the subtleties that are involved in the (^{7}BeX$^-$) case. For example, the photodisintegration cross section for (^{4}HeX$^-$) is well-represented by Equation 3.25, whereas the corresponding cross section for (^{7}BeX$^-$) was about 30% low, as discussed in Section 4.1.[1] Also, it is unnecessary to consider proton- and neutron-destruction channels or internal conversions as were required for the (^{7}BeX$^-$)

[1]The reason for the inaccuracy in the (^{7}BeX$^-$) case was due to the fact that the Bessel Function (Equation 3.19) was used to represent the free-particle wave function of ^{7}Be, assuming point-particle behaviour of the ^{7}Be. As seen in the comparison of the true and point-like *bound state* wave functions in Section 2.3, the (^{7}BeX$^-$) wave function deviates significantly from one which assumes point-particle behaviour. The (^{4}HeX$^-$) wave function, on the other hand, is not significantly different than the point-like wave function in the bound state, and one can safely approximate the *free* wave function as the Bessel function, 3.19.

system. Furthermore, ^{4}He is stable on its own, and is the second most abundant element in the universe, after Hydrogen. In what follows, the Boltzmann Equation will be used as the "true" indicator of the evolution of the (^{4}HeX$^-$) abundance, though solutions to the Saha Equation will also be presented for comparison.

Since ^{4}He is so abundant in the universe (the mass fraction of helium in the universe is about $\frac{1}{4}$ [16]), it would not be logical to study the fraction of ^{4}He locked into the bound state, as this fraction will always be much less than unity, assuming that the X$^-$ is less abundant than ^{4}He. Instead, it is better to study the fraction of X$^-$ that is locked into (^{4}HeX$^-$). Equations 3.13 and 3.14 are respectively the Saha and Boltzmann equations for the fraction F_{X^-} of X$^-$ particles locked into the bound state (NX$^-$), $F_{\mathrm{X}^-} \equiv n_{(\mathrm{NX}^-)}/n_{\mathrm{X}^-}$. Parameterized in this way, F_{X^-} does not depend on the overall abundance of X$^-$ in the universe, Y_{X^-}, but rather it depends on the abundance $Y_{^4\mathrm{He}}$ of *helium*, which is well known (see for example Refs. [4, 16]).

$$F_{\mathrm{X}^-}^{(Saha)} = \left(1 + \left(\frac{m_{^4\mathrm{He}} T}{2\pi}\right)^{3/2} e^{-I/T} n_{^4\mathrm{He}}^{-1}\right)^{-1} \tag{5.1}$$

$$-H\,T\,\frac{dF_{\mathrm{X}^-}^{(Boltz)}}{dT} = \langle\sigma_{\mathrm{rec}} v\rangle n_{^4\mathrm{He}} \left(1 - F_{\mathrm{X}^-}^{(Boltz)}\right) - \langle\sigma_{\mathrm{ph}}\rangle n_\gamma F_{\mathrm{X}^-}^{(Boltz)} \tag{5.2}$$

The Saha Equation 5.1 depends only on the mass of ^{4}He, $m_{^4\mathrm{He}} = 3727.379\,\mathrm{MeV}$ [23], and on the Ionization energy, $\mathrm{I} = 346\,\mathrm{keV}$ from Table 3.1. The Boltzmann Equation 5.2 also depends on the Hubble Rate, the recombination and photodisintegration

cross sections, and the number densities of ^{4}He and photons. The Hubble Rate H is given by Equation 3.8, and the photodisintegration cross section for (^{4}HeX$^-$) is given in Equation 3.25. The recombination cross section is one-to-one related to the photodisintegration cross section, through Equation 3.29, and the quantity $\langle \sigma_{\rm rec} v \rangle$ is obtained by averaging the recombination cross section over the thermal distribution of ^{4}He nuclei in the universe, as was done in Equation 3.32. These quantities are repeated below for ease of reference.

$$H(T) \approx 0.3798 \left(\frac{T}{\rm MeV} \right)^2 \ {\rm s}^{-1} \tag{5.3}$$

$$\sigma_{ph} \approx 0.118 \, {\rm barn} \, , \tag{5.4}$$

$$\langle \sigma_{\rm rec} v \rangle = \frac{4 \, I^2 \, \sigma_{\rm ph}}{\sqrt{2\pi} \ m_{^4{\rm He}}^{3/2}} \ T^{-1/2}. \tag{5.5}$$

The number density of photons as a function of temperature is simply the integral over the Planck distribution, Equation 3.27. With temperature T in MeV, this is $n_\gamma = 2.64 \times 10^{-8} T^3 \, {\rm fm}^{-3}$. The *mass fraction* of ^{4}He in the universe is about 0.248 [4], which can be converted to an abundance relative to baryons of $n_{^4{\rm He}}/n_{\rm B} \approx 0.06$, assuming that the universe is primarily composed of helium and hydrogen. The baryon density is $n_{\rm B} = \eta n_\gamma$, where the baryon-to-photon ratio, η, is defined by this equation. The WMAP 3-year data favours a value of $\eta = 6.116 \times 10^{-10}$ [4].

Using these quantities as input, numerical solutions are found to Equations 5.1 and 5.2 using the mathematical analysis program `Maple 9.5`. The solutions of the Boltzmann and Saha Equations in the limit of long X$^-$ lifetime are shown below in Figure 5.1, where the fraction of X$^-$ locked into bound state, $F_{\mathrm{X}^-} = n_{(^4\mathrm{HeX}^-)}/n_{\mathrm{X}^-}$, is plotted as a function of temperature, comparing the Boltzmann solution to the Saha approximation.

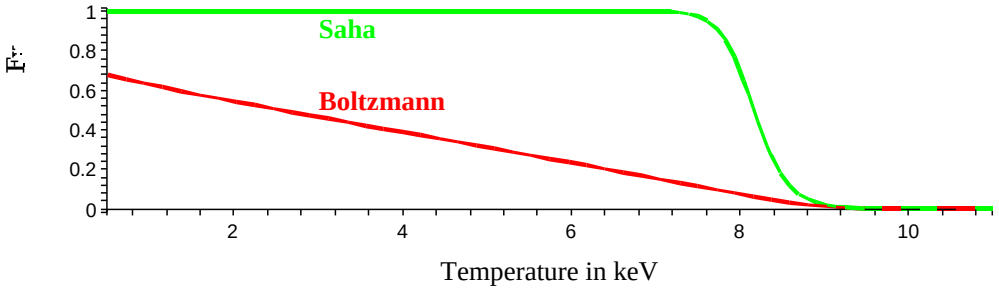

Figure 5.1: Fraction F_{X^-} of X$^-$ locked into (^{4}HeX$^-$) as a function of temperature in the limit of long X$^-$ lifetime. The numerical solution to the Boltzmann Equation is shown in red, with the Saha approximation to it shown in green.

Both the Boltzmann and the Saha expressions can be modified for a unstable X$^-$ by including a factor of $e^{-t/\tau_{\mathrm{X}^-}}$, where τ_{X^-} is the lifetime of the X$^-$. Converting t from units of time to units of temperature (using Equations 3.4 and 3.8) gives $e^{-1.316/T^2\tau_{\mathrm{X}^-}}$, where T is in MeV and τ_{X^-} is in seconds. The fraction of bound states relative to the *initial* X$^-$ density is therefore given by $F_{\mathrm{X}^-} \rightarrow F_{\mathrm{X}^-}e^{-1.316/T^2\tau_{\mathrm{X}^-}}$. In this case, F_{X^-} denotes $n_{(^4\mathrm{HeX}^-)}/n^{initial}_{\mathrm{X}^-}$, where $n^{initial}_{\mathrm{X}^-}$ is the initial X$^-$ number density in the universe before the X$^-$ began to decay, and $n_{(^4\mathrm{HeX}^-)}$ is the number density of bound (^{4}HeX$^-$) systems, which changes as a function of temperature.

A plot of $\log(F_{X^-})$ as a function of temperature for various X^- lifetimes is presented in Figure 5.2, comparing the Boltzmann and Saha solutions. Lifetimes of 1000 s, 2000 s, and 4000 s are plotted, as well as the limiting case of infinite lifetime.

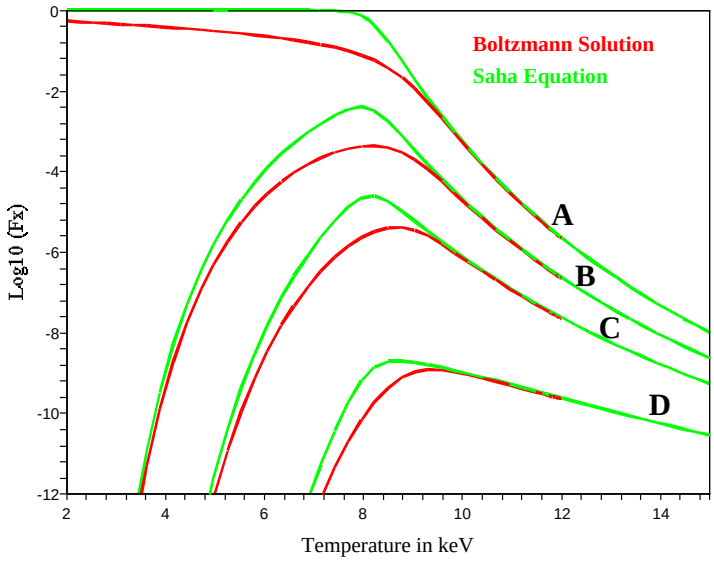

Figure 5.2: Fraction F_{X^-} of initial X^- locked into (^{4}HeX$^-$) as a function of temperature. The curves marked A represent infinite X^- lifetime. Curves B, C, and D represent τ_{X^-} of 4000 s, 2000 s, and 1000 s respectively. The numerical solutions to the Boltzmann Equation are shown in red, with the Saha approximations in green.

The difference between the output of the Boltzmann and Saha Equations is clear, even on the log-scale. The Boltzmann Equation represents the exact solution, however, in many recent publications analysing the CBBN mechanism [31–33], the Saha Equation has been used for analysis. The above plots show that this approximation is *not* a good one, and in this work, the full Boltzmann solution is employed for all results. As such, this work finds significant modifications to the final results of these

publications, as will be demonstrated in the following chapters.

5.2 Catalyzed Production of ^{6}Li

One of the primary reasons to study the (^{4}HeX$^-$) system is that it is highly constrained by the observed ^{6}Li abundance in the universe. As the catalyzed production of ^{6}Li depends on the properties of the X$^-$ (such as the abundance and lifetime), then this constraint will help to put limits on the properties of the X$^-$.

In standard cosmology, ^{4}He combines with a deuteron to form ^{6}Li through the process $^4\mathrm{He} + {}^2\mathrm{H} \rightarrow {}^6\mathrm{Li} + \gamma$. This is the primary SBBN process for the formation of ^{6}Li, and is represented by the Feynman Diagram, Figure 5.3.

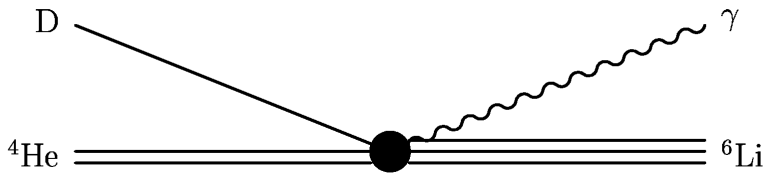

Figure 5.3: Feynman diagram for the standard BBN production of ^{6}Li from ^{4}He and a deuteron.

The NACRE database [21] gives the rate for this formation reaction in astrophysical units, $N_A^{-1}\mathrm{cm}^3\mathrm{s}^{-1}\mathrm{mol}^{-1}$, where N_A is Avagadro's number. This is converted to normal units, s^{-1}, by multiplying by N_A, the number density of ^{4}He, and the abundance of deuterons. From the discussion in the paragraph following Equation 5.5, the number density of ^{4}He is $n_{^4\mathrm{He}} \approx 1.01 \times 10^{-18} T^3\,\mathrm{fm}^{-3}$, where T is in MeV. In the

study of ^{6}Li, all abundances are chosen to be relative to *hydrogen*, as this is the usual way that they are reported in the literature. From Ref. [4], the deuteron abundance relative to hydrogen is $Y_{\rm D} = 2.57 \times 10^{-5}$. Combining these factors, the SBBN rate of ^{6}Li formation in units of s^{-1} is,

$$\begin{aligned} \Gamma_{SBBN}^{form} &= 1.24 \times 10^{-7} T^{7/3} \left(1.00 + 76.26T + 10.23T^2 + 38.76T^3\right) e^{-3.284/T^{1/3}} + \\ & \quad 6.94 \times 10^{-7} T^{7/3} e^{-0.6811/T}. \end{aligned} \tag{5.6}$$

This SBBN rate is "accidentally" suppressed because of the fact that the reaction must proceed through the E2 channel. The E1 amplitude vanishes because of an almost identical charge-to-mass ratio of the deuteron and ^{4}He. In the E2 transition, the cross section scales with the inverse 5^{th} power of the photon wavelength (see for example Ref. [34]). Assuming that the photon energy is on the order of 1 MeV, consistent with the temperature of the universe during standard BBN (see discussion in Section 2.1), then the wavelength is about $\lambda_{SBBN} \sim 200$ fm.

In CBBN, the formation of ^{6}Li is catalyzed by the presence of the bound state (^{4}HeX$^-$). The formation of ^{6}Li can proceed through the catalyzed photonless channel (^{4}HeX$^-$) + ^{2}H $\rightarrow$ ^{6}Li + X$^-$, as shown in the Feynman diagram, Figure 5.4. In this reaction, the real photon from the SBBN process is replaced by a virtual photon, whose wavelength is on the order of the length-scales of the (^{4}HeX$^-$) system. Choosing

$\lambda_{CBBN} \sim a_B = 3.63\,\text{fm}$ (from the Bohr radius of the system given in Table 2.1), then an enhancement could be expected of the CBBN process over the SBBN process by a factor on the order of $(\lambda_{CBBN}/\lambda_{SBBN})^{-5} \approx 5 \times 10^8$. This is a tremendous increase!

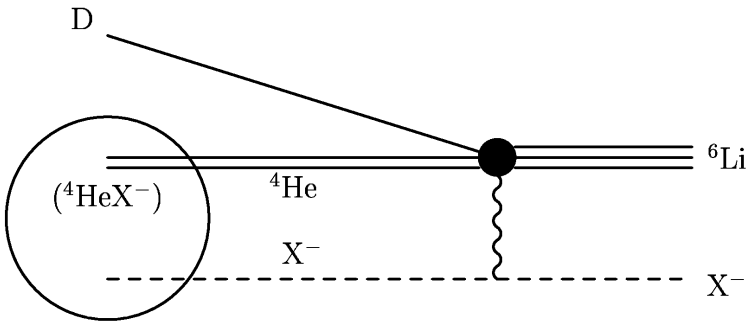

Figure 5.4: Feynman diagram for the CBBN catalyzed production of ^{6}Li.

It remains now only to find a rate for this catalyzed reaction. In Ref. [1], this rate was estimated by modifying the SBBN E2 rate to include the Coulomb field of the X^-. This estimate relies on the approximation of nuclear distances being much smaller than the Bohr radius. As shown in Chapter 2, this estimate may not always hold, especially for larger nuclei. A subsequent 3-body calculation of the Schrödinger Equation by Ref. [31] was able to improve upon the estimate.

In this work, the full 3-body solution from Ref. [31] will be used for the rate of the CBBN production of ^{6}Li. From Equation 4.3 of Ref. [31], the thermally averaged cross section for the CBBN process (converted into the units used here) is,

$$\langle \sigma v \rangle = 7.68 \times 10^{22} T^{-2/3} (1 - 3.95T) e^{-2.354/T^{1/3}} \text{fm}^3 \text{s}^{-1}. \tag{5.7}$$

To get the rate of reaction for the CBBN case, the above cross section must be multiplied by the number density of bound (^{4}HeX$^-$) and the abundance of deuterons relative to hydrogen. The later was already found to be $Y_{\rm D} = 2.57 \times 10^{-5}$. The number density of (^{4}HeX$^-$) is $n_{(^4{\rm HeX}^-)} = \left(\frac{n_{(^4{\rm HeX}^-)}}{n_{\rm X^-}}\right) n_{\rm X^-} = \left(\frac{n_{(^4{\rm HeX}^-)}}{n_{\rm X^-}}\right) Y_{\rm X^-} n_{\rm B}$, where $Y_{\rm X^-}$ is the abundance of X$^-$ relative to baryons. In the case of unstable X$^-$, $Y_{\rm X^-} \rightarrow Y_{\rm X^-} e^{-1.316/T^2 \tau_{\rm X^-}}$, where T is in MeV, $\tau_{\rm X^-}$ is in seconds, and $Y_{\rm X^-}$ now represents the *initial* X$^-$ abundance. The CBBN rate of formation of ^{6}Li in units of s^{-1} is therefore,

$$\Gamma^{form}_{CBBN} = 31.83 T^{7/3} F_{\rm X^-}(T) Y_{\rm X^-} e^{-1.316/T^2 \tau_{\rm X^-}} (1 - 3.95T) e^{-2.354/T^{1/3}}. \qquad (5.8)$$

where $F_{\rm X^-} = \left(\frac{n_{(^4{\rm HeX}^-)}}{n_{\rm X^-}}\right)$ is the fraction of X$^-$ locked into the bound state (^{4}HeX$^-$), and can be taken from the numerical results of Section 5.1. Incidentally, the CBBN creation of ^{6}Li is another *destruction* mechanism for (^{4}HeX$^-$). When this channel is included in the Boltzmann Equation for the evolution of (^{4}HeX$^-$), the results do not differ from those given in Section 5.1, since this rate is small compared to the other mechanisms considered there.

When analysing the evolution of ^{6}Li, the *destruction* mechanisms of ^{6}Li must be considered as well as those of production. The primary mechanism for destroying ^{6}Li is ^{6}Li + p $\rightarrow$ ^{3}He + ^{4}He [21]. The NACRE database rate is converted into the units used here by multiplying by the appropriate conversion factors as described

above, and by the number density of protons and the abundance of ^{6}Li. Assuming that the mass fraction of protons in the universe is 1 minus the mass fraction of ^{4}He, one finds that the proton density is $n_{\rm p} \approx 1.21 \times 10^{-17} T^3\,{\rm fm}^{-3}$, where T is in MeV. The abundance of ^{6}Li relative to protons, $Y_{^6{\rm Li}}$, is left as a variable. Combining these factors, the destruction rate of ^{6}Li in units of s^{-1} is,

$$\Gamma^{dest} = 1.39 \times 10^8 T^{7/3}\, Y_{^6{\rm Li}}\, (1 - 1.59T + 3.25T^2 - 2.00T^3) e^{-3.717/T^{1/3}}. \tag{5.9}$$

Now that the primary creation and destruction mechanisms of ^{6}Li are accounted for, the evolution of the abundance of ^{6}Li both with and without the CBBN contribution can be studied. The preferred method of analysis is again to use the Boltzmann Equation, which sets the rate of change of the abundance of ^{6}Li equal to the difference in rates of creation mechanisms minus destruction mechanisms. The evolution of the abundance of ^{6}Li relative to protons is therefore governed by the following equation,

$$\frac{dY_{^6{\rm Li}}}{dt} = -H(T)\,T\,\frac{dY_{^6{\rm Li}}}{dT} = \Gamma^{form}_{SBBN} + \Gamma^{form}_{CBBN} - \Gamma^{dest}. \tag{5.10}$$

The Hubble rate, $H(T)$, is given in Equation 3.8, and the other rates in this equation were all developed in this section. Since Γ^{dest} is proportional to $Y_{^6{\rm Li}}$, this differential equation is non-trivial and must be solved numerically. It is also important to recall that Γ^{form}_{CBBN} depends on both the initial X^- abundance relative to baryons Y_{X^-},

as well as the X^- lifetime τ_{X^-}. These two quantities are taken as input parameters which must be chosen and inserted into the equation "by hand." Γ^{form}_{CBBN} also depends on F_{X^-}, the fraction of X^- locked in to the bound state ($^4HeX^-$) as a function of temperature. This quantity is given by the numerical solution to the differential equation (Equation 5.2) that was developed in Section 5.1. As such, to study the ^{6}Li evolution, one must solve a system of two coupled differential equations. In this analysis, the software package `Maple 10` was used for this purpose.

The solution to Equation 5.10 gives the CBBN prediction for the ^{6}Li abundance as a function of temperature with two input parameters, the lifetime and the initial abundance of the X^-. The SBBN prediction is obtained by setting Y_{X^-} to zero in Γ^{form}_{CBBN}, and solving the reduced Equation 5.10.

In previous work on this topic, a satisfactory solution for the evolution of $Y_{^6Li}$ has not been found. In Ref. [1], the CBBN rate of formation for ^{6}Li was inaccurate due to oversimplified approximations, as explained earlier in this section. Although Ref. [31] corrected this problem, there were other oversights made in their analysis. Instead of solving the system of coupled differential equations given by the Boltzmann Equations 5.2 and 5.10, a modified version of Equation 5.10 was used, neglecting both the SBBN creation rate and the destruction rate. They claim (correctly) that these rates are small at the time of CBBN reactions, so this approximation on its own is reasonable. The detrimental simplification that both they and Ref. [32] make is in

using the Saha approximation, Equation 5.1 (modified for an unstable X^-) for the abundance of ($^4HeX^-$), instead of using the full Boltzmann solution. This causes a significant discrepancy.

In this work, the full Boltzmann solution to the coupled Equations 5.2 and 5.10 was found numerically using the `Maple 10` software, and a plot of $Y_{^6Li} = {}^6Li/H$ is given in Figure 5.5 for two values of Y_{X^-}, in the limit of long X^- lifetime.

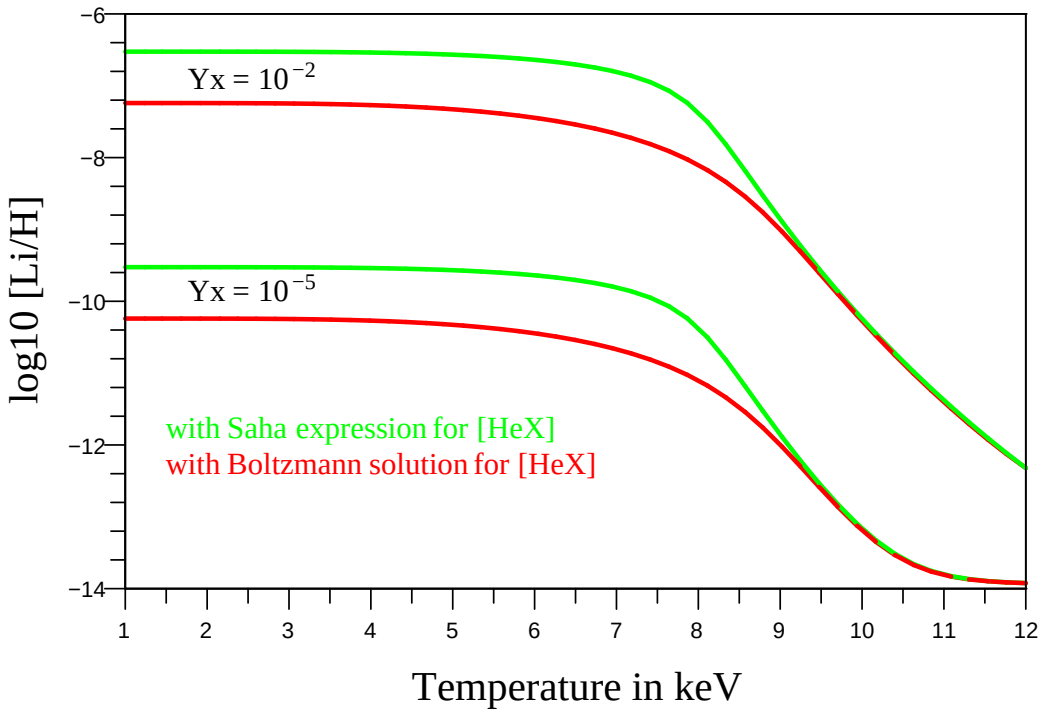

Figure 5.5: Evolution of the ^{6}Li abundance comparing Boltzmann and Saha solutions for two different values of Y_{X^-} in the limit of long X^- lifetime.

The $Y_{^6Li}$ approximation using the Saha abundance for ($^4HeX^-$) was also calculated, and solutions for two values of Y_{X^-} are shown in green on Figure 5.5 in

comparison to the Boltzmann solutions for the same Y_{X^-}. Clearly, the Saha solution is unsatisfactory, as there is a discrepancy of almost a factor of ten at low temperature in the estimation of the primordial ^{6}Li abundance. It has now been clearly shown in several different situations that the Saha Equation is not appropriate for the accurate study of the systems in the CBBN theory. The Saha solutions will no longer be considered, and the rest of the results in this work are all derived from the Boltzmann Equation.

Taking the ^{6}Li abundance at $T = 1\,\mathrm{keV}$ as the "primordial" value, the following result is obtained in the limit of long X^- lifetime,

$$Y_{^6\mathrm{Li}} = \left(\frac{n_{^6\mathrm{Li}}}{n_\mathrm{p}}\right) = 5.73 \times 10^{-6} Y_{X^-}, \tag{5.11}$$

where Y_{X^-} is the abundance of X^- relative to baryons.

The effects of finite X^- lifetime are shown in Figure 5.6, where the CBBN predictions of the ^{6}Li abundance are plotted as a function of temperature for two values of Y_{X^-}. The limit of long X^- lifetime and the case where $\tau_{X^-} = 10^4\,\mathrm{s}$ are both shown in each of the two Y_{X^-} scenarios. In addition, the SBBN prediction from Equation 5.10 with $Y_{X^-} = 0$ is also shown for comparison.

It is clear from Figure 5.6 that the prediction of the primordial abundance of ^{6}Li can be increased by up to 7 orders of magnitude relative to the SBBN results,

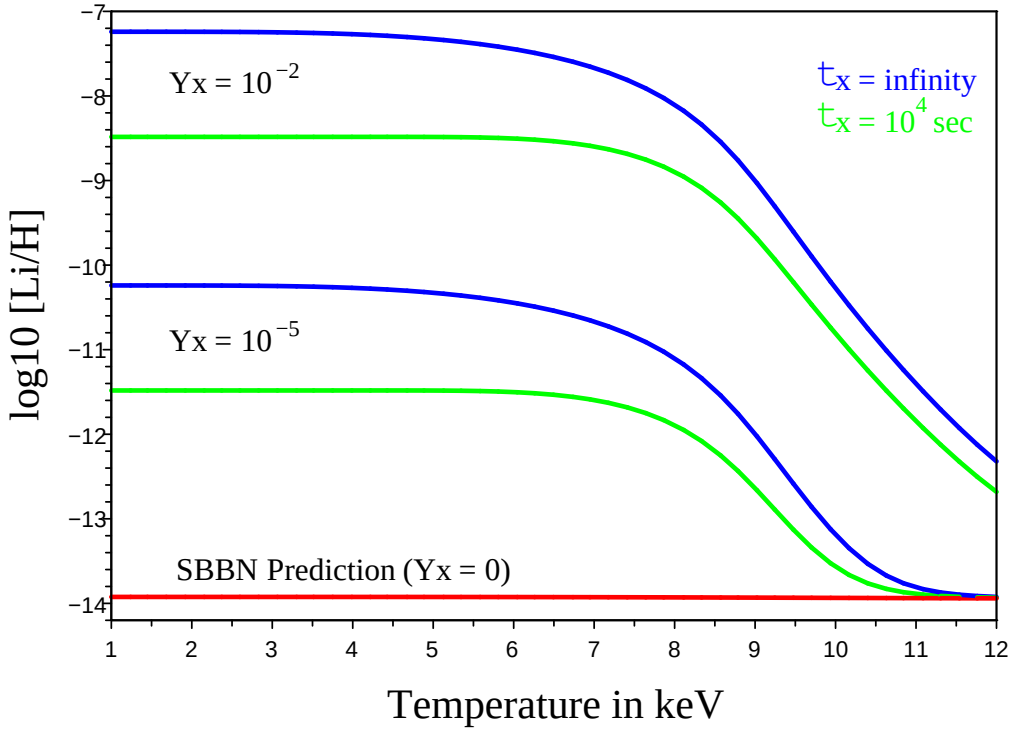

Figure 5.6: Evolution of the CBBN and SBBN predictions of the ^{6}Li abundance for two different values of Y_{X^-}. The CBBN solutions in the limit of long X^- lifetime are shown in blue, while the green curves show the CBBN solutions for $\tau_{X^-} = 10^4$ s. In red is the SBBN prediction.

depending on the values of the parameters chosen for the X^- properties. This is a significant enhancement, and since the CBBN predictions are so sensitive to the properties of the X^-, the observed ^{6}Li abundance in the universe will able to put a stringent constraint on these properties, as discussed in the following chapter.

Chapter 6

Using ^{6}Li Limits to Constrain the Properties of X^-

In the previous chapter, it was shown that the primordial abundance of ^{6}Li depends strongly on the properties (namely the abundance and the lifetime) of the X^- particle, due to catalysis processes involving the ($^4HeX^-$) system. In this chapter, this dependence will be exploited in order to constrain the properties of the X^- based on the observed ^{6}Li abundance. Section 6.1 remains model-independent, but subsequent sections are forced to make further assumptions as to the identity of the X^-. The cases of a Dirac Fermion and a Scalar particle are considered in Sections 6.2 and 6.3 respectively, and constraints on the mass, lifetime, and abundance of the X^- are developed for each of these two scenarios.

6.1 Constraining Y_{X^-} as a Function of τ_{X^-}

As shown in Section 5.2, one can find the ^{6}Li abundance as a function of temperature given the lifetime and abundance of the X^- as input. It is evident from Figures 5.5 and 5.6 that the predicted ^{6}Li abundance is relatively constant for temperatures lower than about 5 keV, so in this work the abundance at 1 keV is considered to be the "primordial" value.

For a given X^- lifetime, it is possible to find the value of Y_{X^-} that gives a specific primordial value of ^{6}Li, by scanning over the parameter space of X^- abundance. Setting a primordial value of ^{6}Li (presumably from observational data), one can therefore generate a plot of Y_{X^-} versus τ_{X^-}, by finding the value of Y_{X^-} for various τ_{X^-} that gives the correct primordial abundance.

Unfortunately, observational data on primordial ^{6}Li is not very precise, and there is some disagreement in the community as to how it should be reported (see Refs. [40] and [43] and references therein). Generally, ^{6}Li is measured in low-metalicity halo stars, but this abundance may not accurately represent the *primordial* abundance, as ^{6}Li is produced by cosmic ray spallation, and also by α-α interactions in the interstellar medium. ^{6}Li may also suffer depletion in stars due to nuclear burning (more so than ^{7}Li, as it is more fragile). Furthermore, many of the ^{6}Li abundance measurements rely on the ^{7}Li abundance, and as discussed in Chapter 4 there is significant discrepancy about this quantity.

Ref. [40] concludes that a "safe" 2-σ upper limit on the observational ^{6}Li primordial abundance relative to hydrogen is $Y_{^6\mathrm{Li}} \lesssim 2\times10^{-11}$. Ref. [43] sets a "conservative" range for the ^{6}Li abundance (again relative to hydrogen) of $Y_{^6\mathrm{Li}} = \left(1.10^{+5.00}_{-0.92}\right)\times10^{-11}$, where the errors are at the 2-σ level. This corresponds to an upper limit of $Y_{^6\mathrm{Li}} \lesssim 6.1\times10^{-11}$. When analysing the (^{4}HeX$^-$) system, Ref. [1] used the first limit to set X$^-$ constraints, while Ref. [31] used the second.

In this analysis, the value of Y_{X^-} that gives a specified primordial $Y_{^6\mathrm{Li}}$ value is found as a function of X$^-$ lifetime for various ^{6}Li exclusion limits. Plots of Y_{X^-} versus τ_{X^-} are generated for the two upper limits mentioned above, as well as for several other values of $Y_{^6\mathrm{Li}}$ ranging from 10^{-13} to 10^{-9} to account for any possible systematic errors in the observed ^{6}Li abundance. The (τ_{X^-}, Y_{X^-}) phase space with various $Y_{^6\mathrm{Li}}$ limits is shown in Figure 6.1. For a given $Y_{^6\mathrm{Li}}$, the phase space above the curve is excluded.

Now, clearly it would be useful to be able to define a "natural" range for the abundance Y_{X^-} in order to further constrain the lifetime of the X$^-$ particle. Not only can this be done, but in fact, even better can be achieved with minimal assumptions. Assuming that X$^+$ (the antiparticle to the X$^-$) is equally as abundant as the X$^-$, and also that X$^-$ and X$^+$ annihilate through the s-channel into two photons, then the abundance Y_{X^-} is one-to-one related to the mass of the X$^-$ (see for example Ref. [16]).

The s-channel annihilation of X$^-$ and X$^+$ into two photons, X$^-$ + X$^+$ $\rightarrow \gamma\gamma$,

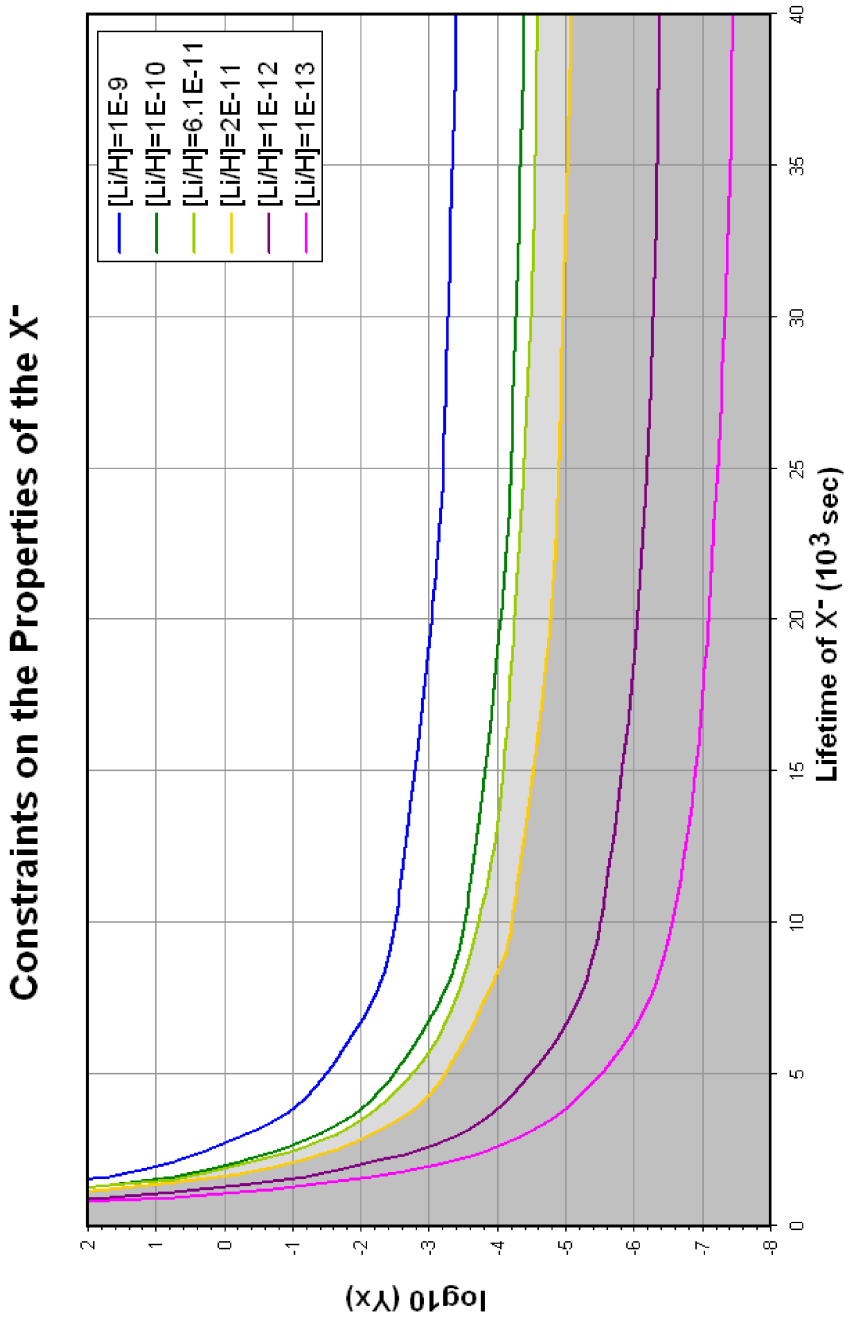

Figure 6.1: The (τ_{X^-}, Y_{X^-}) phase space with ^{6}Li constraints. For a given $Y_{^6\mathrm{Li}}$, the phase space *below* the curve is *allowed*. The dark grey region is allowed by the 2-σ observational limit $Y_{^6\mathrm{Li}} \lesssim 2 \times 10^{-11}$ from Ref. [40], and the light grey region is allowed by the 2-σ observational limit $Y_{^6\mathrm{Li}} \lesssim 6.1 \times 10^{-11}$ from Ref. [43].

is represented by the Feynman diagram in Figure 6.2. Assuming this annihilation mechanism, the abundance of the X^- is approximately proportional to its mass (see for example Refs. [16, 44]).

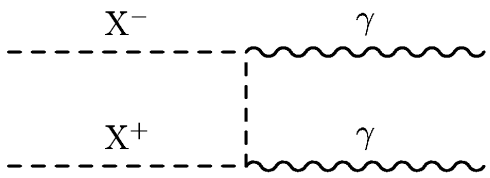

Figure 6.2: Feynman diagram for the annihilation of X^- and X^+ into photons.

Following the standard calculations for relic abundance (see for example Ref. [16]), let $x \equiv m/T$, where m is the mass of the relic particle (in this case denoting m_{X^-}), and T is the temperature. Since the universe is at a temperature of $T \approx 10\,\mathrm{keV}$ at the time of formation of ($^4\mathrm{HeX}^-$) (as shown by Figures 5.1 and 5.2), then $T \ll m_{X^-}$, or $x \gg 1$, and the X^- particle is non-relativistic. On theoretical grounds, one expects the annihilation cross section to have velocity dependence $\sigma_A|v| \propto v^{2l}$, where $l = 0$ corresponds to s-channel annihilation, $l = 1$ corresponds to p-channel, etc. Since temperature is a measure of kinetic energy, then $\langle v \rangle \sim T^{1/2}$, and one expects the thermally averaged annihilation cross section to scale like $\langle \sigma_A v \rangle \propto T^l$.[1] In terms of the parameter x, this reduces to $\langle \sigma_A v \rangle = \sigma_0 x^{-l}$. Since $x \sim \mathcal{O}(10^7)$ for a $100\,\mathrm{GeV}$ particle X^-, only the $l = 0$ s-channel annihilation is considered here.

[1]Note that if σ_A is inversely proportional to the speed v (as is the case for s-channel scattering [45]), then in the thermally averaged cross section for $m \gg T$, the integral over the Boltzmann distribution is unity and, $\langle \sigma_A v \rangle \approx \sigma_A v \equiv \sigma_0$.

In order to derive the mass-dependence of the X^- abundance, one must first define the freeze-out temperature, T_F, at which all the X^- species interaction rates fall below the Hubble Rate. For temperatures less than its freeze-out temperature, the abundance of a stable particle will remain relatively constant [16]. From Refs. [16] and [44], the x parameter at freeze-out is,

$$x_F = m/T_F \simeq \ln[(l+1)a\lambda] - (l+1/2)\ln(\ln[(l+1)a\lambda]), \tag{6.1}$$

where,

$$a = \left(45/2\pi^4\right)(\pi/8)^{1/2}(g/g_{*S}) \approx 0.145\,(g/g_{*S}), \tag{6.2}$$

and, measuring σ_0 in units of inverse mass squared,

$$\lambda = 0.264\left(g_{*S}/g_*^{1/2}\right) M_{\rm Pl}\, m\, \sigma_0. \tag{6.3}$$

In Equation 6.3, $M_{\rm Pl}$ is the Planck Mass, $M_{\rm Pl} = 1.22 \times 10^{19}\,{\rm GeV}$. Using these definitions, the initial abundance of a species (before it begins to decay) is [16, 44],

$$\begin{aligned} Y_{initial} &= \frac{(l+1)}{\lambda}\, x_F^{l+1} \\ &= \frac{3.79\,(l+1)\,x_F^{l+1}}{\left(g_{*S}/g_*^{1/2}\right) M_{\rm Pl}\, m\, \sigma_0}, \end{aligned} \tag{6.4}$$

where this abundance is measured relative to the entropy, s, of the universe [16],

$$\begin{aligned} s &= \frac{2\pi^2}{45} g_{*S} T^3 \\ &= \frac{1.8 g_{*S}}{\eta} n_{\mathrm{B}}. \end{aligned} \tag{6.5}$$

In this equation, η is the baryon-to-photon ratio, $\eta = 6.116 \times 10^{-10}$ [4], and n_{B} is the baryon number density. The quantity g_* was initially defined in Equation 3.6,

$$g_* = \left(\sum_B g_B \left(\frac{T_B}{T} \right)^4 + \frac{7}{8} \sum_F g_F \left(\frac{T_F}{T} \right)^4 \right), \tag{6.6}$$

where B and F are the bosons and fermions with masses much less than the temperature T of the universe. The quantity g_{*S} is similarly defined [16],

$$g_{*S} = \left(\sum_B g_B \left(\frac{T_B}{T} \right)^3 + \frac{7}{8} \sum_F g_F \left(\frac{T_F}{T} \right)^3 \right). \tag{6.7}$$

The degrees-of-freedom variables g_* and g_{*S} must be evaluated at the freezeout temperature, T_F. As an estimate, this is typically around 5% of the particle mass. Assuming that the X^- has a mass larger than about 100 GeV, then the freezeout temperature is larger than about 5 GeV. At this temperature, all particle species are in equilibrium with the universe, and all the temperature parameters in Equations 6.6 and 6.7 are equal, $T_i = T$. In this limit, g_* and g_{*S} also become identical.

Using the step-function put forth by Ref. [30], $g_* = g_{*S} = 86.25$ in the temperature range $m_{\mathrm{bottom}} < T < m_{\mathrm{W,Z}}$, which corresponds to about $4\,\mathrm{GeV} < T < 80\,\mathrm{GeV}$.

Setting $l = 0$, the abundance $Y_{initial}$ relative to entropy can therefore be calculated as a function of mass. The only further input required is g, the number of degrees of freedom of the X^- particle, and $\sigma_0 = \sigma_A v$, from the s-channel annihilation cross section.

$$x_F \approx \ln[0.00412 g M_{\mathrm{Pl}}\, m\, \sigma_0] - 1/2 \ln(\ln[0.00412 g M_{\mathrm{Pl}}\, m\, \sigma_0]) \tag{6.8}$$

$$Y_{initial} \approx \frac{3.79\, x_F}{M_{\mathrm{Pl}}\, m\, \sigma_0}, \tag{6.9}$$

Since σ_0 scales with m^{-2} (even just from a dimensional argument), then $Y_{initial}$ is approximately proportional to m, except for a logarithmic dependence through x_F.

To this point, all the calculations have been fairly model-independent, the only assumption required being the existence of a heavy metastable charged particle. To proceed further with Equation 6.4, however, one needs to make some further assumptions as to the identity and properties of the X^-. Two basic cases are considered below. Section 6.2 studies the case where X^- is a spin-1/2 particle. Since the X^- is charged, this means that it is a *Dirac* Fermion. In Section 6.3, the case of a Scalar X^- is investigated. This case is of particular interest in SUSY models, as many SUSY scenarios include a charged scalar particle at about 100 GeV. For many of the constraints made in Section 6.3, the X^- assumes the identity of the stau, $\tilde{\tau}$, which is the

superpartner to the tau lepton.

6.2 Constraints on an X^- Dirac Fermion

The case of X^- X^+ annihilation in which the X particles are Dirac Fermions can be treated analogously to the well-studied e^- e^+ annihilation, as the only difference from a particle physics point of view is the masses. As a spin-1/2 fermion, the X^- particle has two spin degrees of freedom (spin "up" and spin "down"), so $g = 2$. The s-channel annihilation cross section can be taken analogously from the electron-positron annihilation cross section [45],

$$\begin{aligned} \sigma_A &= \frac{4\pi}{v}\left(\frac{\alpha}{m}\right)^2 \\ \sigma_0 &\approx 6.69 \times 10^{-4}\ m^{-2}. \end{aligned} \tag{6.10}$$

Measuring m in units of 100 GeV ($m \equiv m_{X^-}/100\,\mathrm{GeV}$), the freeze-out parameter is,

$$\begin{aligned} x_F &= \ln\left[\frac{6.73 \times 10^{11}}{m}\right] - 1/2 \ln\left(\ln\left[\frac{6.73 \times 10^{11}}{m}\right]\right) \\ &\approx 25.58 - \ln(m), \end{aligned} \tag{6.11}$$

where the approximation holds if m_{X^-} is not significantly different from 100 GeV.

The initial abundance of X^- from Equation 6.9 is,

$$Y_{initial} = 4.64 \times 10^{-14}\, m\, (25.58 - \ln(m))\,. \tag{6.12}$$

Equation 6.5 can be used to convert the above abundance (which is measured relative to entropy) into an abundance relative to baryons. At the temperatures relevant for CBBN, $g_{*S} \approx 3.91$, and one finds,

$$Y_{\mathrm{X}^-} = 5.34 \times 10^{-4} \left(\frac{m_{\mathrm{X}^-}}{100\,\mathrm{GeV}}\right)\left(25.58 - \ln\left(\frac{m_{\mathrm{X}^-}}{100\,\mathrm{GeV}}\right)\right). \tag{6.13}$$

With this relationship between abundance and mass, the analysis of Section 6.1 can now be used to constrain both the abundance *and* the mass of the X^- as a function of the lifetime τ_{X^-}. A mass axis can therefore be added to Figure 6.1 to generate Figure 6.3, a plot of the ^{6}Li constraints imposed on the (τ_{X^-}, m_{X^-}) plane. This alone does not help to constrain the allowed parameter space, but now experimental and theoretical limits on the *mass* of the X^- can be used to reduce the allowed parameter space, whereas there is not much known *a priori* about the abundance.

Direct detector searches (for example at LEP and at the Tevatron) were able to put a lower limit of $m > 85.2\,\mathrm{GeV}$ [3] on the existence of any charged exotic particle (see also the discussion in the footnote on Page 13), while the spin-1/2 chargino limit is slightly more strict, $m > 94\,\mathrm{GeV}$ [3]. In Figure 6.3, the more conservative

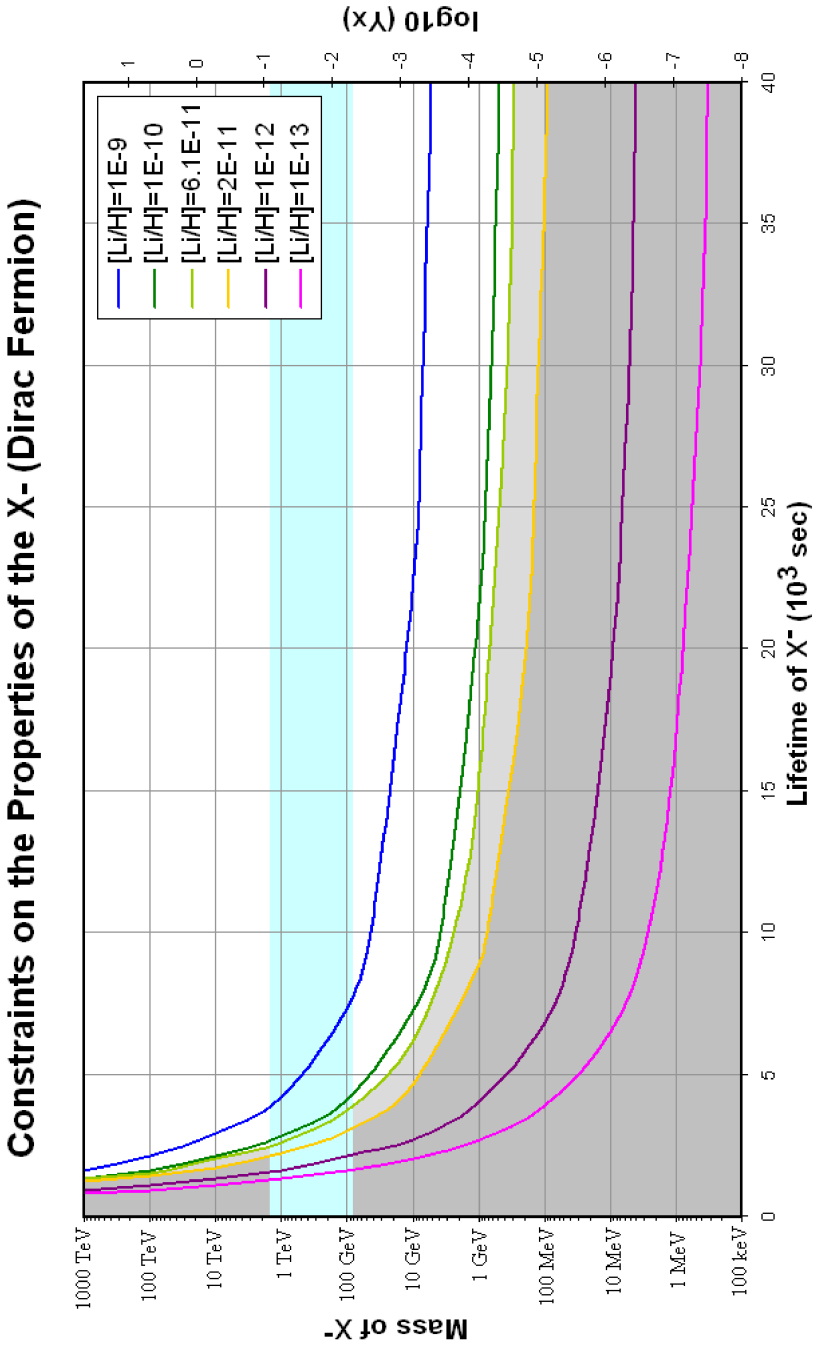

Figure 6.3: The (m_{X^-}, Y_{X^-}) phase space for an X$^-$ Dirac Fermion, with ^{6}Li constraints as in Figure 6.1. The light blue band corresponds to the probable mass range. The lower limit of 85.2 GeV comes from direct detector searches, while the upper limit of 1.5 TeV is the "natural" heavy limit in most SUSY models.

$m_{X^-} > 85.2\,\text{GeV}$ is used as a lower limit. The "natural" upper limit on the mass of any particle from a theory intending to help solve the gauge hierarchy problem should be on the order of the electroweak symmetry breaking scale, about 1 TeV (see for example Ref. [40] and references therein). Most theoretical models of Supersymmetry don't consider chargino masses above about 1.5 TeV (for example, Refs. [46–48]), so this is used as an indicative upper bound on the X^- fermion mass in order to constrain the phase space.

In Figure 6.3, the overlap between the light blue region and the grey regions is the probable phase space for the X^- properties. Although the upper bound on the ^{6}Li abundance should be enforced, a *lower* limit on the primordial ^{6}Li abundance is harder to determine. As a speculative lower limit, the 2-σ lower bound of 1.8×10^{-12} from Ref. [43] could be used. To err on the side of caution, the dark purple constraint on Figure 6.3 ($Y_{^6\text{Li}} = 10^{-12}$) is be taken as the lower bound. This is not a legitimate limit like the upper bound, and should only be taken as suggestive. If the observed ^{6}Li that led to the limit in Ref. [43] was not entirely primordial, but rather produced through cosmic rays or other mechanisms, then this limit would not properly reflect primordial lithium.

Using these limits, the results of this chapter indicate that if the X^- is a Dirac Fermion, then one would expect for it to have a mass of a few hundreds of Gev, a lifetime between about 1500 s to 3000 s, and an initial primordial abundance of about

$Y_{X^-} \approx 0.01$ relative to baryons. Since the lower bound on the lifetime depends on the lower limit of $Y_{^6\mathrm{Li}}$, it should also be taken as suggestive, rather than as a strict limit such as the upper bound.

These are remarkable constraints considering how few assumptions were made. Since the NLSP scalar $\tilde{\tau}$ is one of favoured scenarios both for particle physics and for cosmology (see for example Ref. [49] and references therein), final conclusions of this work will wait for the consideration of the Scalar system in Section 6.3. Comparisons will then be made with the results of previous work on the topic.

6.3 Constraints on an X^- Scalar

For the case of X^- X^+ annihilation in which the X particles are Scalar particles, $g = 1$, but the cross section is not as easy to parameterize as was the case for the Dirac Fermion. The fermion case could be studied in analogy with e^- e^+ annihilation, but there is no such analogue for scalars. No fundamental scalar particle has been discovered to date.

In order to find the annihilation cross section and thus derive the mass dependence of the X^- abundance, several results from the literature are now considered. Two main

annihilation channels are presented in Ref. [50],

$$\begin{aligned} \textit{Channel } 1 \quad &: \quad \tilde{\tau}\tilde{\tau}^* \rightarrow \gamma\gamma,\, Z\gamma,\, ZZ,\, W^+W^-,\, f\bar{f},\, h^0h^0 \\ \textit{Channel } 2 \quad &: \quad \tilde{\tau}\tilde{\tau} \rightarrow \tau\tau \end{aligned}$$

The annihilation cross section for Channel 1 is [50],

$$\langle \sigma_A^{(1)} v \rangle \simeq 2\sigma_{\tilde{\tau}\tilde{\tau}^* \rightarrow \gamma\gamma} = 4\pi \left(\frac{\alpha}{m_{\tilde{\tau}}} \right)^2 + \mathcal{O}\left(\frac{T}{m_{\tilde{\tau}}} \right). \tag{6.14}$$

This is the same as the annihilation cross section for the Dirac Fermion case, Equation 6.10. It will therefore result in an identical relation between Y_{X^-} and m_{X^-} as for the fermion case (within a factor of $\ln 2$, for the difference in g between the scalars and fermions). The cross section for Channel 2 is [50],

$$\langle \sigma_A^{(2)} v \rangle \simeq \frac{16\pi\alpha^2 m_{\tilde{B}}^2}{\cos^4\theta_W \left(m_{\tilde{\tau}}^2 + m_{\tilde{B}}^2 \right)^2} + \mathcal{O}\left(\frac{T}{m_{\tilde{\tau}}} \right), \tag{6.15}$$

where $\theta_W = 28.7^\circ$ [45], and $m_{\tilde{B}}$ can be taken as $1.1 m_{\tilde{\tau}}$ in the conservative case [50]. Using these cross sections and Equations 6.8 and 6.9, the abundance is calculated numerically as a function of mass. The resulting abundance (relative to entropy) for Channel 1 alone, and for Channels 1 and 2 together are plotted as a function of mass in Figure 6.4. In addition, Ref. [50] notes the possibility that the cross section for

Channel 1 could be enhanced by a factor of 5 relative to that given above. In Figure 6.4, the abundance as a function of mass is therefore also given in the case of the enhanced Channel 1 combined with Channel 2.

Other references forego giving an expression for the annihilation cross section, and just quote results relating the abundance of the relic scalar particle to its mass. Assuming the stau is the NLSP, Ref. [49] finds that the stau abundance relative to entropy is $Y_{\tilde{\tau}} = 1.2 \times 10^{-13}(m_{\tilde{\tau}}/100\,\mathrm{GeV})$. The ($^4\mathrm{HeX}^-$) analysis in Ref. [32] assumes a scalar lepton NLSP, and uses $Y_{\tilde{l}} = 7 \times 10^{-14}(m_{\tilde{l}}/100\,\mathrm{GeV})$, in agreement with $Y_{\tilde{\tau}} = 0.142 \times 10^{-12.3}(m_{\tilde{\tau}}/100\,\mathrm{GeV})$ from Ref. [51]. In Ref. [51], the model-dependence of the result is acknowledged, and the authors say that $Y_{\tilde{\tau}} = (0.142/3) \times 10^{-12.1}(m_{\tilde{\tau}}/100\,\mathrm{GeV}) \approx 4 \times 10^{-14}(m_{\tilde{\tau}}/100\,\mathrm{GeV})$ is also possible.

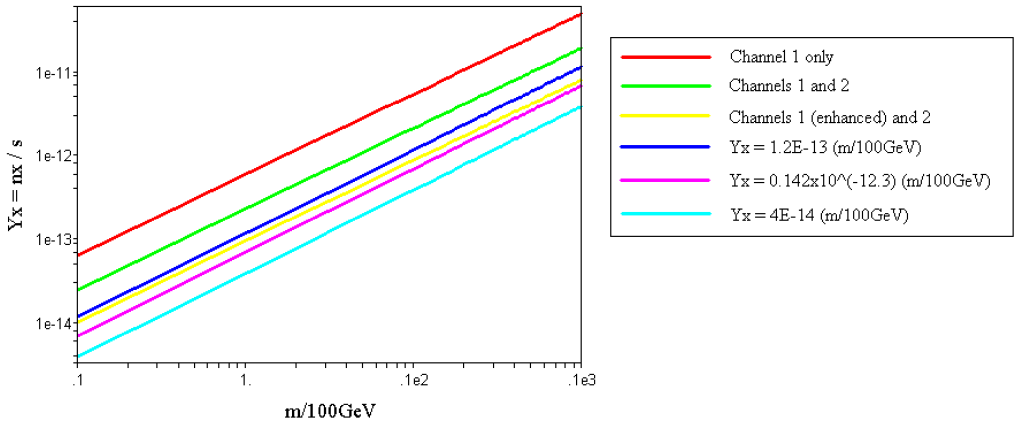

Figure 6.4: The abundance Y_{X^-} relative to entropy as a function of m_{X^-} in various different parameterizations (see text for references and explanation).

All these different estimates of the abundance as a function of scalar mass are plotted in Figure 6.4. There is more than an order of magnitude spread in the various results. The highest estimate corresponds almost exactly with the expression found in Section 6.2 in the case where X^- is a Dirac Fermion. Therefore, Figure 6.3 represents the upper limiting case for the Scalar X^- as well. The estimate $Y_{\tilde{\tau}} = 0.142 \times 10^{-12.3}(m_{\tilde{\tau}}/100\,\mathrm{GeV})$ from Ref. [51] will serve as the other limit.[2] Since the upper limit for the correspondence between Y_{X^-} and m_{X^-} was already given in Figure 6.3, in this section the *lower* limit of this relation will be used, employing $Y_{\tilde{\tau}} = 0.142 \times 10^{-12.3}(m_{\tilde{\tau}}/100\,\mathrm{GeV})$ instead of trying to find a central value within the different estimates of Y_{X^-}. Ultimately, this will mean that the true Scalar results may lie between what is presented in Figure 6.3, and what is presented later in this section in Figure 6.5.

The limiting abundance from Ref. [51], $Y_{\tilde{\tau}} = 0.142 \times 10^{-12.3}(m_{\tilde{\tau}}/100\,\mathrm{GeV})$ is measured relative to entropy. Equation 6.5 is used to convert this into an abundance relative to baryons,

$$Y_{X^-} \simeq 8.19 \times 10^{-4} \left(\frac{m_{X^-}}{100\,\mathrm{GeV}}\right). \tag{6.16}$$

This result is used to replace the Y_{X^-} axis in Figure 6.1 with a mass axis. In order to constrain the properties of the X^- Scalar, mass limits are required. The lower

[2] Although $Y_{\tilde{\tau}} \approx 4 \times 10^{-14}(m_{\tilde{\tau}}/100\,\mathrm{GeV})$ is an even lower estimate, this comes from the same reference, and is not the preferred result [51].

limit is the same as was used in the Fermion case, $m > 85.2\,\mathrm{GeV}$ from direct detector searches at LEP [3].

If the X^- is the NLSP stau with gravitino Dark Matter LSP, then Ref. [49] suggests an upper limit on its mass of $m \lesssim 203\,\mathrm{GeV}$. This is used as one (model-dependent) upper limit on the (m_{X^-}, τ_{X^-}) phase space here. A second more generous upper limit is also used. In many Supersymmetry models, stau masses up to about 1 TeV are considered (see for example Refs. [46–48]). In Ref. [48], four bench-mark SUSY scenarios are studied. They are consistent with models of mSUGRA (minimal Super Gravity) and cosmological limits, in the case where the gravitino is the Dark Matter LSP, and the stau is the NLSP. In these four scenarios, the lightest stau mass varies from 154 GeV to 1140 GeV. The bench-mark that gives the upper limit $m_{\tilde{\tau}} = 1140\,\mathrm{GeV}$ is also in the ^{6}Li- and ^{7}Li-friendly region. Since this seems indicative of an mSUGRA / SUSY "natural" upper limit on the stau mass, it is used to constrain the (m_{X^-}, τ_{X^-}) phase space in Figure 6.5.

If the X^- is the NLSP, then in R-parity conserving SUSY models with the gravitino as the lightest Supersymmetric particle, the dominant decay mode of the stau is $\tilde{\tau} \rightarrow \tilde{g}_{3/2} + \tau$. The standard decay rate for this process is (see for example Refs. [32, 49–52]),

$$\Gamma_{\tilde{\tau}\rightarrow\tilde{g}_{3/2}+\tau} = \frac{1}{48\pi}\frac{m_{\tilde{\tau}}^5}{M_*^2 m_{3/2}^2}\left(1 - \frac{m_{3/2}^2}{m_{\tilde{\tau}}^2}\right)^4, \tag{6.17}$$

where M_* is the *reduced* Planck scale, $M_* = 2.436\times10^{18}\,\mathrm{GeV}$, and $m_{3/2}$ is the gravitino

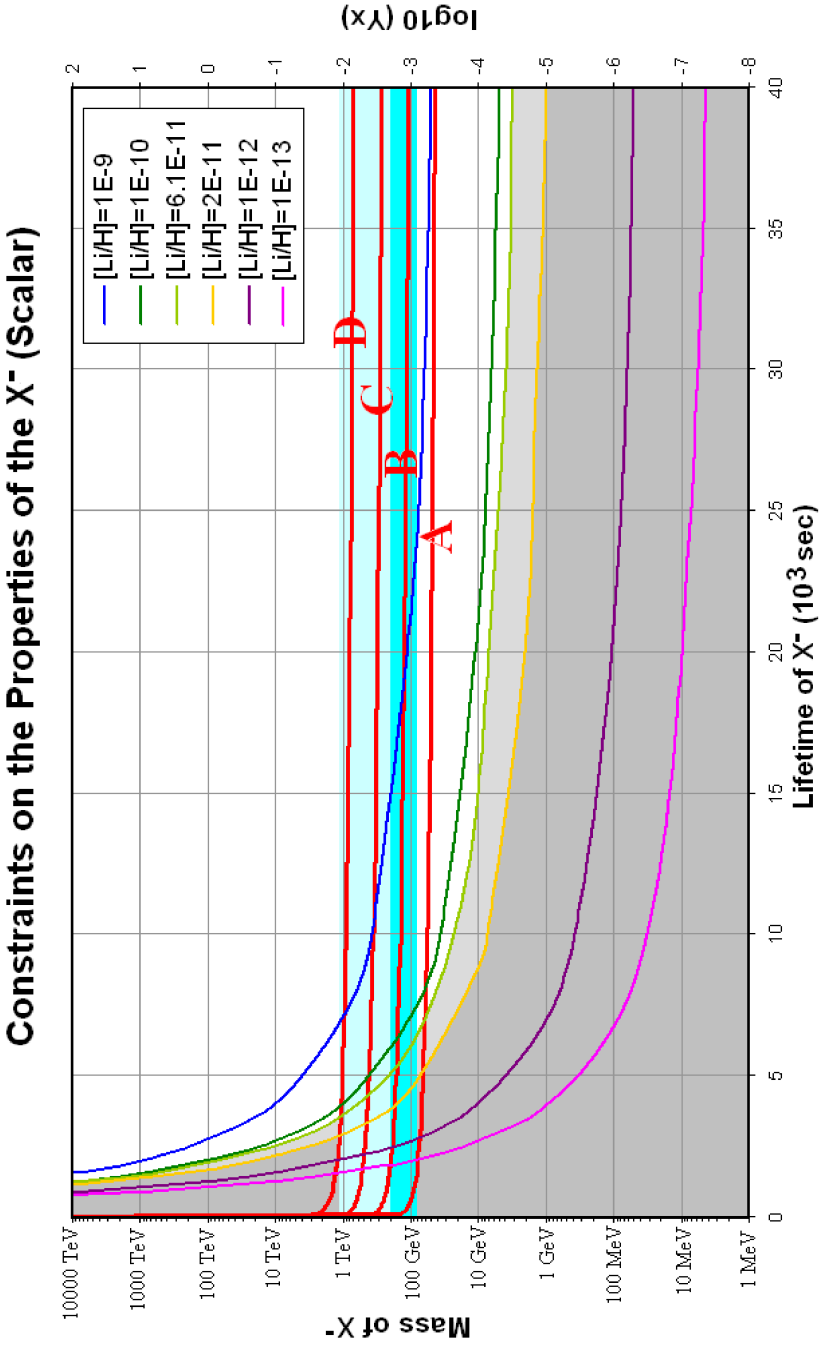

Figure 6.5: The (m_{X^-}, Y_{X^-}) phase space for an X^- Scalar, with ^{6}Li constraints as in Figure 6.1. The bright blue band corresponds to the most probable mass range. The lower limit of 85.2 GeV is from direct detector searches, while the upper limit of 203 GeV is suggestive if X^- is the NLSP stau. The light blue band extends to the "natural" SUSY limit of $m_{\tilde{\tau}} \lesssim 1140$ GeV. The red curves are m_{X^-} vs. τ_{X^-} predictions for gravitino masses of A: 0.1 GeV, B: 1 GeV, C: 10 GeV, and D: 100 GeV.

mass. The above equation is actually a simplification in the limit where m_{stau} is much greater than both $m_{3/2}$ and m_τ. The full decay width is [48],

$$\Gamma_{\tilde{\tau}\to\tilde{g}_{3/2}+\tau} = \frac{\left(m_{\tilde{\tau}}^2 - m_{3/2}^2 - m_\tau^2\right)^4}{48\pi\, M_*^2\, m_{3/2}^2\, m_{stau}^3} \left(1 - \frac{4\, m_{3/2}^2\, m_\tau^2}{\left(m_{\tilde{\tau}}^2 - m_{3/2}^2 - m_\tau^2\right)^2}\right)^{3/2}, \tag{6.18}$$

where $m_\tau = 1.777\,\mathrm{GeV}$ [53] is the tau lepton mass.

Equation 6.18 constrains the Scalar X^- lifetime ($\tau_{X^-} = 1/\Gamma$) as a function of its mass, with only one model-dependent parameter, the gravitino mass $m_{3/2}$. This gravitino constraint is a useful addition to the (m_{X^-}, τ_{X^-}) phase space plot for the Scalar X^-, as it adds another independent constraint on the X^- properties. The phase space now contains direct mass limits, constraints imposed by the ^{6}Li abundance (which fundamentally constrain Y_{X^-} as a function of τ_{X^-}, but use X^- X^+ annihilation information generate mass constraints), and now gravitino constraints, which directly relate mass to lifetime.

In general, the gravitino LSP is usually assumed be be heavier than about 10 GeV (see for example Refs. [49,51,54]), however in some scenarios (especially ones in which leptogenesis occurs non-thermally), the gravitino can be the Dark Matter particle for masses lighter than 10 GeV [31, 50, 54]. Depending on the Reheating Temperature of the universe, the gravitino could be as light as 1 keV (see Ref. [50] and references therein). A more likely scenario, however, is to have a heavier gravitino (with a

mass of $m_{3/2} \gtrsim 100\,\mathrm{MeV}$) for gauge-mediated SUSY breaking models [50]. Even more interesting is the fact that if the gravitino mass lies between $\mathcal{O}(1)\,\mathrm{GeV}$ and $\mathcal{O}(10)\,\mathrm{GeV}$ and the NLSP is a charged slepton, then not only is the gravitino a good Dark Matter candidate, but in this scenario, the Super Gravity theory can be tested in collider experiments (see Ref. [31] and references therein).

As an upper limit, the gravitino is sometimes considered to be as heavy as 10 TeV [40, 51], though this is not in the regime for a gravitino LSP. In this analysis, the gravitino must be lighter than the X^- if Equation 6.18 is to hold, since the decay would otherwise be kinematically forbidden. An upper limit of $m_{3/2} \lesssim 100\,\mathrm{GeV}$ is therefore used in this analysis, and constraints for gravitino masses of 100 GeV, 10 GeV, 1 GeV, and 0.1 GeV are included on Figure 6.5.

Although the model with gravitino Dark Matter and an NLSP stau is attractive and had received a lot of attention in the literature, this is not the only scenario in which the CBBN results apply. The CBBN mechanism requires that the heavy relic X^- must be long lived. There are two generic ways in which this can be achieved. One is that it has a small coupling with the particle that it decays into. This would be the case if the LSP was a gravitino, as gravitational couplings are very small, and there is no hadronic current between $\tilde{\tau}$ and $\tilde{g}_{3/2}$. The second way to generate a long lifetime for the X^- is for it to be almost degenerate in mass with the LSP. In this case, the LSP is generally presumed to be a neutralino, which should have a mass

on the order of 300 GeV, plus or minus a couple hundred GeV [46–48]. To generate the lifetime of the X^-, the mass splitting between X^- and the neutralino must be $\mathcal{O}(100)$ MeV.

Replacing the gravitino LSP constraints with the neutralino ones would result in a limit on the X^- mass of $100\,\text{GeV} \lesssim m_{X^-} \lesssim 500\,\text{GeV}$. This constraint is already covered by the light blue regions on Figure 6.5, which represent a lower limit from detector searches, and a "natural" SUSY upper limit. The neutralino constraint is thus almost redundant. The lower limit it proposes is similar to the lower limit from the gravitino constraint marked A (corresponding to $m_{\tilde{g}_{3/2}} = 0.1\,\text{GeV}$). The upper limit is similar to the gravitino constraint marked C (corresponding to $m_{\tilde{g}_{3/2}} = 10\,\text{GeV}$). As such, the neutralino constraints are slightly more stringent than the gravitino constraints, since the gravitino constraints allow all the phase space up to the curve marked D (corresponding to $m_{\tilde{g}_{3/2}} = 100\,\text{GeV}$). Since the gravitino constraints are more conservative, and since they do not exclude the neutralino phase space, they will be the ones used in the following analysis. As a result, much of the following discussion will assume a model with the gravitino as the Dark Matter LSP, and the stau as the NLSP.

6.4 Results

In Figure 6.5, the overlapping area between the blue regions and the grey regions is the probable phase space for the Scalar X^- properties. Some of the constraints, such as those generated by considering the decay of X^- into a gravitino, further assume that the X^- is the NLSP stau.

As discussed in the case of an X^- Dirac Fermion, the lower bound on the primordial ^{6}Li abundance is hard to determine, and not reliable. As in Section 6.2, however, the dark purple curve representing $Y_{^6\mathrm{Li}} = 10^{-12}$ is chosen as a reasonably conservative lower bound, suggested at the 2-σ level by Ref. [43]. It should be emphasized that this limit (and the resulting lower limit on X^- lifetime) should be seen as somewhat speculative, while the upper limit should be strictly observed.

The *abundance* constraints generated by the ^{6}Li limits are therefore bounded by the dark purple curve ($Y_{^6\mathrm{Li}} = 10^{-12}$) from below, and the light green curve ($Y_{^6\mathrm{Li}} = 6.1 \times 10^{-11}$) from above. The *mass* constraints on the X^- are represented by the blue shaded regions, with the bright blue region being the stau preferred region. The *decay* constraints relate to the gravitino mass, and are represented by the red curves marked A-D in Figure 6.5. The X^- properties should lie within the phase space bounded by curves A and D.

Combining these constraints, the allowed phase space for the X^- properties is quite restrictive, and quantitative results can be obtained. It is now possible to

present the results of this analysis, using the predictions of Figures 6.3 and 6.5. Recall from the discussion in Section 6.3 that Figure 6.5 represents a limiting case for the Scalar particle in terms of how the abundance, Y_{X^-}, relates to the mass, m_{X^-}. The other limit is well represented by superimposing the gravitino limits onto Figure 6.3. The true Scalar results may lie between what is presented in these two figures, and this is taken into account in assigning limits to the X^- properties.

The results presented below apply to the case where the X^- is a heavy, metastable charged scalar particle, assumed to be the NLSP stau. Model-independent properties can be read from Figure 6.1, but these are not as well constrained.

The lower limit on the lifetime τ_{X^-} comes from the intersection point between the purple curve ($Y_{^6\mathrm{Li}} = 10^{-12}$) and the red gravitino curve D ($m_{3/2} = 100\,\mathrm{GeV}$). Figures 6.3 and 6.5 read $\tau_{X^-} = 1600\,\mathrm{s}$ and $\tau_{X^-} = 2000\,\mathrm{s}$, respectively for this point, so the lower limit on the lifetime is set as $\tau_{X^-} > 1600\,\mathrm{s}$. Since the lower $Y_{^6\mathrm{Li}}$ constraint is not strict, this limit should also be seen just as suggestive.

The upper limit on the mass of the X^- comes from the same intersection point, giving in both cases an upper limit of about $m_{X^-} < 1000\,\mathrm{GeV}$. From Figure 6.3, this relates to $Y_{X^-} < 0.07$ relative to baryons, while Figure 6.5 reads $Y_{X^-} < 8 \times 10^{-3}$. The higher of these two, $Y_{X^-} < 0.07$, is chosen as the upper limit on the abundance. Since the X^- mass (and abundance) do not change much along the gravitino line D as a function of the $Y_{^6\mathrm{Li}}$ value, these limits are meaningful even in the case that the

lower bound on $Y_{^6\mathrm{Li}}$ is inaccurate.

The upper limit on the X^- lifetime is defined by the intersection point between the light green curve ($Y_{^6\mathrm{Li}} = 6.1 \times 10^{-11}$) and the red gravitino curve A ($m_{3/2} = 0.1\,\mathrm{GeV}$). Figures 6.3 and 6.5 read $\tau_{X^-} = 4000\,\mathrm{s}$ and $\tau_{X^-} = 7000\,\mathrm{s}$, respectively for this point. The strict upper limit on the X^- lifetime is therefore $\tau_{X^-} < 7000\,\mathrm{s}$.

This point also defines the lower limit on the mass. Both plots read $m_{X^-} = 60\,\mathrm{GeV}$ at this point, so the lower limit on the mass is $m_{X^-} > 60\,\mathrm{GeV}$. This gives $Y_{X^-} > 4 \times 10^{-3}$ from Figure 6.3, and $Y_{X^-} > 5 \times 10^{-4}$ from Figure 6.5. The lower limit on the abundance relative to baryons is thus $Y_{X^-} > 5 \times 10^{-4}$.

These results are summarized and compared with four other studies of CBBN in Table 6.1. The analysis methods of these four references will now be briefly reviewed and examined.

Table 6.1: Comparison of CBBN Results from Several Publications

Ref.	Source	$Y_{X^-} = n_{X^-}/n_\mathrm{B}$	τ_{X^-} (s)	m_{X^-} (GeV)
[1]	^{6}Li	$\lesssim 3 \times 10^{-7}$	$\lesssim 5 \times 10^3\,\mathrm{s}$	
[31]	^{6}Li	10^{-3} to 10^{-4}	(3300 - 3700) s	
[2]	^{7}Li	> 0.02	(1000 - 2000) s	
[33]	^{7}Li	$\gtrsim 1.2 \times 10^{-10}$	(730 - 1736) s	$\sim m_{LSP}$
Here	^{6}Li	5×10^{-4} to 0.07	(1600 - 7000) s	(60 - 1000) GeV

Ref. [1] examines catalysis effects from the ($^4\mathrm{HeX}^-$) system, using the ^{6}Li constraint of $Y_{^6\mathrm{Li}} < 2 \times 10^{-11}$ to deduce the properties of the X^-. The analysis is model-independent, in that no assumptions are made as to the identity of the X^-,

other than to assume that it is heavy, metastable, and charged. As discussed in Section 5.2, however, the CBBN production rate of ^{6}Li that was used in Ref. [1] was an estimate. At shorter lifetimes than in Table 6.1, the abundance limit as a function of the X^- lifetime becomes $Y_{X^-} \exp(-2.2 \times 10^4\,\mathrm{s}/\tau_{X^-}) < 10^{-6}$.

Ref. [31] attempts to resolve the reaction rate discrepancy in Ref. [1], and re-examines the (^{4}HeX$^-$) system using the ^{6}Li limit of $Y_{^6\mathrm{Li}} < 6.1 \times 10^{-11}$ to constrain the properties of the X^-. The analysis is also model-independent, but the authors use the Saha Equation to find the (^{4}HeX$^-$) abundance, as opposed to the required Boltzmann Equation, so the results may not be satisfactory. The values on Table 6.1 represent the case where m_{X^-} is in the range between 100-300 GeV.

Ref. [2] uses the CBBN mechanism to provide a possible solution to the Lithium Problem by examining the (^{7}BeX$^-$) system and finding the allowed phase space that would give the "correct" ^{7}Li primordial abundance without spoiling the ^{6}Li predictions. The work avoids making model-dependent conclusions, and combines results obtained through ^{7}Li constraints with those obtained earlier in the same author's previous publication [1] using ^{6}Li limits. The ^{7}Li results obtained in Ref. [2] are important constraints to keep in mind. With enough X^- in the universe, the predicted ^{7}Li abundance can be brought into agreement with observations. Ref. [2] sets a lower limit on the abundance of X^- required to solve the Lithium Problem. This is quite high compared to the *upper* limits set by Refs. [1] and [31], but this is compensated

for by the fact that the lifetime of the X^- is required to be relatively short compared to the lifetimes considered in the other two references.

Ref. [33] also attempts to resolve the Lithium Problem through CBBN mechanisms using the (^{7}BeX$^-$) system and ^{7}Li constraints. They assume a neutralino LSP with a mass of $m_{LSP} = 300\,\mathrm{GeV}$ and infer a mass splitting between the NLSP X^- and the neutralino of $\delta m \approx (100 - 200)\,\mathrm{MeV}$. This reference is included in Table 6.1 solely because of the fact that it is one of the few papers to address the Lithium Problem using the CBBN mechanism. The results are not reliable, however, as this group also uses the Saha approximation to find abundances. As shown earlier, this is an inappropriate approximation, and will lead to erroneous results.

Comparing the results of this current work to those of the four other studies in Table 6.1, it is clear that there is some overlap. The lifetime range found in this work is consistent with the results of all the other groups. The important (^{7}BeX$^-$) results [2] prefer the very low end of the range found here, $1600\,\mathrm{s} \lesssim \tau_{X^-} \lesssim 2000\,\mathrm{s}$. It is reassuring to see this concurrence. It means that the results found here are not excluded by ^{7}Li constraints (or vice versa) and is supportive of the fact that the CBBN mechanism may indeed supply many of the missing pieces in cosmology, as well as provide good particle physics constraints on the SUSY properties.

The X^- abundance found in this current work is again consistent with the ^{7}Li results of Ref. [2]. The abundance result from Ref. [1] as shown in Table 6.1 does not

agree with the current findings, but in the case of shorter lifetime, the agreement is good. Using the lifetime range found here in this current work, the results of Ref. [1] are, $2 \times 10^{-5} \lesssim Y_{\mathrm{X}^-} \lesssim 0.9$. Not only are the current findings consistent with this, but they also give a tighter constraint.

This current work is the only one that finds a likely mass range for the X^-. The constraints here mainly arise due to an assumption that the X^- is the NLSP and that it decays into a gravitino with very small couplings. This is only one possible way through which the X^- could obtain its long lifetime. The other generic possibility is for the X^- to be nearly degenerate in mass with its daughter particle. This is presumably the case if the LSP is a nautralino. Neutralino constraints on the X^- mass are not too interesting, though. Since the particles are assumed to be nearly degenerate, a mass limit on the X^- requires direct knowledge of the neutralino mass. In this work, a wide range of gravitino masses were considered, and the X^- mass constrained to (60 - 1000) GeV. It is interesting that the lower limit found here is actually slightly less than the current detector limit of about 85 GeV.

One further paper [15] also addressed the CBBN implications to cosmology. This reference assumes a gravitino LSP and thoroughly examines the effects of a charged relic in the early universe. It includes analysis of the bound state effects as well as the consequences of the injections of both electromagnetic and hadronic energy during and after the Nucleosynthesis era. The detailed analysis in this paper uses the proper

Boltzmann Equation for analysing abundances, and also calculates two- and three-body decays of the stau NLSP. Ref. [15] concludes that for a stau with a lifetime longer than about $10^3 - 10^4$ s, it is not possible to bring both the ^{7}Li and the ^{6}Li abundances into agreement with observation without spoiling the BBN predictions of one of the other isotopes, such as deuterium.

For the particular case when the stau NLSP lifetime is about 1500 s and the gravitino mass is about 80 GeV, Ref. [15] finds that it *is* possible to both reduce the predicted ^{7}Li abundance, while at the same time increase the predicted ^{6}Li amount. They comment that it may indeed be possible to solve both the Lithium Problems, as described in Section 1.3 through the CBBN mechanism.

The allowed values of $\tau_{X^-} = 1500$ s and $m_{3/2} = 80$ GeV from Ref. [15] are both within the ranges predicted in this work.

All in all, the results obtained in this current work are generally consistent with the ranges of values obtained in previous works. The results here are in many cases more stringent and more complete than in other references. Combining these results with the CBBN limits imposed by ^{7}Li constraints in Ref. [2] gives one of the most sensitive probes for exotic electroweak scale relics known to date. Some of the possible cosmological implications of these results will be discussed in the following chapter.

Chapter 7

Conclusions

In the previous chapters, the CBBN mechanism was studied, and applications to the (^{7}BeX$^-$) and (^{4}HeX$^-$) systems were shown. Bound states with nuclei lighter than ^{4}He are not important. By the time the universe has cooled enough for those states to form, all the free X$^-$ are bound into the (^{4}HeX$^-$) system, as shown in Chapter 5. In Chapter 6, ^{6}Li constraints on the catalyzed (^{4}HeX$^-$) system were used to deduce the properties of the X$^-$. These were found to be consistent with the X$^-$ properties found by Ref. [2] using ^{7}Li constraints on the (^{7}BeX$^-$) system. In this chapter, a summary of the results found in this work will be presented. A brief discussion of implications to cosmology will also be included, in which it is shown that the findings in this work are consistent with Dark Matter constraints.

7.1 Cosmology: Dark Matter

As discussed in Chapter 1, one of the primary goals in particle physics and cosmology today is to explain what the Dark Matter in the universe is composed of. Approximately 20% of the energy density of the universe is Dark Matter, and there is to date no conclusive and proven theory to explain what it is.

An attractive feature of Supersymmetry is that it provides a possible Dark Matter solution. If R-parity is conserved (see discussion in Chapter 1), then the lightest SUSY particle must be stable, since there is nothing that it can decay into in an energy conserving process. This lightest SUSY particle (LSP) is therefore a Dark Matter candidate.

In the discussion here of the CBBN process, the required X^- particle cannot itself be Dark Matter, since it is charged. If the Dark Matter in the universe was charged, it could be observed through electromagnetic interactions and emitted radiation. The decay product of the X^- could, however, be Dark Matter in the case where it is stable, neutral, and weakly interacting.

Assume for the sake of argument that the only production mechanism of the LSP is through X^- decays. In reality, the LSP could also be produced thermally, through vacuum fluctuations and pair production. For now, however, consider only the case where the non-thermal X^- decays dominate the production rate.

If the branching ratio for the decay of X^- into the LSP is unity, then all the X^-

particles will eventually be converted to Dark Matter. The number density of the LSP in the current universe will therefore be the same as the number density that the X^- would have had today if it had not decayed at all,

$$n_{LSP}^{non-th} = 2n_{X^-}. \tag{7.1}$$

The factor of 2 is inserted here to account for the X^+ particles, which presumably would have the same abundance as their anti-particle, the X^-, and could also decay into the LSP.

In astrophysics, the cosmic abundance of Dark Matter is usually referred to in terms of the density parameter Ω_{DM}, which is defined for a generic system as $\Omega = \rho/\rho_{crit}$. The mass density ρ is obtained from the number density n through the simple relationship, $n = \rho/m$, where m is the mass of the particle. The current critical density required for the closure of the universe is defined as $\rho_{crit} = 3H_0^2/8\pi G_N$, and takes a value $\rho_{crit} \approx 1.01 \times 10^{-26}\,\mathrm{kg/m^3}$ [4, 53].

Using these definitions, Equation 7.1 can be reformulated as,

$$\begin{aligned} \frac{\rho_{crit}\Omega_{LSP}^{non-th}}{m_{LSP}} &= 2\,\frac{\rho_{crit}\Omega_{X^-}}{m_{X^-}} \\ \Omega_{LSP}^{non-th} &= 2\,\frac{m_{LSP}}{m_{X^-}}\,\Omega_{X^-}. \end{aligned} \tag{7.2}$$

The density Ω_{X^-} is needed in order to find the density of the LSP. From the results

of Section 6.4, the initial X^- abundance relative to baryons is $5 \times 10^{-4} \lesssim Y_{X^-} \lesssim 0.07$. Using the fact that the baryons in the universe are about 25% by mass ^{4}He [4], and the remainder predominantly Hydrogen, then the abundance Y_{X^-} can be converted into a density Ω_{X^-},

$$\begin{aligned} Y_{X^-} &= \frac{n_{X^-}}{n_B} \\ &= \frac{\rho_{crit}\Omega_{X^-}}{m_{X^-}} \frac{m_B}{\rho_{crit}\Omega_B} \\ &= \frac{m_B}{m_{X^-}} \frac{\Omega_{X^-}}{\Omega_B} \\ &= \frac{0.75 m_H + 0.25 m_{^4He}}{m_{X^-}} \frac{\Omega_{X^-}}{\Omega_B} \\ &\approx \frac{1.6\,\mathrm{GeV}}{m_{X^-}} \frac{\Omega_{X^-}}{\Omega_B}. \end{aligned} \tag{7.3}$$

If the X^- hadn't decayed, then the current energy density of the X^- particles in the universe today would be,

$$\begin{aligned} \Omega_{X^-} &\approx \frac{m_{X^-}}{1.6\,\mathrm{GeV}} Y_{X^-}\, \Omega_B \\ &\approx \frac{m_{X^-}}{38\,\mathrm{GeV}} Y_{X^-}, \end{aligned} \tag{7.4}$$

where $\Omega_B = 0.042$ was used [4, 53].

Inserting this expression into Equation 7.2 gives the LSP density,

$$\Omega_{LSP}^{non-th} \approx \frac{m_{LSP}}{19\,\mathrm{GeV}}\, Y_{\mathrm{X}^-}. \tag{7.5}$$

In the limiting case where all the Dark Matter is produced through the decay of the X^-, then $\Omega_{LSP}^{non-th} = \Omega_{DM}$. From the WMAP 3-year results, the Dark Matter density is $\Omega_{DM} = 0.20^{+0.02}_{-0.04}$ [4, 53]. Using a 2-σ range for Ω_{DM}, then limits can be placed on the allowed abundance of the X^- at a given LSP mass. Using the upper limit of $m_{LSP} \lesssim 100\,\mathrm{GeV}$ (which is the heaviest allowed if the mass of the X^- is approximately 100 GeV), then Y_{X^-} must be in the range,

$$0.023 \lesssim Y_{\mathrm{X}^-} \lesssim 0.046, \tag{7.6}$$

where Y_{X^-} is measured relative to baryons, as in the rest of this work. This range overlaps with the upper end of the allowed X^- abundance found in Section 6.4, which was $5 \times 10^{-4} \lesssim Y_{\mathrm{X}^-} \lesssim 0.07$. It also agrees with the ^{7}Li constraints on the X^- properties from Ref. [2]. Considering lower LSP masses, however, would *raise* the limits in Equation 7.6.

Equation 7.6 assumes that all the Dark Matter is produced non-thermally through the X^- decay. Allowing for thermal production of the LSP, then the equivalence between Ω_{LSP}^{non-th} and Ω_{DM} should be replaced by the inequality, $\Omega_{LSP}^{non-th} \leq \Omega_{DM}$. This

will allow the X^- abundance to be *lower* than indicated in Equation 7.6, and will also allow for lighter gravitino masses. In order to make any more conclusions, the thermal production rate must be accounted for. This can be hard to do, especially since there is so little known for certain at the moment as to the identity and interactions of the LSP.

There has been a significant effort in the literature lately to determine the thermal production of gravitinos if they are the lightest SUSY particle (for example, papers relevant to this discussion include Refs. [49–51, 54]). This can be parameterized in many different ways, but in general always depends on the reheating temperature of inflation, T_R. In inflationary models where a scalar field, X, is responsible for inflation, its decay can cause reheating of the universe. The reheating temperature is constrained in thermal leptogenesis scenarios, and this constraint is often used to bound the abundance of the gravitino LSP, which is presumed to be the eventual decay product of the reheating decay.

Very little is known about inflation, and there is no current understanding of the mechanisms of inflation, nor what caused it. It would be premature and speculative to attempt to put any limits on the reheating temperature based on the conclusions of this work.

It suffices to acknowledge the fact that thermal production of the LSP is possible, and this will reduce the Dark Matter limits set in Equation 7.6. These limits already

overlap with the accepted X^- abundance range in the case where the gravitino mass is 100 GeV. Reducing the limits will make the agreement better, and may also allow for lighter gravitinos while still remaining consistent with the Y_{X^-} findings in this work.

7.2 Summary

In Chapters 2 and 3, some of the basic properties of the bound (NX^-) systems were found. These include the binding energy of the system, the average distance from the centre of the nucleus to the X^- particle, and a temperature scale at which the bound state could be expected to begin to form.

In general, it was found that the finite size of the nucleus N caused the binding energy of the (NX^-) system to be less than the naïve Rydberg energy that one might expect. Although the average distance $\langle r \rangle$ from the X^- particle to the centre of the nucleus N was always found to be larger than the nuclear radius, it was often the case that the Bohr Radius was well *within* the nuclear radius.

The temperature of formation of the system (NX^-) was estimated to be the temperature at which the photodisintegration rate became less than the Hubble Rate. This was generally found to happen at a temperature of about 2.5% of the binding energy of the system. The temperature of formation and the other bound state properties from Chapters 2 and 3 are summarized in Table 7.1.

Table 7.1: Summary of the Bound State Properties of (NX^-)

Nucleus N	a_B (fm)	$\langle r \rangle$	Ry (keV)	$\lvert E_g \rvert$ (keV)	T_f (keV)
^{1}H	28.82	1.50 a_B	25.0	25.0	0.6
^{2}H	14.42	1.53 a_B	49.9	48.8	1.2
^{3}H	9.63	1.54 a_B	74.8	72.5	1.8
^{3}He	4.81	1.66 a_B	299	267	6.3
^{4}He	3.63	1.70 a_B	397	346	8.2
^{6}Li	1.61	2.47 a_B	1342	794	19
^{7}Li	1.38	2.63 a_B	1566	870	21
^{7}Be	1.03	3.00 a_B	2784	1336	33
^{8}Be	0.91	3.18 a_B	3176	1427	36

In Chapter 4, work on the (^{7}BeX$^-$) system was briefly reviewed. For a detailed analysis, the reader is referred to Ref. [2]. The possibility of an X^- decay within the bound state (^{7}BeX$^-$) was also thoroughly examined in that chapter. It was found that such an occurrence would not significantly affect Nucleosynthesis.

Chapter 5 was devoted to the study of the (^{4}HeX$^-$) system. It was found that the presence of the bound state (^{4}HeX$^-$) in the universe would catalyze the production of ^{6}Li. Using the conservative 2-σ upper limit on the abundance of ^{6}Li relative to protons, $Y_{^6\mathrm{Li}} \lesssim 6.1 \times 10^{-11}$ [43], Equation 5.11 was used to find the initial abundance of X^- in the universe in the limit of long X^- lifetime. In the limit that $\tau_{X^-} \to \infty$, the X^- abundance relative to baryons is,

$$Y_{X^-} \lesssim 10^{-5}\,, \ for\ \tau_{X^-} \to \infty. \tag{7.7}$$

With a shorter lifetime, the initial X^- abundance could be much larger than this, as was discovered in Chapter 6. Chapter 5 also showed the important differences between the Boltzmann and Saha Equations, and it was concluded that the Saha Equation is inappropriate for the study of CBBN.

In Chapter 6, both the case where the X^- is a Dirac Fermion, and the case where it is a Scalar particle were considered. Assuming a primordial origin for the observed ^{6}Li in the universe, ^{6}Li constraints on the (^{4}HeX$^-$) system were used to constrain the abundance and lifetime properties of the X^- particle. A "natural" mass range (bounded below by the direct detector search limit) was added as an additional constraint. By considering X^-X^+ annihilation, a restriction of the X^- abundance as a function of its lifetime was also used to constrain the mass of the X^-. In the case of the Scalar particle, decays of the X^- into a gravitino were considered, leading to further constraints on the X^- properties. The results are presented below.

$$\textbf{Dirac Fermion}: \begin{cases} Y_{X^-} \sim 0.01 \\ 1500\,\text{s} \lesssim \tau_{X^-} \lesssim 3000\,\text{s} \\ m_{X^-} \sim \mathcal{O}(100)\,\text{GeV} \end{cases}$$

$$\textbf{Scalar Particle}: \begin{cases} 5 \times 10^{-4} \lesssim Y_{X^-} \lesssim 0.07 \\ 1600\,\text{s} \lesssim \tau_{X^-} \lesssim 7000\,\text{s} \\ 60\,\text{GeV} \lesssim m_{X^-} \lesssim 1000\,\text{GeV} \end{cases}$$

These limits were based entirely on considerations of the (^{4}HeX$^-$) system, but they are in good agreement with the best results from analysis of the (^{7}BeX$^-$) system. Using ^{7}Li constraints on the (^{7}BeX$^-$) system, Ref. [2] found $Y_{\mathrm{X}^-} > 0.02$ and $1000\,\mathrm{s} \lesssim \tau_{\mathrm{X}^-} \lesssim 2000\,\mathrm{s}$. Together, these provide one of the most stringent and model-independent probes of exotic electroweak-scale relic particles known to date. It is all the more encouraging to see that the analysis in Section 7.1 confirms that the results in this work are consistent with Dark Matter constraints, in the case where the X$^-$ is the NLSP and decays to the LSP Dark Matter. This supports the fact that Catalyzed Big Bang Nucleosynthesis may be in important part of early universe cosmology.

Bibliography

[1] M. Pospelov. Particle Physics Catalysis of Thermal Big Bang Nucleosynthesis. *Phys. Rev. Lett.*, 98(231301), 2007. [arXiv:hep-ph/0605215].

[2] C. Bird, K. Koopmans, and M. Pospelov. Primordial Lithium Abundance in Catalyzed Big Bang Nucleosynthesis. *arXiv:hep-ph/0703096v1*, 2007.

[3] Particle Data Group. Review of Particle Physics. *J. Phys. G: Nucl. Part. Phys*, 33:1120–1147, 2006. Supersymmetry Searches Review.

[4] D.N. Spergel et al. [WMAP Collaboration]. Wilkinson Microwave Anisotropy Probe (WMAP) Three Year Observations: Implications for Cosmology. *ApJ,* in press. Also available online at *arXiv:astro-ph/0603450v2*, Jan. 2007.

[5] F. Spite and M. Spite. Abundance of lithium in unevolved halo stars and old disk stars - Interpretation and consequences. *Astronomy and Astrophysics*, 115(2):357–366, 1982.

[6] S.G. Ryan, T.C. Beers, K.A. Olive, B.D. Fields, and J.E. Norris. Primordial Lithium and Big Bang Nucleosynthesis. *Astrophys. J. Lett.*, 530(L57), 2000.

[7] R.H. Cyburt, B.D. Fields, and K.A. Olive. Primordial nucleosynthesis in light of WMAP. *Phys. Lett. B*, 567:227 – 234, 2003.

[8] P. Bonifacio et al. The Lithium Content of the Globular Cluster NGC 6397. *Astron. Astrophys.*, 390:91, 2002.

[9] J. Melendez and I. Ramirez. Reappraising the Spite Lithium Plateau: Extremely Thin and Marginally Consistent with WMAP Data. *Astrophys. J.*, 615(L33), 2004.

[10] A. Coc, E. Vangioni-Flam, A. Descouvemont, A. Adahchour, and C. Angulo. Updated Big Bang Nucleosynthesis compared with Wilkinson Microwve Anisotropy Probe Observations and the Abundance of Light Elements. *Astrophys. J.*, 600:544, 2004.

[11] R.H. Cyburt, B.D. Fields, and K.A. Olive. Solar neutrino constraints on the BBN production of Li. *Phys. Rev. D*, 69(123519), 2004.

[12] C. Angulo et al. The ^{7}Be(d,p)2α Cross Section at Big Bang Energies and the Primordial ^{7}Li Abundance. *Astrophys. J.*, 630(L105), 2005. [arXiv:astro-ph/0510636].

[13] A.J. Korn et al. A probable stellar solution to the cosmological lithium discrepancy. *Nature*, 442(657), 2006. [arXiv:astro-ph/0608201].

[14] M. Asplund, D.L. Lambert, P.E. Nissen, F. Primas, and V.V. Smith. Lithium Isotopic Abundances in Metal-Poor Halo Stars. *The Astrophysical Journal*, 644:229–259, 2006.

[15] R.H. Cyburt, J. Ellis, B.D. Fields, K. Olive, and V.C. Spanos. Bound-State Effects on Light-Element Abundances in Gravitino Dark Matter Scenarios. *arXiv:astro-ph/0608562*, 2006. [CERN-PH-TH/2006-168].

[16] E. Kolb and M. Turner. *The Early Universe*. Addison-Wesley Publishing Company, 1990.

[17] P.J. Karol. Nucleus-nucleus reaction cross sections at high energies: Soft-spheres model. *Phys. Rev. C*, 11(4):1203–1209, 1975.

[18] L. Visscher and K.G. Dyall. Dirac-Fock atomic electronic structure calculations using different nuclear charge distributions. *Atom. Data Nucl. Data Tabl.*, 67:207, 1997.

[19] D. Griffiths. *Introduction to Quantum Mechanics*. Prentice Hall Inc., 1995.

[20] K. Krane. *Introductory Nuclear Physics*. John Wiley and Sons, 1988.

[21] NACRE Collaboration. http://pntpm.ulb.ac.be/nacre/nacre.htm. The NuBase database website is hosted by Université Libre de Bruxelles.

[22] NNDC National Nuclear Data Center. http://www.nndc.bnl.gov. The NuDat 2.3 database website is hosted by Brookhaven National Laboratory.

[23] G. Audi, A.H. Wapstra, and C Thibault. The AME2003 Atomic Mass Evaluation. *Nuclear Physics*, A(729):337–676, 2003.

[24] I. Tanihata, H. Hamagaki, O. Hashimoto, Y. Shida, and N. Yoshikawa. Measurements of interaction cross sections and nuclear radii in the light p-shell region. *Phys. Rev. Letters*, 55(24):2676–2679, 1985.

[25] G.G. Simon, Ch. Schmitt, F. Borkowski, and V.H. Walther. Absolute electron-proton cross sections at low momentum transfer measured with a high pressure gas target system. *Nucl. Phys. A*, 333:381–391, 1980.

[26] A. Huber, Th. Udem, B. Gross, J. Reichert, M. Kourogi, K. Pachucki, M. Weitz, and T.W. Hänsch. Hydrogen-deuterium $1s - 2s$ isotope shift and the structure of the deuteron. *Phys. Rev. Lett.*, 80(3):468–471, Jan 1998.

[27] D.H. Beck, S.B. Kowalski, M.E. Schulze, W.E. Turchinetz, J.W. Lightbody, X.K. Maruyama, W.J. Stapor, H.S. Caplan, G.A. Retzlaff, D.M. Skopik, and R. Goloskie. Tritium form factors at low q. *Phys. Rev. C*, 30(5):1403–1408, Nov 1984.

[28] P.C. Dunn, S.B. Kowalski, F.N. Rad, C.P. Sargent, W.E. Turchinetz, R. Goloskie, and D.P. Saylor. ^{3}He magnetic form factor. *Phys. Rev. C*, 27(1):71–82, Jan 1983.

[29] D. Perkins. *Introduction to High Energy Physics*. Cambridge University Press, 4th edition.

[30] Particle Data Group. Review of Particle Physics. *J. Phys. G: Nucl. Part. Phys*, 33:1120–1147, 2006. Astrophysics and Cosmology Review.

[31] K. Hamaguchi, T. Hatsuda, M. Kamimura, Y. Kino, and T.T. Yanagida. Stau-catalyzed ^{6}Li Production in Big-Bang Nucleosynthesis. *arXiv:hep-ph/0702274v4*, 2007.

[32] M. Kawasaki, K. Kohri, and T. Moroi. Big-Bang Nucleosynthesis with Long-Lived Charged Slepton. *arXiv:hep-ph/0703122v2*, March 2007.

[33] T. Jittoh, K. Kohri, and M. Koike. Possible solution to the ^{7}Li problem by the long lived stau. *arXiv:hep-ph/0704.2914v1*, April 2007.

[34] L. Landau and E. Lifshitz. *Relativistic Quantum Theory*. Pergamon Press, 1971.

[35] L. Landau and E. Lifshitz. *Quantum Mechanics: Non-Relativistic Theory*. Pergamon Press, 1958.

[36] Wikipedia. Photon Gas. *http://en.wikipedia.org/wiki/Photon_gas*, Dec. 2006.

[37] P. Mohr, K. Vogt, M. Babilon, J. Enders, T. Hartmann, C. Hutter, T. Rauscher, S. Volz, and A. Zilges. Experimental simulation of a stellar photon bath by bremsstrahlung: the astrophysical γ-process. *arXiv:nucl-ex/0007003v1*, July 2000.

[38] D. Clayton. *Principles of Stellar Evolution and Nucleosynthesis*. University of Chicago Press, 1983.

[39] Wikipedia Online Encyclopedia. The Maxwell-Boltzmann Distribution. *http://en.wikipedia.org/wiki/Maxwell-Boltzmann_distribution*, May 2007.

[40] R.H. Cyburt, J. Ellis, B.D. Fields, and K. Olive. Updated Nucleosynthesis Constraints on Unstable Relic Particles. *Phys. Rev. D*, 67(103521), 2003. [arXiv:astro-ph/0211258], [CERN-TH/2002-207].

[41] M.H. Reno and D. Seckel. Primordial nucleosynthesis: The effects of injecting hadrons. *Phys. Rev. D.*, 37(12):3441–3462, 1988.

[42] K. Jedamzik. Big Bang Nucleosynthesis Constraints on Hadronically and Electromagnetically Decaying Relic Particles. *arXiv:hep-ph/0604251*, April 2006.

[43] M. Kawasaki, K. Kohri, and T Moroi. Big-Bang Nucleosynthesis and Hadronic Decay of Long-Lived Massive Particles. *arXiv:astro-ph/0408426v2*, March 2005.

[44] R.J. Scherrer and M.S. Turner. On the relic, cosmic abundance of stable, weakly interacting massive particles. *Phys. Rev. D*, 33(6):1585 – 1589, 1986.

[45] D. Griffiths. *Introduction to Elementary Particles*. John Wiley and Sons, 1987.

[46] M. Battaglia, A. De Roeck, J. Ellis, F. Gianotti, K.T. Matchev, K.A. Olive, L. Pape, and G. Wilson. Proposed Post-LEP Benchmarks for Supersymmetry. *arXiv:hep-ph/0106204v2*, June 2001.

[47] A. Djouadi, M. Drees, and J.-L. Kneur. Updated Constraints on the Minimal Supergravity Model. *arXiv:hep-ph/0602001v2*, March 2006.

[48] O. Cakir, I. Cakir, J.R. Ellis, and Z. Kirea. Measurements of Metastable Staus at Linear Colliders. *arXiv:hep-ph/0703121*, March 2007.

[49] W. Buchmüller, L. Covi, J. Kersten, and K. Schmidt-Hoberg. Dark Matter from Gaugino Mediation. *arXiv:hep-ph/0609142v2*, Nov. 2006.

[50] T. Asaka, K. Hamaguchi, and K. Suzuki. Cosmological Gravitino Problem in Gauge-Mediated Supersymmetry Breaking Models. *arXiv:hep-ph/0005136v2*, Aug. 2000.

[51] M. Fujii, M. Ibe, and T. Yanagida. Upper Bound on Gluino Mass from Thermal Leptogenesis. *arXiv:hep-ph/0310142v2*, Nov. 2003.

[52] J. Ellis, K. Olive, Y. Santoso, and V.C. Spanos. Gravitino Dark Matter in the CMSSM. *arXiv:hep-ph/0312262v4*, June 2004.

[53] Particle Data Group. Review of Particle Physics. *J. Phys. G: Nucl. Part. Phys*, 33, 2006.

[54] F. Takahashi. Gravitino Dark Matter from Inflation Decay. *arXiv:hep-ph/0705.0579v1*, May 2007.

Appendix A

Abbreviations and Symbols

Table A.1: List of Abbreviations and Symbols

Abbreviation	Full Form
BBN	Big Bang Nucleosynthesis
CBBN	Catalyzed Big Bang Nucleosynthesis
SBBN	Standard Big Bang Nucleosynthesis
SM	Standard Model
SUSY	Supersymmetry
CMSSM	Constrained Minimal Supersymmetric Standard Model
mSUGRA	Minimal Super Gravity
LSP	Lightest Supersymmetric Particle
NLSP	Next-to-Lightest Supersymmetric Particle
T	Temperature
t	Time
rms	Root-mean-square
a_B	Bohr radius
R_{N}	Nuclear radius of nucleus N
I	Ionization energy
E_B	Binding energy (equivalent to Ionization energy)
E_g	Ground state energy (< 0)
Ry	Rydberg energy, $Ry = \frac{1}{2}Z^2\alpha^2 m$
(NX^-)	Bound state between nucleus N and relic X^-
τ_{X^-}	Lifetime of the X^- particle
Y_i	Abundance of species i relative to some standard

Appendix B

Physical Constants

Table B.1: Numerical Values of Physical Constants and Other Quantities

Quantity	Symbol	Value
Fine Structure Constant	α	$1/137.036$
Boltzmann Constant	k_B	$8.6173423 \times 10^{-11}\,\mathrm{MeV/K}$
Atomic Mass Unit	amu or u	$931.502\,\mathrm{MeV}/c^2$
Astrophysical Temperature Unit	T_9	$1\mathrm{T}_9 = 10^9\,\mathrm{K} = 0.0861734\,\mathrm{MeV}$
Planck's Constant	$\hbar$	$6.58211915 \times 10^{-22}\,\mathrm{MeV}\cdot\mathrm{s}$
Speed of Light	c	2.99792458×10^8 m/s
Planck Mass	M_{Pl}	$1.22 \times 10^{19}\,\mathrm{GeV}$
Reduced Planck Mass	M_*	$2.436 \times 10^{18}\,\mathrm{GeV}$
h-bar c	$\hbar c$	$197.327\,\mathrm{MeV}\cdot\mathrm{fm}$
Baryon-to-Photon Ratio	η	6.116×10^{-10}
Newton's Gravitational Constant	G_N	$6.7087 \times 10^{-39}\,\mathrm{GeV}^{-2}$